A GENERALIZED LOG-LAW FORMULATION FOR A WIDE RANGE OF BOUNDARY ROUGHNESS CONDITIONS ENCOUNTERED IN STREAMS

James Read Plott

Thesis submitted to the faculty of the Virginia Polytechnic Institute and State University in partial fulfillment of the requirements for the degree of

Master of Science
In
Civil Engineering

Panayiotis Diplas, Committee Chair
Clinton L. Dancey
Glenn Emery Moglen

August 30, 2011
Blacksburg, VA

Keywords: log law, boundary layers, bed forms, open channel flow, zero-plane displacement, sediment transport

A GENERALIZED LOG-LAW FORMULATION FOR A WIDE RANGE OF BOUNDARY ROUGHNESS CONDITIONS ENCOUNTERED IN STREAMS

James Read Plott

Abstract

It is demonstrated that the method for locating a velocity profile origin, or plane of zero velocity, by fitting log profiles to streamwise velocity measurements is applicable to a larger range of roughness scales than previously expected. Five different sets of detailed, experimental velocity measurements were analyzed encompassing sediment-scale roughness elements, roughness caused by rigid vegetation, and large-scale roughness elements comprised of mobile bedforms. The method resulted in similar values of normalized zero-plane displacement for all roughness types considered. The ratios of zero-plane displacement, d_h, to roughness height, k_s, were 0.20 and 0.26 for the sediment- and vegetation-scale experiments, respectively. The results for the two experiments with bedform dominated roughness were 0.34 and 0.41. An estimate of d_h/k_s ranging from 0.2 to 0.4 is therefore recommended for a range of roughness types with the higher end of the range being more appropriate for the larger, bedform-scale roughness elements, and the lower end for the sediment-scale roughness elements. In addition, it is demonstrated that the location of the plane of zero velocity is temporally constant even when the bed height is not. The effects of roughness element packing density were also examined with the identification of a possible threshold at 4%, above which zero-plane displacement is independent of packing density. The findings can be applied to field velocity measurements under mobile bed conditions, facilitating the calculation of turbulence parameters such as shear velocity, by using point measurements and providing guidelines for the estimation of an appropriate value for zero-plane displacement.

Acknowledgements

I would like to thank my advisor, Panos Diplas, for his support and input throughout my research as well as his patience during the completion of this thesis. I would also like to thank my committee members Glenn Moglen and Clint Dancey; Glenn Moglen for his understanding in the classroom and support during my research, and Clint Dancey for his expert input on the subject.

I would also like to thank Jess Kozarek for her help in designing and conducting experiments as well as data analysis and general guidance. I thank Craig Hill for answering all of my technical questions with instrumentation as well as experiment design and data collection and Fotis Sotiropoulos for providing the one of a kind, state of the art facilities to conduct the research.

I would like to acknowledge NCHRP for providing the impetus to undertake the experiments I conducted. I would also like to acknowledge Kris Guentzel for assistance collecting OSL data and for his moral support. He was always available for a good laugh when research was tedious and monotonous. I thank Seokkoo Kang for experimental planning and data analysis support. And finally, June Sayers, Tom Wangerin (for being the butt of many jokes), Anna Dooley, Chris Millren, and Jeff Heur for keeping the OSL operating and making each experiment interesting and enjoyable.

Table of Contents

List of Figures

List of Tables

Notation

a	Largest dimension of a spheroid roughness element [m]
b	Intermediate dimension of a spheroid roughness element [m]
b_r	Intercept of linear regression
c	Smallest dimension of a spheroid roughness element [m]
C_D	Drag coefficient [m^{-1}]
d	Diameter of a sphere [m]
d_h	Zero-plane displacement [m]
d_m	Mean grain diameter [m]
d_X	Grain size at which X% of material is finer by weight [m]
D	Sieve dimension [m]
g	Gravitational constant [9.81 m/s^2]
h	Characteristic size of roughness elements (generally height or diameter) [m]
H	Flow depth [m]
k_s	Representative roughness height [m]
m_r	Slope of linear regression
p	Proportionality constant between zero-plane displacement and roughness height
Q	Volumetric flow rate [m^3/s]
R^2	Coefficient of determination for a curve of best fit
S	Energy slope [m/m]
SF	Shape factor
u	Time averaged streamwise velocity component [m/s]
u'	Fluctuation of streamwise velocity from the mean [m/s]
$\langle u \rangle$	Time-average streamwise velocity [m/s]
u_h	Streamwise velocity at height z = h [m/s]
u_i	Instantaneous streamwise velocity [m/s]
u_τ	Shear velocity [m/s]
U	Velocity magnitude [m/s]
w	Vertical velocity component [m/s]
w'	Fluctuation of vertical velocity from the mean [m/s]
y	Distance from the river right bank in the transverse direction [m]

z	Vertical distance from the bed [m]
z_0	Measure of boundary roughness height often used in atmospheric fluid mechanics

Greek Symbols

Γ	Constant of integration for log law
δ_e	Penetration depth [m]
θ_u	Median absolute deviation of the streamwise velocity [m/s]
κ	von Karman's constant (0.4)
λ	Roughness element packing density
u_τ	Shear velocity [m/s]
τ_0	Bed shear stress [Pa]
ρ	Fluid density [kg/m^3]
ν	Fluid Kinematic viscosity [m^2/s]

Chapter 1: Introduction

This thesis presents a study to determine if the traditional method of locating the plane of zero velocity, found in Detert et al. (2010) for example, is appropriate for all boundary roughness conditions. The study consisted of five separate data sets with varying roughness height scales representative of sediment particles, submerged vegetation, and bedform roughness. In order to outline the method used, and since the method used has been shown to be applicable under such conditions, spherical roughness elements at maximum packing density were studied. Cylindrical, rod-like vertical roughness elements simulating rigid vegetation with a fixed packing density were studied in order to assess the validity involving flows through large-scale roughness elements. Roughness elements simulating mobile bedforms were examined in two separate experimental conditions: in a straight flume and in a controllable, meandering channel. A fifth data set was obtained in order to study spherical roughness elements at different packing densities in an effort to determine the effects that packing density has on the zero-plane displacement. The bedform roughness experiments will be examined in more detail than the other experiments since they are original experiments and have not been published before. The research presented has been submitted to the Journal of Geophysical Research – Earth Surface for review and possible publication.

Included is discussion involving the relationship between zero velocity plane and the datum chosen, or bed height, the effects of packing density on zero-plane displacement along with a threshold for packing density above which the effects are minimized. It is also acknowledged that the selection of bedform roughness height is not solely dependent on wave height as was chosen for simplicity during the analyses of bedform roughness. Finally, it is demonstrated that global flow parameters can be obtained from using point measurements, instead of spatially averaged quantities, within the inner flow region.

1.1 Background Information

The location of the boundary in flows over flat, smooth surfaces is apparent and undisputable. However, for hydraulically rough boundaries common in natural rivers and atmospheric flows, the problem of defining a representative boundary is much more complicated. The challenge arises from the presence of voids having sizes significantly larger than a hypothetical viscous

sublayer thickness, which in turn allows for hyporheic flow. The irregularity of boundaries due to either variable roughness element sizes, shapes, and arrangement (Church et al., 1987), the existence of a bedload layer and saltating particles under mobile bed conditions, or bedforms and their migration (Smart, 1999) further complicates the situation. In an attempt to simplify the problem, a fictitious boundary is often considered corresponding to the asymptote of an assumed logarithmic velocity profile.

It is well accepted practice to quantitatively describe turbulent flows by assuming the existence of a logarithmic distribution of mean, streamwise velocity, u, over a certain distance from the boundary, z, known as the log law (Schlichting, 2000)

$$u/u_\tau = 1/\kappa \cdot \ln(z/k_s) + \Gamma \quad (1)$$

for fully rough-boundaries in uniform flow, where u_τ is shear velocity ($u_\tau = (\tau_0/\rho)^{0.5}$ and where τ_0 is bed shear and ρ is the fluid density), k_s is a representative roughness height, κ is von Karman's constant (0.4), and Γ is a constant. A boundary is classified as fully rough if $k_s > 70 \cdot \nu/u_\tau$ where ν is the kinematic viscosity of the fluid (Schlichting, 2000). The difficulty is in defining the origin of the logarithmic distribution where often times the boundary is comprised of irregular roughness elements varying in size and shape, in which case the average bed elevation may not be representative of the actual, local bed elevation. Further difficulties arise from the fact that the roughness elements are frequently mobile, constantly shifting due to forces imposed by the flow above and around them. Often times during mobile bed conditions there are large-scale fluctuations in bed elevation due to bedforms, thereby causing roughness to be dominated by continually migrating bedforms instead of individual sediment particles. It is also possible to have significant sediment-scale roughness elements superimposed on top of bedform-scale roughness. The presence of a roughness sublayer further complicates the problem of boundary layer theory where the individual roughness elements interact with the flow near the boundary, displacing it upwards (Raupach et al., 1991) and causing complex, not well understood patterns of shear and turbulence due to separation of flow around upstream roughness elements (Recking, 2009).

Defining a flow's boundary is important because it is the location at which the fluid-sediment interaction takes place. It is also important because of the spatial dependence of many aspects of

fluid mechanics, such as the location of boundary layers. Much research has been performed on defining boundaries with static roughness elements, but at present, limited information is available discussing how to define the boundary at a location in a stream where large-scale fluctuations in bed elevation occur due to active bedform migration.

To clarify the notation used herein, zero-plane displacement is defined as the distance from the top of the roughness elements to the zero-velocity plane. The zero-velocity plane is the elevation that the logarithmic velocity profile approaches as the velocity asymptotes to zero velocity. It is sometimes referred to as the plane of zero velocity, the velocity profile origin, origin offset, or the representative or theoretical boundary. Clarification of terms may be found by examining Figure 1.

Chapter 2: Literature Review

For flows with rough, static boundaries, it has been verified numerous times that a representative boundary is located a certain distance below the top of the roughness elements (Figure 1). Einstein and El-Samni (1949) were some of the first to investigate the location of the theoretical boundary. They performed flume experiments with roughness elements of identical plastic spheres and again with a bed of natural gravel. The location of the zero velocity plane was selected such that it caused the velocity distribution to appear as a straight line on a semi-log plot when considering the logarithmic region to extend over the entire flow depth. The flow depth for these experiments was not reported, although no measurements were obtained above 18 cm. Given the particle size of 6.9 cm, and assuming the flow depth to be approximately 18 cm, the ratio of flow depth to particle size is relatively large so that under such conditions it is appropriate to consider the log law valid over the entire depth. For the experiment with uniform, spherical roughness elements, their results indicated that the datum should be located $0.2 \cdot d$ below the top of the roughness elements where d is the sphere diameter. For the second experiment using a bed of natural gravel, the origin producing the best fit of the log profile to the data was located 1.2 cm below the top of the gravel layer, which equates to $0.2 \cdot d_{67}$ and where d_{67} is the sieve size at which 67% of the bed material is finer by weight (Einstein & El-Samni, 1949). It should be noted that their results are only comparable to conclusions drawn here if the natural sediments were placed in the flume in a random way and were not allowed to be rearranged by the flow. It is unclear whether or not this was the case.

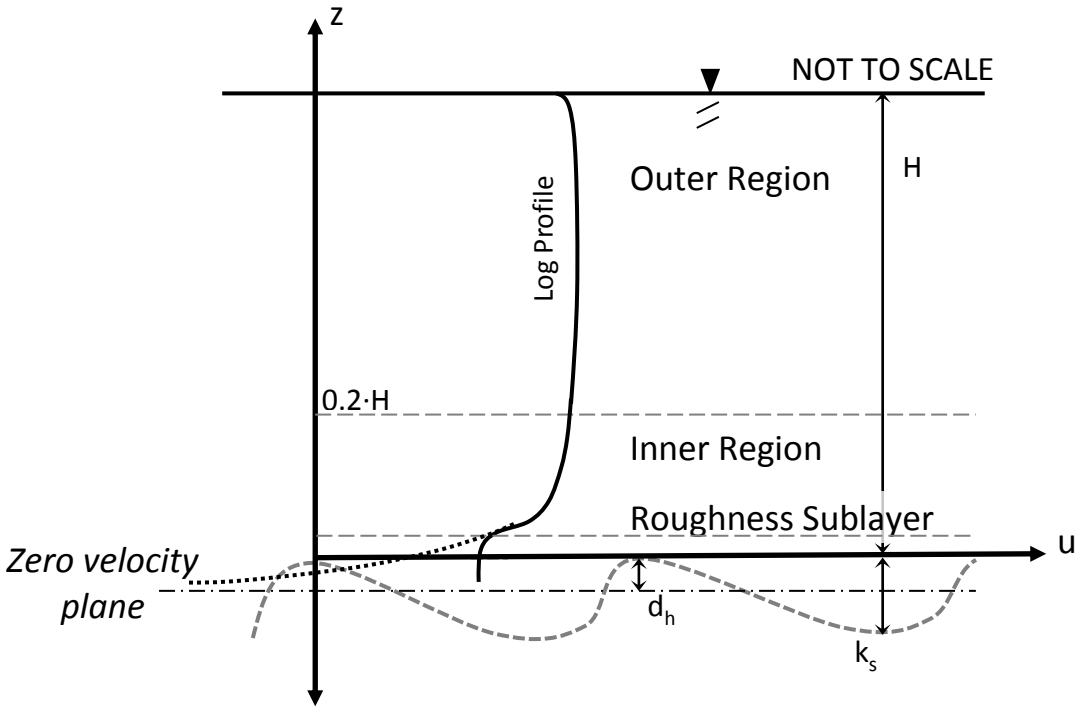

Figure 1: A sketch of an idealized, exaggerated velocity profile over a bed of the three different roughness types discussed herein.

It should also be noted that sieve diameter is not necessarily representative of a roughness element's height. Generally, for flow-worked sediments, the height of a natural sediment particle corresponds to the particle's c-axis, where the c-axis is the smallest dimension of a three dimensional sediment particle having an ellipsoidal shape and the a- and b-axes are the largest and intermediate axes, respectively. Sediment will typically arrange itself such that the particle's a-b plane lies parallel to the bed with the c-axis perpendicular to the bed. This orientation results in the maximum surface area in contact with the bed and the smallest protrusion, resulting in the maximum resistance to motion. Natural gravel has been shown to have a shape factor, *SF*, of 0.7 (Chang, 1988) where

$$SF = c\cdot(a\cdot b)^{-0.5} \tag{2}$$

and *a*, *b*, and *c* are the particle's largest, intermediate, and smallest dimensions, respectively. Considering the following relationship between sieve dimension, *D*, and a particle's c and b dimensions for ellipsoidal particles (Church et al., 1987)

$$D/b = 2^{-0.5} \cdot [1 + (c/b)^2]^{0.5} \quad (3)$$

it is possible to obtain Equation 4 by combining and manipulating Equations 2 and 3 to read,

$$D/c = [1/(0.98 \cdot a/b) + 0.5]^{0.5} \quad (4)$$

Using Equation 4, it can be shown that the possible ratios of D/c range from 1.00 to 1.23 by considering the two limiting cases a/b of unity (b/c = 1.43) and b/c of unity (a/b = 2.04). Therefore, a sieve diameter $d_{67} = D$ = 6.1 cm reported by Einstein & El-Samni (1949), could correspond to a roughness height, or sediment c-axis dimension as low as 4.9 cm. Assuming the c-axis dimension is representative of roughness height ($k_s = c$), the ratio of zero-plane displacement to roughness height could range from 0.20 to 0.25 for the gravel experiment outlined in Einstein & El-Samni (1949). The resulting value of d_h/k_s is remarkably similar to the values reported in the literature for other fixed, roughness boundaries (Kironoto & Graf, 1995; Raupach et al., 1991; Kanellopoulos, 1998).

Kironoto & Graf (1995) performed two sets of experiments similar to those of Einstein & El-Samni (1949), one with a rough plate made of fastened crushed grains ($k_s = d_m$ = 4.8 mm where d_m is the mean grain diameter) and one with natural gravel ($k_s = d_{50}$ = 23 mm). Recall that Einstein & El-Samni (1949) considered $k_s = d_{67}$ when it was determined that $d_h = 0.2 \cdot d$, whereas Kironoto & Graf (1995) considered $k_s = d_{50}$ while also assuming $d_h = 0.2 \cdot d$. Kironoto & Graf (1995) only considered measurements to follow a logarithmic profile within the bottom 20% of the flow depth. The ratios of particle size to flow depth are much larger than that presumed to be used by Einstein & El-Samni (1949), who considered the log region to cover the entire flow depth, so that the discrepancy in analyses is appropriate. Kironoto & Graf (1995) concluded that the log law (Equation 1) described their data well in the inner region.

Perry & Joubert (1963) performed experiments in a wind tunnel with 3.2 mm square bar roughness elements spanning the entire width of the tunnel and spaced at 12.7 mm. The height to spacing ratio, a measure of packing density, was 4. The location of the velocity profile origin was found by plotting multiple profiles with different origin locations until a range of zero-plane displacements were found that matched the measured data well. Measured points that clearly did not follow the straight line trend on a semi-log plot were omitted, presumably because they were outside of the inner region; no well-defined limit to the inner region, such as 20% of the flow

depth, was used. According to their results, the location of the origin was, on average, 2.54 mm below the top of the roughness elements, which results in d_h/k_s of 0.8 using $k_s = h$ where h is the height of the roughness elements.

The location of the origin has been examined theoretically by Jackson (1981). From the derivation of the log law, Jackson (1981) concluded that the location of the origin is where the mean surface shear appears to act and that the zero-plane displacement adjusts the reference to that location. Furthermore, Jackson (1981) discussed the effects of roughness density, or packing density, λ, on the zero-plane displacement and indicated that there may exist a threshold for λ above which packing density has virtually no effect on zero-plane displacement. Below the threshold, zero-plane displacement is linearly dependent on packing density. Jackson (1981) gave no clear expression describing the relationship, nor any indication of the threshold value for λ, only that one exists. The only remaining question is value of the threshold and the exact relationship between zero-plane displacement and packing density below that value.

One way to explain this behavior is to consider rod or bar-like roughness elements, such as those used by Perry & Joubert (1963). As λ increases, the boundary will approach a smooth condition, so that d_h will approach zero as the packing density reaches a maximum. As λ increases, the flow becomes less capable of penetrating down into the voids due to the decrease in spacing between elements. Defining penetration depth, δ_e, as the distance that Kelvin-Helmholtz vortices penetrate vertically into a vegetated canopy of height h, Nepf & Ghisalberti (2008) found the direct relationship between d_h and δ_e (Equation 5) by considering $z = h - d_h$ to be the location of the centroid of momentum absorption and that momentum absorption is constant for $h - \delta_e < z < h$

$$d_h = \delta_e/2 \tag{5}$$

where d_h and δ_e are measured from the top of the roughness elements and z is measured from the bed. Therefore, as packing density increases and penetration depth decreases, zero-plane displacement decreases. This is in conflict with the conclusion drawn by Jackson (1981) that for large packing densities, above the threshold, zero-plane displacement is constant. It is worth noting that a smooth boundary is not reached for large, sphere-like roughness elements at the

maximum packing density, which may explain the disagreement in conclusions drawn by Nepf & Ghisalberti (2008) and Jackson (1981).

By considering the large scale turbulent kinetic energy budget, Nepf & Ghisalberti (2008) found that the penetration depth ranged from $0.17/(C_D \cdot \lambda) < \delta_e < 0.29/(C_D \cdot \lambda)$ where C_D is a canopy drag coefficient. Murphy et al. (2007) used the penetration depth to divide the flow within the vegetation into two separate zones: a wake zone ($0 < z < h - \delta_e$) and an exchange zone ($h - \delta_e < z < h$). In the exchange zone, mixing is dominated by the Kelvin-Helmholtz vortices (Murphy et al., 2007) and momentum absorption is constant (Nepf & Ghisalberti, 2008), whereas in the wake zone, mixing is dominated by the stem-wake turbulence which is characterized by much shorter length and velocity scales (Murphy et al., 2007). As a result, the penetration depth is identifiable by analyzing the turbulence patterns when estimation of a drag coefficient is complicated by the need to account for factors like rigidity and orientation.

Smart (1999) took detailed velocity measurements from five gravel bed rivers in New Zealand under both static and mobile bed conditions. Log profiles were fit to the data in the form of Equation 6

$$u_i/u_\tau = 1/\kappa \cdot \ln((z + d_h)/z_0) \quad (6)$$

where u_i is the instantaneous streamwise velocity, z is the elevation above the top of the roughness elements, d_h is the origin offset and z_0 is another measure of boundary roughness height ($z_0 = 0.033 \cdot k_s$ if $\Gamma = 8.5$ in Equation 1). He assumes there is little skewness in the distribution of u_i such that the instantaneous value is likely to be equal to the average value ($<u>$). Shear velocity, u_τ, and roughness height, z_0, were used as regression parameters and only the portion of the data that appeared as a straight line on a semi-log plot of u_i vs. z was considered in the profile fitting. The origin displacement, d_h, was then calculated by varying its value until a maximum correlation coefficient was obtained for the regression. Smart (1999) found that there was no correlation between d_h and the size of the bed material for the mobile bed conditions; however, a relationship between d_h and z_0 was evident, $d_h/z_0 = 1.1$. It should be noted that the bed type was not made clear, although most data was collected under flood conditions. Since grain roughness appears to be irrelevant and considering the flood conditions, it is safe to assume that the flow encompassed the upper flow regime and that some form of bedform was

present, most likely antidunes, making up the majority of the bed's roughness. This seems to indicate that the zero-plane displacement is not proportional to bed material size for mobile beds, but could instead be proportional to the bedform height. This conclusion is reasonable given that the total roughness height, bedform height plus sediment height, is almost always dominated by the larger height of the bedforms.

Raupach et al. (1991) performed a comprehensive review of the subject and suggested that for static, regular roughness elements, $0 < d_h < h$ since the zero velocity plane represents the location where the mean surface shear acts and the shear must act on some portion of the roughness elements of height h. For atmospheric experiments over different types of canopies, values of zero-plane displacement and z_0 were given and reproduced in Table 1; data shown was presented originally in Jarvis et al (1976), Raupach (1988), and Raupach et al. (1986). The equivalent sand grain roughness k_s was not included and was calculated assuming the flow was fully rough (Γ = 8.5). The values of d_h/k_s for the data given ranged from 0.16 to 1.00 with an average value of 0.51, similar to other values reported in the literature (Table 2) and slightly higher than values found here (Table 3). Note that the d_h/k_s values for the Jarvis et al. (1976) data are slightly higher (average of 0.62) than the values for the Raupach (1988) and Raupach et al. (1986) data (average of 0.23). This could be attributed to the much larger z_0 values found in the Jarvis et al. (1986) data encompassing data taken from natural forests.

Table 1: Contains values of d_h/k_s found in Raupach (1991) for atmospheric modeling, both natural and in wind tunnels.

Original Author (year)	Roughness Type	λ	z_0 (m)	k_s (m)[a]	d_h (m)	d_h/k_s
Jarvis et al (1976)	Forest	2.8[b]	0.5	15.0	7.6	0.51
Jarvis et al (1976)	Forest	3.1[b]	0.66	19.8	19.8	1.00
Jarvis et al (1976)	Forest	4.3[b]	0.93	27.9	11.8	0.42
Jarvis et al (1976)	Forest	0.8[b]	0.45	13.5	3	0.22
Jarvis et al (1976)	Forest	1.7[b]	1.15	34.5	19.1	0.55
Jarvis et al (1976)	Forest	9.6[b]	0.35	10.5	9.7	0.92
Raupach (1988)	Wheat	0.47	0.004	0.12	0.035	0.29
Raupach et al (1986)	Aluminum Strips[c]	0.23	0.0087	0.26	0.043	0.16
					Average	0.51

[a] k_s not reported and was calculated using $k_s = z_0 \cdot e^{-3.4}$ which assumes $\Gamma = 8.5$

[b] λ calculated using LAI/2 where LAI is the "Leaf Area Index"

[c] 10 mm x 1 mm vertical aluminum strips 60 mm tall

Other methods have been proposed for determining the location of the theoretical origin, such as by Kanellopoulos (1998) where detailed, two-dimensional velocity measurements were collected in a flume using a 2-D laser Doppler velocimeter. Bed shear was calculated using $\tau_0 = -\rho \cdot \langle u'w' \rangle$ where u' and w' are the instantaneous fluctuations of streamwise and vertical velocity components, respectively, about the mean, and brackets < > denote a time average. Knowing the bed shear allowed the shear velocity, u_τ, to be calculated. Therefore, κ and Γ in Equation 1 were left unknown and were used as regression parameters. The location of the profile origin was varied until the expected value of $\kappa = 0.4$ was reached; the value of Γ was not constrained. Measurements from the study will be utilized in the analyses presented and elaborated on in subsequent chapters.

More recently, Afzalimehr & Rennie (2009) used an equation in the form of

$$u/u_\tau = 1/\kappa \cdot \ln((z + p \cdot k_s)/k_s) + \Gamma \qquad (7)$$

where p is a proportionality constant between the zero-plane displacement and a representative roughness height, or $p = d_h/k_s$. They considered an origin offset equal to $d_h/k_s = 0.25$ by maximizing the coefficient of determination between u and $\ln[(z + p \cdot k_s)/k_s]$ for data collected in

four different gravel bed rivers in Iran and Canada under non-uniform flow conditions. Because of the greater influence on roughness by the larger grains, they took a roughness coefficient of $k_s = d_{84}$. They also reported a 20% difference in bed shear estimates from the log law when considering d_h/k_s ranging from 0.1 to 0.25. Furthermore, Afzalimehr & Rennie (2009) found that the log law was valid for their data from as low as $0 < z < 0.22 \cdot H$, where H is the flow depth, to as high as $0 < z < 0.68 \cdot H$.

Table 2: Summary of previous research into determining the location of the velocity profile origin. Note that for all experiments, beds were static and there was no sediment motion (except for Smart, 1999).

Author (year)	Roughness Type	Roughness Size	k_s	λ	d_h/k_s	Notes
Einstein & El-Samni (1949)	Plastic spheres & natural gravel	d = 69 mm, d_{50} = 69 mm	d	Not reported[a]	0.2	Considered velocities over entire flow depth
Perry & Joubert (1963)	Horizontal square bars	h = 3.2 mm	d	0.25	0.8	Velocity-determined inner region; wind data
Jackson (1981)	n/a	n/a	z_0[b]	0 to 0.33	0.7	Theoretical study
Raupach et al. (1991)	n/a	n/a	z_0[b]	n/a	0.51	Theoretical study; atmospheric flows
Kironoto & Graf (1995)	Crushed grains & natural gravel	d_m[c] = 2.8 mm, d_{50} = 23 mm	d_m, d_{50}	Not reported[d]	0.2	Considered velocities within bottom 20% of depth
Kanellopoulos (1998)	Lead spheres	d = 8 mm	d_{50}	0.7	0.5	Used iterative technique; κ = 0.4 as objective
Smart (1999)	Natural gravel	23 mm < d_{50} < 85 mm	z_0[e]	Mobile Gravel Bed Rivers	0.04	Velocity-determined inner region; found that d_h/z_0 = 1.1
Afzalimehr & Rennie (2009)	Natural gravel	14 mm < d_{50} < 23 mm	d_{84}	Gravel Bed Rivers	0.25	Used objective of maximum R^2; assumed Γ = 4.4; non-uniform flow

[a] Little was included about the experimental setup, only that uniform spheres were used in one experiment and natural gravel in the other; no description of the particle arrangement was given

[b] z_0 (Equation 6) was considered instead of k_s (Equation 1), common practice in atmospheric fluid mechanics

[c] d_m = mean grain diameter

[d] No information regarding the roughness particles' arrangements was included

[e] Smart (1999) considered $z_0 = 0.033 \cdot k_s$ and z_0 was a regression parameter in the analysis

Chapter 3: Summary of Experiments

Velocity measurements from five different experiments were analyzed to study the effects of three different roughness scales on the flow field within the inner flow region as well as the effects of packing density on the zero-plane displacement. Packing density, λ, is defined here as the ratio of the roughness element area projected onto a plane perpendicular to the flow direction to the unit ground area surrounding the roughness element (frontal area per unit ground area). The three roughness scales analyzed were representative of river sediments, submerged woody vegetation, and natural bedforms. Three of the five experimental setups were performed by previous researchers and their descriptions can be found in detail in Kanellopoulos (1998), Liu et al. (2008), and Balakrishnan (1997). The two bedform-scale experiments were conducted by the authors and have not yet been reported in the literature; therefore they will be explained in greater detail.

The sediment-scale experiment consisted of 8 mm diameter spheres arranged at a maximum packing density and is described in detail in Kanellopoulos (1998). Experiments were conducted in a rectangular, tilting-bed flume that is 0.6 m wide and 0.3 m deep. The flume boundary was comprised of immobile lead spheres 8 mm in diameter. Detailed, streamwise velocity measurements were taken in vertical profiles using a two-dimensional Laser Doppler Velocimeter (LDV) system with a high measurement density near the bed and decreasing density as distance from the bed increased. Streamwise and vertical velocity components were measured simultaneously in the experimental section of the flume with fully-developed flow. This data set was used as a control since the method for locating the zero-velocity plane had already been shown in the literature to be valid for static, rough beds with uniform roughness elements such as this one. Note that Kanellopoulos (1998) employed a slightly different method for determining d_h than the method used here and discussed earlier in this document. His results indicate a ratio of zero-plane displacement to roughness height of 0.5.

The roughness representative of submerged rigid vegetation was replicated using rigid, acrylic dowels 6.35 mm in diameter, d, and 7.62 cm in height, h, attached to a plexiglass bed in a staggered arrangement (Figure 2). The roughness packing density λ was approximately 0.12. In addition to the smooth dowels and channel bed, different surface roughnesses were applied to both the dowels and the bed using water-resistant fine and coarse sandpaper, placed around each

dowel like a sleeve and covering the bed. The median grain size diameters for the fine and coarse sandpapers were 0.2 mm and 0.45 mm, respectively. However, Liu et al. (2008) determined that the additional roughness had little influence on the flow's behavior, probably because the total roughness is dominated by the height of dowels making the additional sandpaper roughness inconsequential. More simply put, the height of the sandpaper grains is negligible when compared to the height of the dowels. The flume was 0.3 m wide with a slope of 0.3% and a flow rate of 0.0114 m^3/s with flow depths ranging from 11 cm to 12 cm. Detailed streamwise velocity measurements were taken with a one-dimensional LDV system. Measurements were taken for 20 seconds at a rate of 75 Hz at points both within and above the dowel array. For more information regarding the experimental setup see Liu et al. (2008).

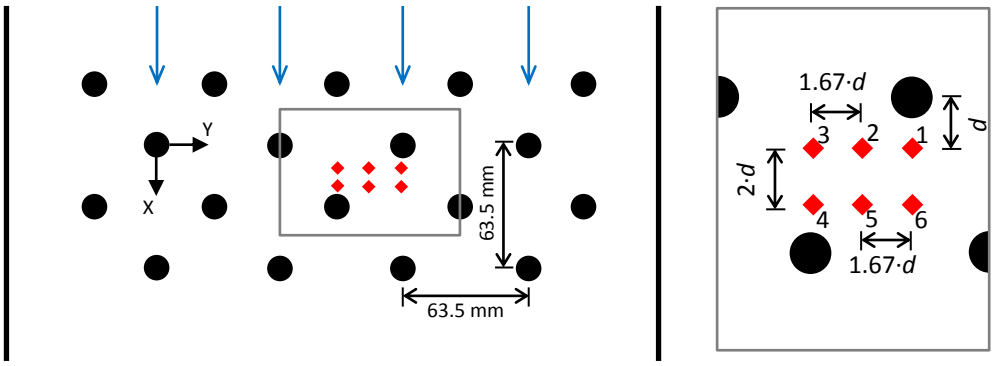

Figure 2: Top view of dowel arrangement for vegetation-scale experiment found in Liu et al. (2008). Not to scale. Circles represent dowels. Diamonds represent locations of velocity profile measurements.

Bedform-scale roughness was studied using two separate data sets: one in a tilting bed flume with crushed gravel where a single, scour-induced bedform migrated downstream and the other data set in a meandering, sandy-bed channel (Figure 3) at bankfull flow where bedforms developed naturally. These experiments have not been reported in the literature before and will therefore be explained in detail here.

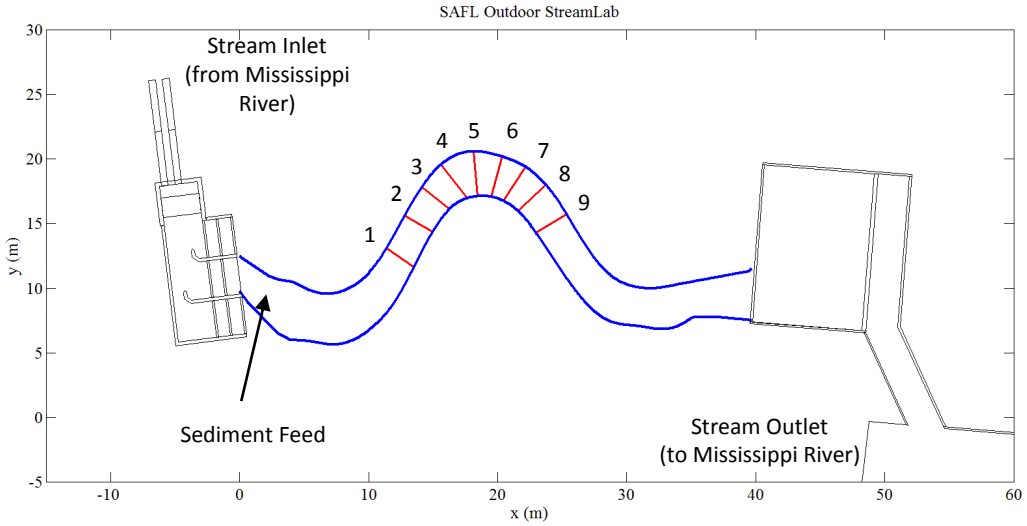

Figure 3: Top view of the meandering channel and location of nine permanent cross sections (numbered and shown in red). Flow in the channel is from left to right.

For the first bedform-scale roughness experiment, data was collected in a 15 m long, 0.9 m wide and 0.6 m deep tilting bed flume at the University of Minnesota's St. Anthony Falls Laboratory in Minneapolis, Minnesota. The flume slope and the flow depth at the time of the experiment were not recorded and are therefore unknown. Water was routed into the flume and through a series of flow straighteners at the flume entrance. Flume sediment consisted of crushed gravel with a d_{50} of approximately 1.8 mm and a d_{90} of 2.4 mm. During the 120 minute recording period, the bed elevation changed by approximately 2.3 cm due to the migration of a bedform through the flume. The 400 second segment encompassing the large change in bed elevation due to the bedform migration is shown in Figure 4, beginning at t = 4400 seconds and ending at t = 4800 seconds. The single bedform was caused by the scouring of material around a rock structure installed upstream of the measurement location. Three-dimensional velocity data was collected continuously at one location, for 120 minutes using a Nortek Vectrino II profiling ADV at a rate of 100 Hz. The instrument takes 30 instantaneous measurements, vertically spaced at 1 mm, giving it the ability to measure an instantaneous, 3 cm velocity profile. Of the 30 measurements, only the ten top-most measurements exhibited no interference from the rising bed; therefore, the bottom-most 20 measurements were neglected. The instrument also records simultaneous bed elevation at a rate of 1 Hz.

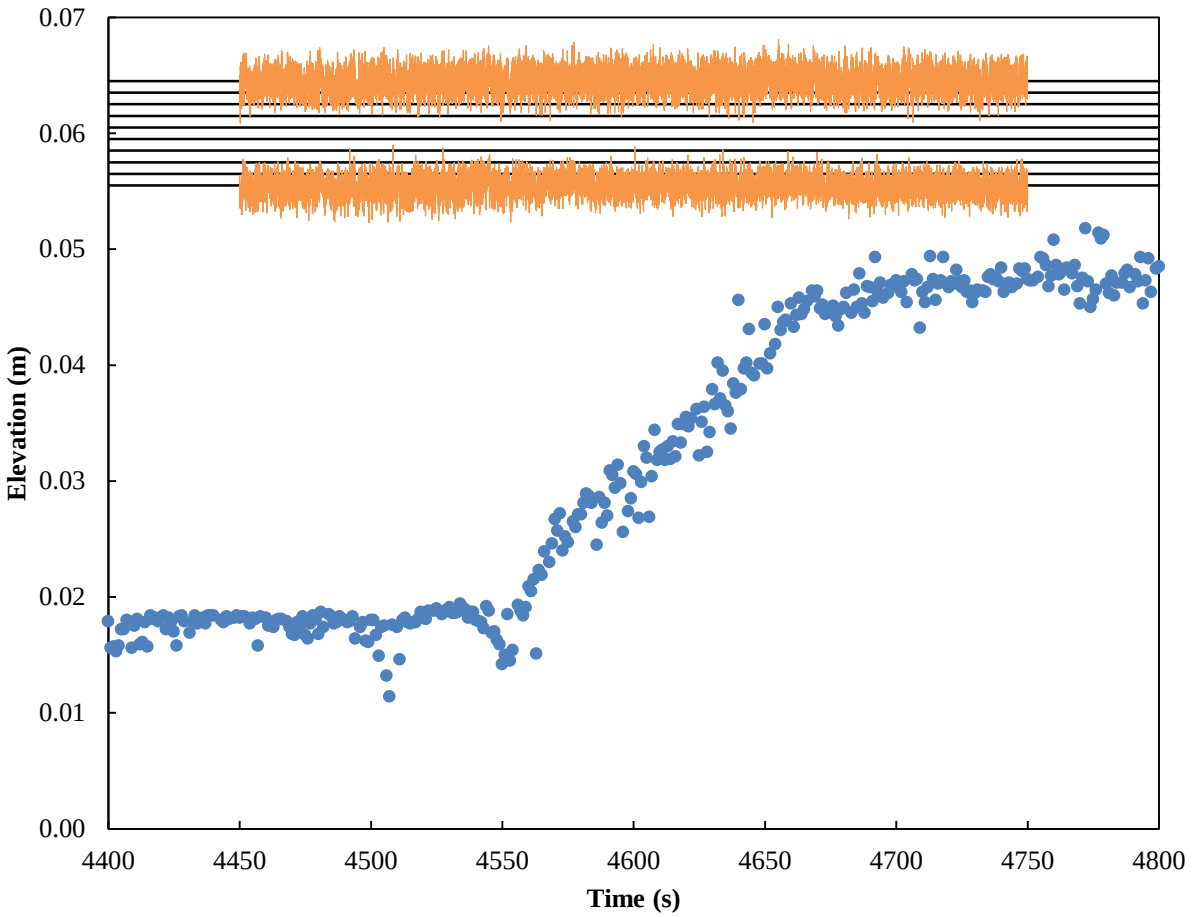

Figure 4: Location of ten velocity records relative to the changing bed elevation (top-most and bottom-most of the ten velocity records are shown). Black horizontal lines represent the elevation of the ten records. ● – Average bed elevation measurements; ▬ – velocity record samples for the lowest and highest of the ten velocity records considered.

The second bedform-scale roughness experiment was conducted in the Outdoor StreamLab (OSL) also at the University of Minnesota's St. Anthony Falls Laboratory. The meandering channel with sinuosity of 1.3, was run at bankfull conditions with an average depth of 21 cm, an average width of 230 cm and a slope of approximately 0.7%. Flow was diverted from the Mississippi River into the channel via an abandoned spillway, and was maintained at a relatively constant 280 L/s using a manual gate valve, then released back into the river at the tail of the stream (Figure 3). The channel sediment (d_{50} = 0.7 mm and d_{90} = 2.0 mm) collected in a tailbox at the end of the stream was recirculated to a storage tank and fed back into the head of the stream at a constant rate using an electronically controlled auger. The sediment feed rate

regulates the amount of bedload transport within the flume and therefore the equilibrium conditions. Velocity measurements were taken at nine permanent cross sections spaced at approximately 2 m (Figure 3) for two separate, but virtually identical, channel and bed configurations as well as flow conditions, termed Baseline1 and Baseline2. The actual velocity measurements for the two scenarios can be found in Appendix B. The point bar experienced significant changes between experiments; however, the stream was allowed to run sufficiently long to reach the same equilibrium state before any measurements were taken during the second experiment. The presence of equilibrium conditions was subjective and considered established when there were no longer observable changes to the size of the point bar. On the order of 35 velocity measurements were taken per cross section, with each cross section made up of four to eight vertical profiles spaced at 16 to 52 cm depending on the width of the stream. Within each profile, measurement points were spaced vertically from 3 to 5 cm. Velocity measurements were taken with a Nortek Vectrino 200 Hz acoustic Doppler velocimeter (ADV). Velocity samples were taken for 4 minutes, which encompasses over 700 integral time scales for the given flow conditions. According to Buffin-Belanger & Roy (2005), the maximum length of record necessary for describing most turbulence statistics is 1.5 minutes; therefore, the 4 minute period of record chosen is a rather conservative selection. Considering each measured vertical profile contained up to ten, 4 minute velocity measurements and that the rate of bedform migration through the meander was as frequent as two per minute, the bed elevation varied considerably and constantly during the period required to record a vertical profile, causing the velocities measured to actually be spatially averaged quantities. The bedforms were approximately 1 m in length and up to 0.5 m in height (Figure 5). The depth averaged velocity, approximately 0.7 m/s, is almost two orders of magnitude higher than the bedform celerity, estimated at 0.08 m/s by assuming a bedform migration rate of two per minute (estimated by simply observing bedforms) and a wave length of 1 m (Figure 5). Since the flow velocity is much larger than the bedform velocity, it is safe to consider the local, point velocity measurements as equivalent to the spatially averaged velocity at that elevation and location across the stream. The fact that many bedforms passed underneath the vertical location while data were being collected also allows for the data to be considered spatially averaged. Another way to consider the situation is to imagine velocity measurements obtained over a static, wavy bed by averaging a number of measurements along the same line, at the same elevation, in the stream-wise direction.

Figure 5: Bedforms in the Outdoor StreamLab under low flow conditions.

Detailed bathymetry was collected using a high-resolution data acquisition carriage (DAQ) equipped with an ultrasonic transducer capable of measuring underwater channel bathymetry at 1 cm horizontal and 1 mm vertical resolutions. The DAQ is equipped with a Keyence LKG laser that is capable of mapping bank topography above the water margin at 1 mm horizontal and sub-millimeter vertical resolutions. Up to eight consecutive, five minute bathymetry scans were repeated at each location in the stream, allowing for the measurement of the temporal evolution of the bed. Average bed elevations from the repeat scans were meshed together to produce a digital elevation map of the entire meander bend for each experiment conducted, allowing for locations of scour and deposition within the channel to be determined. The repeat scans also allowed for the extraction of the maximum bed elevation at the location of each vertical velocity profile.

Both velocity data sets were filtered using a modified phase-space threshold (PST) technique. The original PST technique was developed by Goring & Nikora (2002) and involved plotting the velocity signal against its first and second derivatives in a three-dimensional phase-space plot. From the plot, an ellipsoid cloud, defined by the Universal threshold (i.e. the expected absolute maximum), is created that surrounds the majority of the data. Any points lying outside the ellipsoid cloud are deemed spikes and are removed. Once spikes are removed, they can be replaced by a number of different methods; however, Goring & Nikora (2002) recommend interpolating along a polynomial fit to data on either side of the spike. The method of eliminating and replacing spikes is then repeated until no more spikes are detected. Parsheh et al. (2010) noticed that using the PST technique eliminated some valid data points in the vicinity of spikes. They proposed a modification to the PST technique to insure that points near the probability density function (PDF) peak, but far from the PDF tail, are not erroneously flagged and remain unchanged. They define a range proportional to the median absolute deviation of the streamwise velocity, θ_u, within which instantaneous velocity fluctuations, u', are considered safe and not allowed to be removed by the filter. A second step is used to locate obvious spikes with magnitudes much larger than the rest of the time series before using the phase-space ellipsoid suggested by Goring & Nikora (2002) to remove the remaining spikes. The modified PST technique found in Parsheh et al. (2010) was used in this paper to filter the velocity signals in both bedform-scale roughness data sets.

In an attempt to better understand the relationship between packing density and zero-plane displacement, data from a fifth source, Balakrishnan (1997), were obtained. One of his objectives was to analyze the nature of the fluid-solid interface under different packing densities by measuring turbulence parameters upstream, directly above, and downstream of a selected roughness element (Figure 6). The experiments were conducted in a 0.6 m wide by 0.3 m deep tilting bed flume located at the Baker Environmental Hydraulics Laboratory at Virginia Tech. The flume slope ranged from 0.2% to 1% with discharges ranging from 0.012 m^3/s to 0.026 m^3/s resulting in flow depths from 5.0 cm to 6.8 cm. Three dimensional velocity measurements were obtained using a non-intrusive LDV. The bed was made of four layers of static, glass spheres, 8 mm in diameter with a fifth layer made of lead spheres of the same diameter at varying packing densities. Lead was used to ensure that the spheres were immobile under loosely packed, and therefore more exposed, flow conditions. Four separate packing densities were tested: 2%, 20%,

35%, and 50%. The 2% packing density case was chosen to replicate isolated roughness elements where each roughness element acts independently of the others (wake reattaches to the bed before reaching the next particle downstream), the 20% and 35% cases are representative of the wake interference regime, and the 50% case is representative of the skimming flow regime. The wake interference regime exists when particles are close enough that the wakes from the individual particles interact. The skimming flow regime occurs when particles are close enough that the flow "skims" over the top of the roughness elements. More complete definitions of the three flow regimes can be found in Lee and Soliman (1977). Velocity measurements were obtained at the three verticals shown in Figure 6. More information regarding the setup and results of the experiment can be found in Balakrishnan (1997).

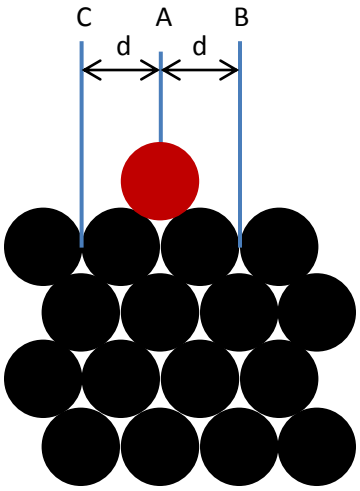

Figure 6: Side view of velocity profiles measured (A, B, and C) for experiments found in Balakrishnan (1997). Black balls indicate static, glass bed material. Red ball indicates a lead test sphere around which velocity measurements were taken.

Chapter 4: Results

It is hypothesized here that in flows containing large scale variations in bed elevation, such as those due to bedform migration, the same zero-plane displacement concept originally proposed by Einstein & El-Samni (1949) for static, rough beds could be employed and that the difference between the measured bed elevation and the location of the zero-plane would be strongly related to the bedform, or roughness, height. In other words, the method is applicable as long as a relevant value of roughness height, k_s, is chosen to represent the total roughness, or dominant height. It will be shown that that $k_s = h$ may be an appropriate relationship, where h is the roughness element height whether it be grain diameter, vegetation height, or bedform height. For bedform roughness, it has been acknowledged before that the roughness is related to the bedform height and wavelength (Smith and McLean, 1977); however, here it is assumed to be solely dependent on bedform height, more specifically the average bedform height estimated using bathymetry data. It is understood that this relationship may not be the most accurate as it does not account for the effects of roughness element orientation, spacing, or shape. The simple relation was chosen for consistency and because the actual, supposed non-linear relationship between k_s, h, and λ is complicated and not well understood. It is much easier to consider one of the parameters affecting the roughness coefficient (roughness height), accounting for all of the variability associated with the other, more subjective parameters, in the value for zero-plane displacement. Note that the ratio of $k_s/h = 1$ is also within the range of values found in Schlichting (2000) for spherical, hemispherical, and conical roughness elements. For measurements in which velocity profiles were taken in close proximity to one another over static beds, measurements were averaged in the streamwise and spanwise directions at each elevation to create a spatially averaged quantity at each elevation. This was done for consistency as the measurements obtained from the two bedform-scale experiments were spatially averaged in nature and the measurements in all other experiments were simply point measurements over static beds. Combining the velocity measurements also allows for the characterization of the entire channel roughness into one parameter, which is useful for determining gross flow characteristics such as discharge and bed shear. Spatial averaging may have ultimately been unnecessary, although, as is discussed in the chapter *Differences Between Profiles of Spatial Averages and Point Measurements*.

4.1 Sediment-scale Experiment (Static Bed)

The location of a theoretical profile origin below the top of the roughness elements in a static, rough bed proposed by Einstein & El-Samni (1949) has been supported numerous times by experiments found in the literature and will be verified here as well. The high quality velocity profiles obtained by Kanellopoulos (1998) above a bed made of uniform, 8 mm diameter spheres and a bed slope of 0.075% was used as an experimental control. The data set will also be used to outline the method employed for determining the zero-plane displacement.

Each data point contains the elevation above an arbitrary datum, generally chosen as the top of the roughness elements, and a matching streamwise velocity measurement. Only data within the bottom 20% of the flow depth was considered to be within the logarithmic inner region in this analysis (Kironoto and Graf, 1995; Detert et al., 2010; Dancey and Diplas, 2008). A linear regression was fit to the data (following Equation 1) with the natural logarithm of the elevations as the abscissa and the original velocity measurements as the ordinate with no zero-plane displacement considered ($d_h = 0$). The regression slope, m_r, and regression intercept, b_r, are representations of shear velocity and Γ, respectively, as shown in Equations 8 and 9 where the variables κ (equal to 0.4) and k_s (equal to particle diameter) are both constants.

$$u_\tau = \kappa / m_r \tag{8}$$

$$\Gamma = -1/\kappa \cdot [b_r - \ln(k_s)] \tag{9}$$

Next, each data point's elevation was iteratively increased by the same amount, which effectively changes the reference elevation, until the constant Γ takes on a value of 8.5 (Schlichting, 2000). The zero-plane displacement is the amount that each data point elevation was increased by, or the difference between the original datum located at the top of the particles and the final reference elevation. A sample spreadsheet showing the calculations used can be found in Appendix A.

After performing the analysis described above to the data from the sediment-scale experiment (Kanellopoulos, 1998), and assuming $k_s = d = 8$ mm and $\kappa = 0.4$, the resulting zero velocity plane is 0.16 cm below the top of the roughness elements ($d_h = 0.16$ cm) with $u_\tau = 2.6$ cm/s and $R^2 = 0.996$ (Figure 7). The resulting ratio of d_h/k_s for the control experiment is 0.20, virtually

identical to the results obtained by Einstein & El-Samni (1949). Recall that Einstein & El-Samni (1949) utilized data over the entire flow depth (ratio of particle size to flow depth of 0.4), whereas here data was only considered in the bottom 20% of the flow depth (ratio of particle size to flow depth of 0.08). Were Kanellopoulos (1998) data considered over the entire flow depth, the results would differ rather significantly (d_h/k_s = 0.07).

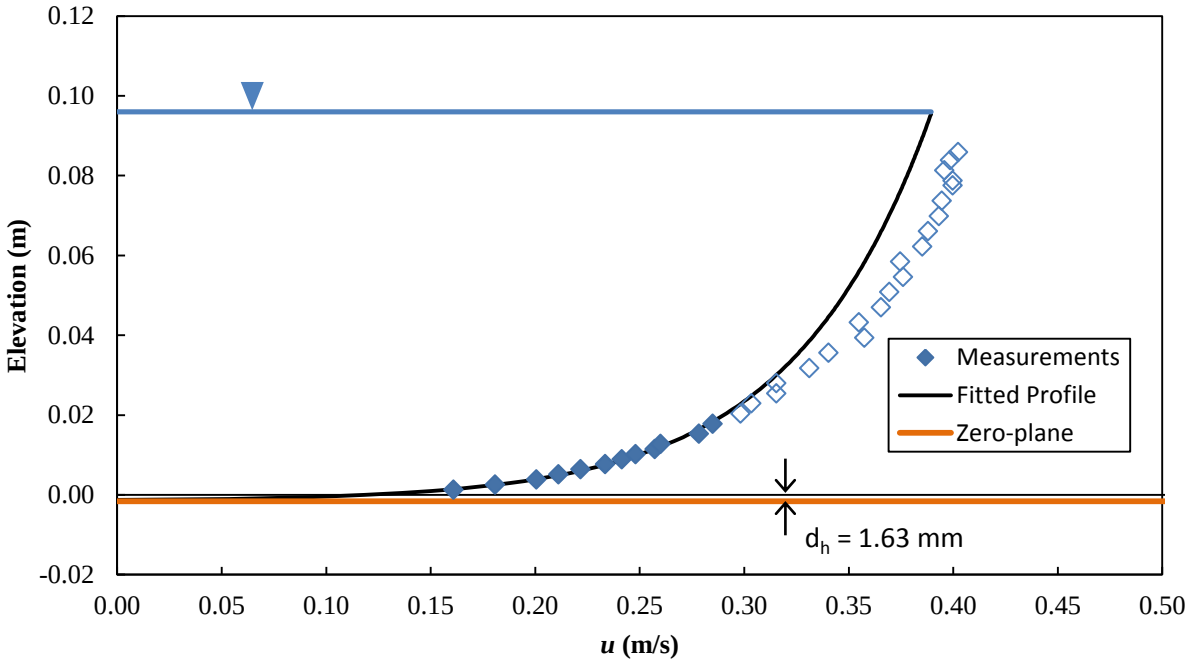

Figure 7: Measured velocity profile and fitted regression for control experiment performed by Kanellopoulos (1998). The datum (z = 0) is the top of the roughness elements. Solid symbols represent those considered within the logarithmic inner region; empty symbols those above, within the outer region.

4.2 Vegetation-scale Experiment (Static Bed)

A similar method of using a logarithmic regression and iterative technique was employed to locate the origin of four profiles of spatially averaged velocity in flow through an array of rigid, 7.62 cm tall acrylic dowels found in Liu et al. (2008). Below the top of the dowels, the velocity profile has been shown to be nearly uniform and non-logarithmic (Liu et al., 2008). Therefore, the only divergence from the method outlined previously is that the regression was fit to all data points above the dowel array (z > 7.62 cm). In other words, no inner layer was considered due to the relatively short distance from the top of the dowels to the water surface. For the four velocity

profiles fit to the data (L1, L2, L3, and L4 in Figure 8), the dowel density was the same (λ = 0.12), the only differences being the roughness added to the dowels and the bed. Profile L1 contained no skin roughnesses, L2 contained skin roughness on the bed and fine skin roughness on the dowels, L3 contained skin roughness on the bed and coarse skin roughness on the dowels, L4 contained skin roughness on the bed and no skin roughness on the dowels. The experiments L1, L2, L3, and L4 correspond to experiments 3.1, 3.2, 3.3, and 3.4, respectively, in Liu et al. (2008). Since it was determined by Liu et al. (2008) that the added skin roughness had little effect on the flow, the experimental conditions for all four profiles are assumed identical. The roughness coefficient, k_s, was assumed to be equal to the dowel height ($k_s = h$ = 7.62 cm). The average value of d_h/k_s for the four profiles was 0.26, similar to the results from the control experiment and values reported in the literature (Table 2). The d_h/k_s ratios were 0.26, 0.25, 0.24, and 0.30 for experiments L1, L2, L3, and L4, respectively. The average R^2 for the four profiles (Figure 8) was 0.994 with a minimum of 0.988.

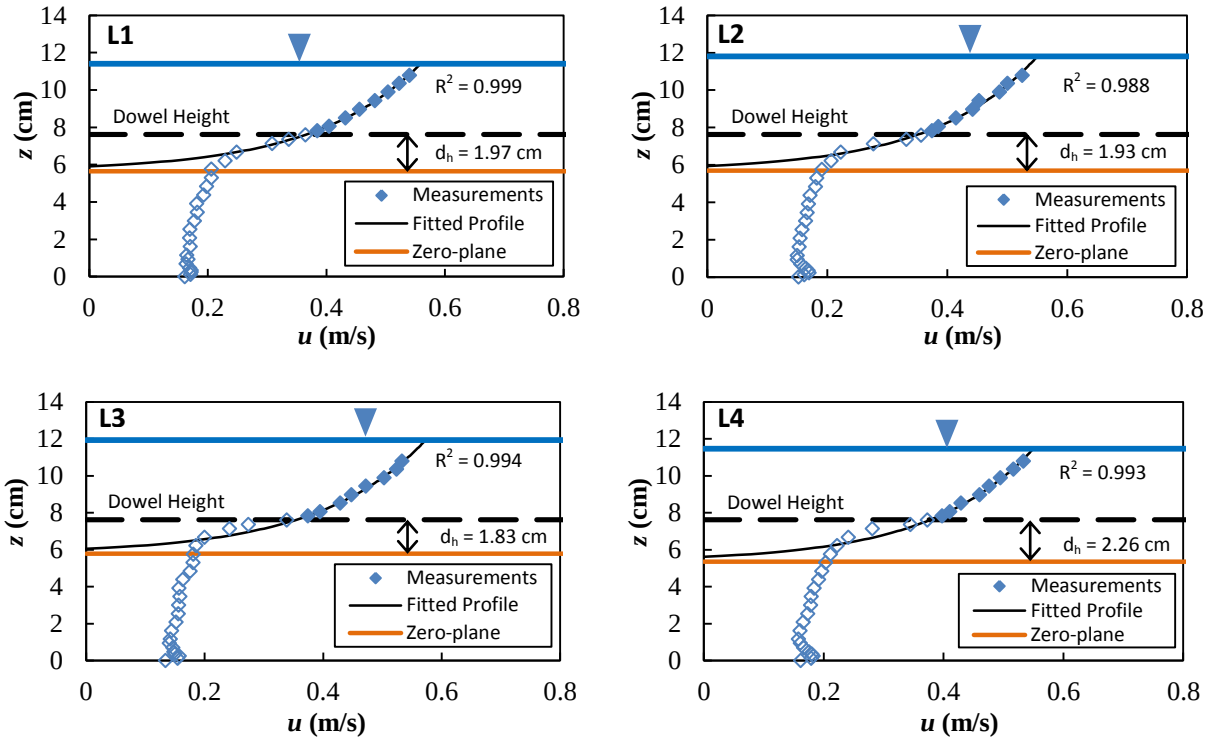

Figure 8: Regressions used to determine d_h for four vegetation experiments found in Liu et al. (2008). Solid symbols represent those considered within the log region; empty symbols those below, within the suspected roughness sublayer. Note that here, z = 0 cm is taken as the flume bed and not the top of the roughness elements as is the case in other velocity profile figures, although d_h *is* measured with respect to the top of the roughness elements.

In an attempt to examine the relationship between zero-plane displacement and penetration depth, penetration depth was calculated using the expression $\delta_e = 0.23/(C_D \cdot \lambda)$ proposed by Nepf & Ghisalberti (2008). The drag coefficient was calculated using $C_D = 2 \cdot u_\tau^2/(\lambda \cdot u_h^2)$ where u_h is the measured streamwise velocity at $z = h$. The resulting zero-plane displacements were 1.50 cm, 1.48 cm, 1.40 cm, and 1.72 cm for experiments L1, L2, L3, and L4, respectively, assuming that $d_h = \delta_e/2$ (Nepf & Ghisalberti, 2008). These d_h values are only slightly lower than those obtained using the iterative technique, which could be adjusted by using the upper bound for δ_e found in Nepf & Ghisalberti (2008). The corresponding ratios of d_h/k_s are 0.20, 0.19, 0.18, and 0.23 with an average value of 0.20. Again, the resulting ratios of d_h/k_s are on the order of 0.2 as was the case for the control profile discussed earlier.

4.3 Bedform-scale Flume Experiment (Mobile Bed)

It has been shown, both in the literature (Table 2) and experiments described above for static roughness elements, that the location of the velocity profile origin is on the order of $0.2 \cdot k_s$ below the top of the roughness elements. During moderate to severe floods, however, sediment is entrained by the flow resulting in a moving boundary, such as in the case of downstream migrating bedforms. It is therefore important to test the validity of the method described for locating the velocity profile origin for static beds under mobile bed conditions and determine the corresponding d_h/k_s ratios to conclude whether or not the method is applicable under such flow conditions. In the presence of bedforms, the dominant bed roughness length scale is the bedform height, k_s, instead of sediment size which contributes a far lesser degree to the overall roughness characteristics of the flow boundary. It is often thought necessary to consider spatially averaged quantities when comparing results from static beds and mobile beds. Velocity is often measured in a single location over mobile beds, which is the equivalent of taking multiple measurements over static beds with comparable static planform geometry. Consider the static bed to be on a running conveyor belt and the velocity probe in a fixed position above the belt. Equivalent conditions are obtained by stopping the conveyor belt and moving the velocity probe over the static bed. The comparison is valid if the mobile bedforms move at a rate much lower than the flow velocity.

If the proposed hypothesis is correct and the method is as applicable to mobile beds as it is to static ones, the zero-plane displacement is expected to be equal to around 20% of the roughness height, or bedform height. For the analysis of velocity records in a flume over a single bedform, only velocity records that exhibited no influence from the rising boundary during the entire 400 second period were analyzed (Figure 4). The twenty lower bins that were at or below the height of the bedform, causing them to be influenced by the approaching bed and exhibiting unreasonable values, were excluded. Since they were not considered in the analysis, they are not shown in Figure 4 or Figure 9. Using the same method described previously for locating the zero velocity plane for static beds and choosing a k_s representative of the bedform height (k_s = 2.34 cm), the resulting profile origin was 0.80 cm below the maximum bed elevation, or the bedform crest (d_h = 0.80 cm) and is shown in Figure 9 along with the time-averaged velocity values for the ten records considered. Taking the maximum bed elevation as the original datum, consistent

with taking the datum at the top of the roughness elements for the static bed experiments, the ratio d_h/k_s is 0.34, only slightly higher than the values of 0.20 and 0.26 found for the two static bed experiments described previously and within the range of values reported in the literature (Table 2).

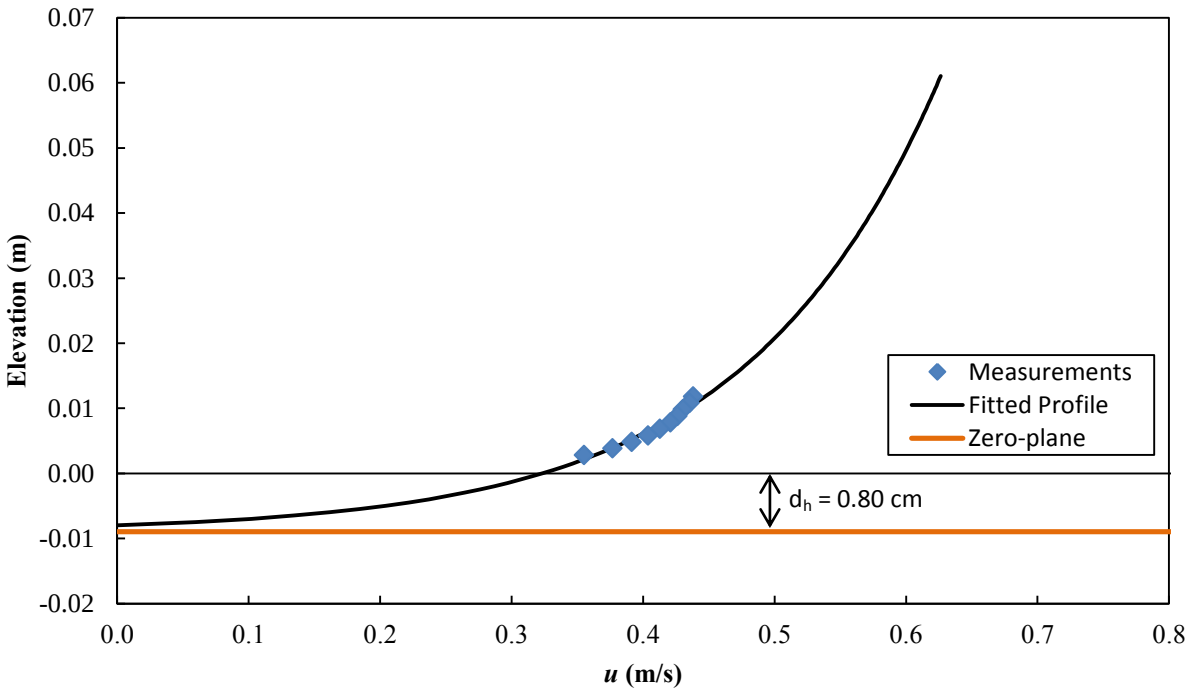

Figure 9: Velocity measurements along with the regression used to determined d_h for indoor, mobile bed experiment. The datum ($z = 0$) is taken as the maximum bed elevation, or bedform crest. Note that the water surface elevation is unknown.

Recall that Perry & Joubert (1963) performed experiments under similar conditions with square bars spanning the entire width of a wind tunnel with a height to spacing ratio of 4. Their results indicated a ratio of zero-plane displacement to roughness height of 0.8 for width-spanning roughness elements. The higher value reported by Perry & Joubert (1963) could be partially attributed to the fact that they considered data over the entire inner region whereas here the log-profile was fit to data within a relatively thin (around 1 cm) portion of the flow where the velocity measurements were taken. Differences could also be attributed to the fact that only a single roughness element was encountered here and Perry & Joubert (1963) had multiple bars, or an entire rough surface.

4.4 Bedform-scale Outdoor Experiment (Mobile Bed)

The need for considering a reference elevation based on the velocity profile asymptote will be presented by comparing results using the original datum (bedform crest, or considering $d_h = 0$) and the velocity profile asymptote as the reference. Figure 10 contains the spread of Γ values for two virtually identical experiments carried out in the meandering channel before iterating ($d_h = 0$). The expected value of 8.5 for fully rough boundaries (Schlichting, 2000) is noted with a bold, dashed line. It is clear that the Γ values vary considerably, with a mean of 6.69 and a standard deviation of 5.31. A similar spread in shear velocities is shown in Figure 11. Shear velocity distribution had a mean of 0.12 m/s and standard deviation of 0.080 m/s.

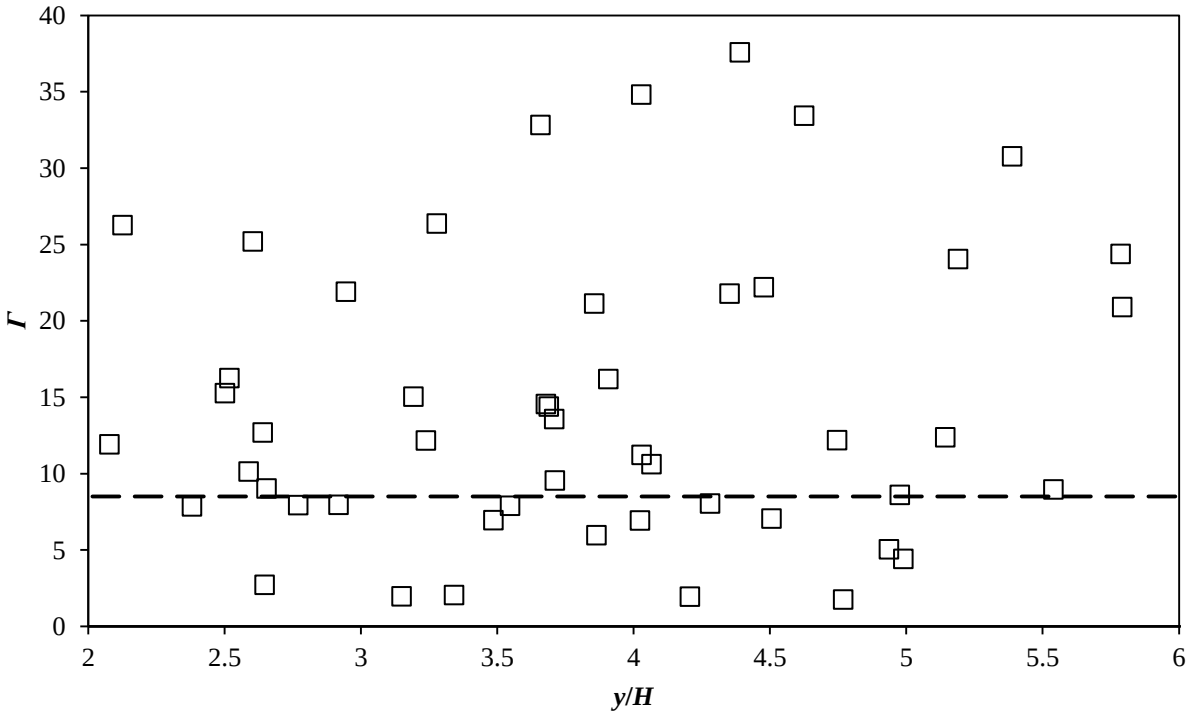

Figure 10: Values of Γ in Equation 1 for outdoor experiments using original boundary elevation ($d_h = 0$). The expected value for fully rough boundaries of $\Gamma = 8.5$ is denoted by a bold, dashed line. Note that y/H is the transverse (y-axis) distance from either bank that the vertical profile is located normalized by the stream depth. Profiles within 2 flow depths of either bank were not included to remove the boundary's influence on the profiles.

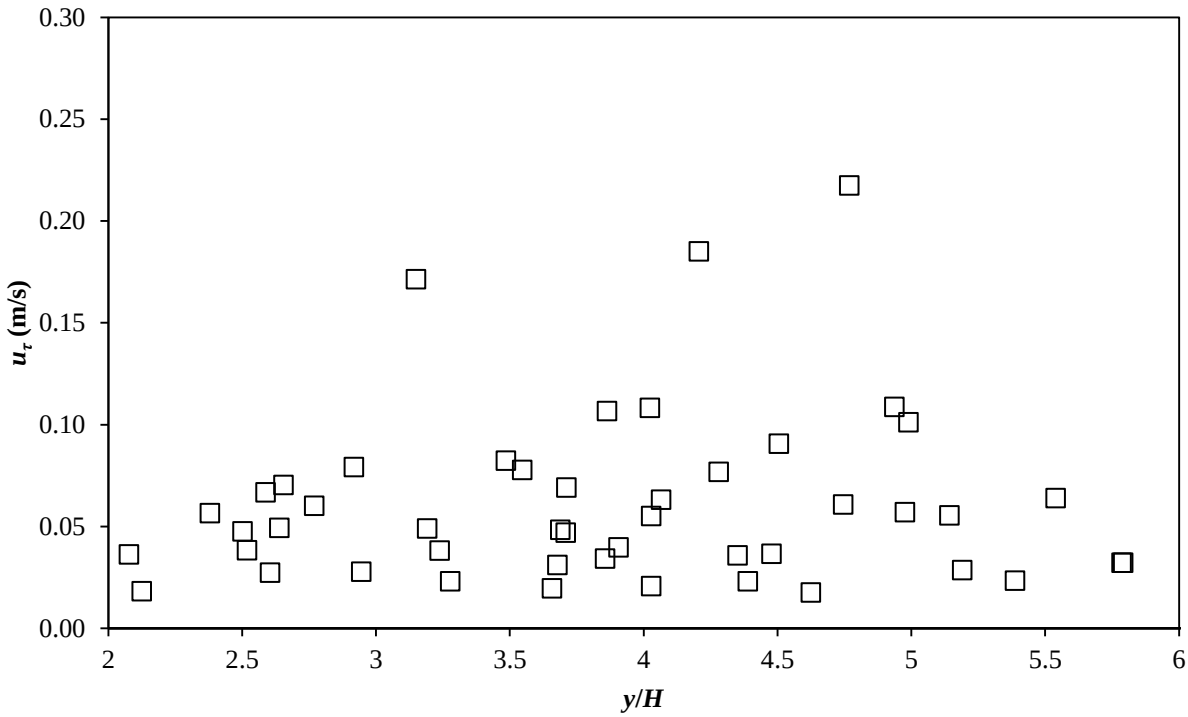

Figure 11: Values of u_τ in Equation 1 for outdoor experiments using original boundary elevation. Note that y/H is the transverse (y-axis) distance from either bank that the vertical profile is located normalized by the stream depth. Profiles within 2 flow depths of either bank were not included to remove the boundary's influence on the profiles.

From the variability in Γ and u_τ, it was apparent that the results assuming no zero-plane displacement did not produce adequate calculations of the turbulence parameters. Therefore, it was decided that iterations were necessary to change the reference elevation. After changing the reference datum to the velocity profile asymptote, by forcing $\Gamma = 8.5$, the resulting shear velocities appear to collapse to a much tighter distribution (Figure 12) compared to Figure 11, with a mean of 0.080 m/s and standard deviation of 0.024 m/s. The average shear velocity is only slightly less than the reach average value of 0.12 m/s calculated using $u_\tau = (g \cdot H \cdot S)^{0.5}$ where g is the gravitational constant and S is bed slope and H is the average flow depth (21 cm). The values match closely, giving further confidence in the method's applicability.

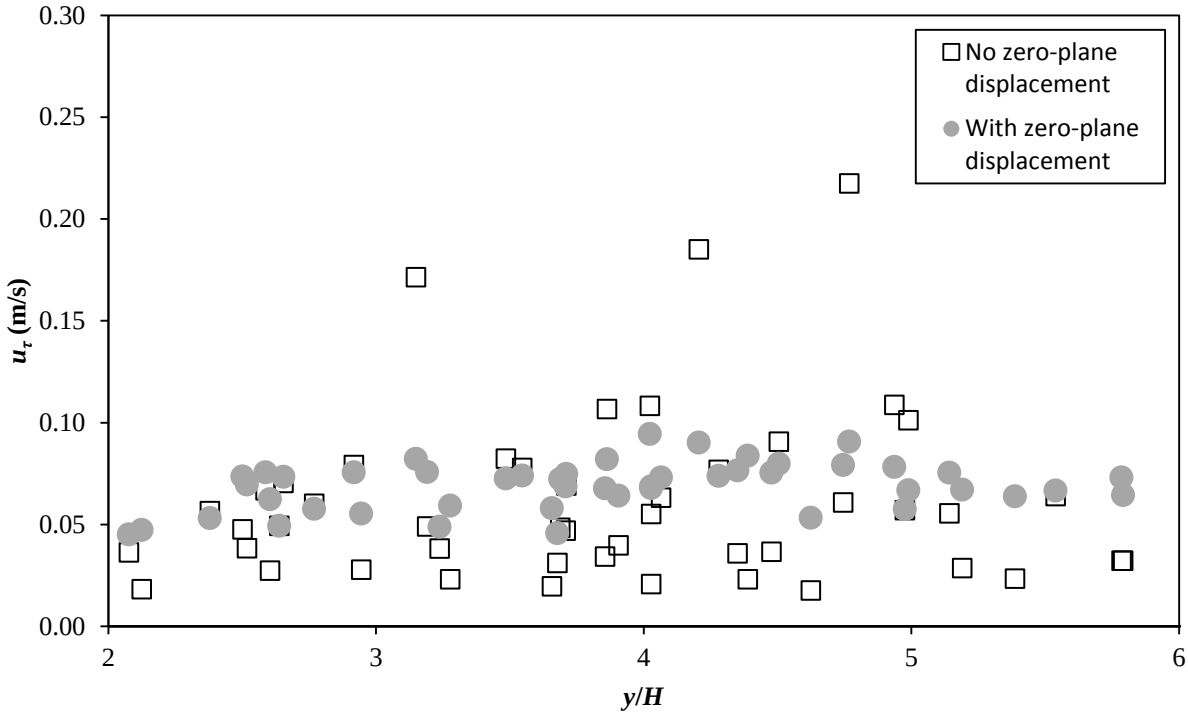

Figure 12: Values of u_τ in Equation 1 for outdoor experiments using zero-plane displacement elevation. Note that y/H is the transverse (y-axis) distance from either bank that the vertical profile is located normalized by the stream depth. Profiles within 2 flow depths of either bank were not included to remove the boundary's influence on the profiles.

For the 50 log-profiles fit to the data in the outdoor channel, the average zero-plane displacement was 1.51 cm below the maximum bed elevation, or bedform crest (shown in Figure 13 normalized by k_s). This corresponds to an average ratio of d_h/k_s of around 0.41 (Figure 13), using k_s = 5 cm which is representative of the spatially averaged bedform height. It is understood that this approximation differs slightly from the traditional method used when studying grain roughness using k_s proportional to the larger grains ($k_s = d_{90}$ or d_{84} for example); however, it is thought that considering the larger bedforms would not change the results significantly as it would also increase the resulting zero-plane displacement values. Note that the value used is a rough estimate and may not precisely depict the actual spatial average of bedform heights throughout the meander. Bedform heights also varied slightly along the streamwise direction and more significantly laterally across the stream; larger bedforms were located along the outer bank, across from the point bar, and smaller bedforms located along the inner bank. A rough estimation of the spatial average bedform height was obtained by subtracting the

maximum and minimum bed elevations, bedform crests and troughs, respectively, throughout the meander bend measured using the precise DAQ bathymetry measurements. At present, there is not a superior method to estimate bedform height. Tabulated values are located in Appendix C.

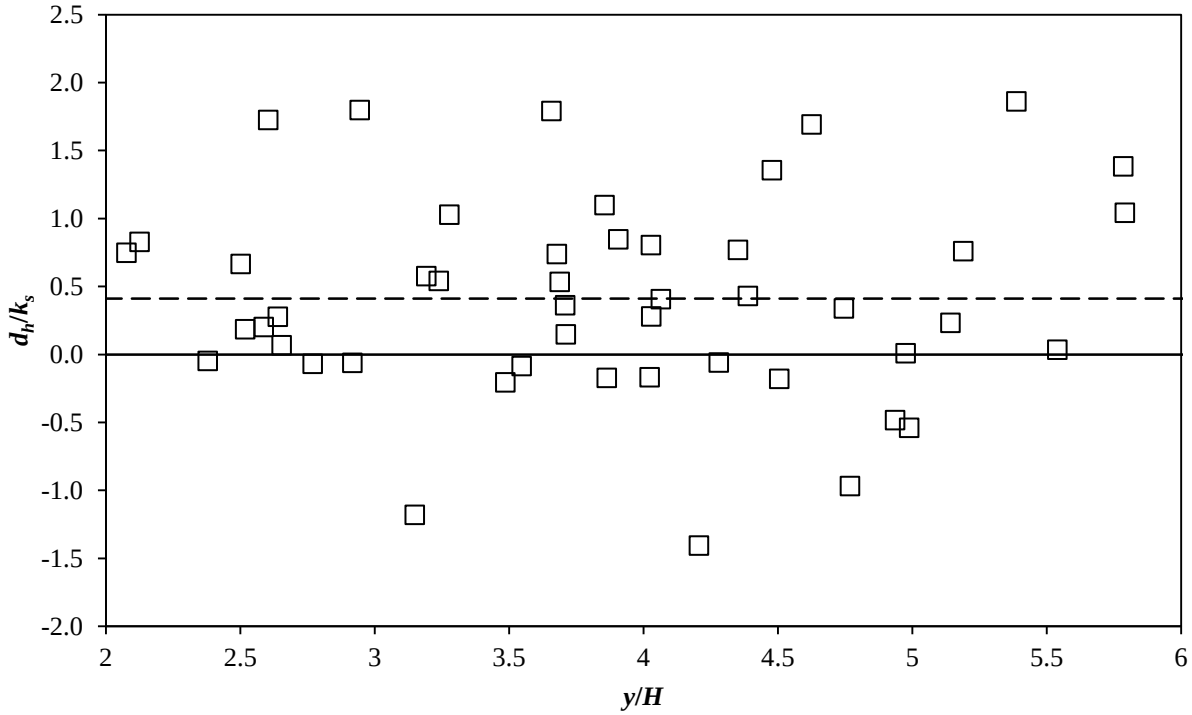

Figure 13: Zero-plane displacement, d_h, normalized by roughness height, k_s, for mobile bed outdoor experiments when considered the zero-velocity plane as the reference elevation. Dotted line represents the average ratio of d_h/k_s. Note that y/H is the transverse (y-axis) distance from either bank that the vertical profile is located normalized by the stream depth. Profiles within 2 flow depths of either bank were not included to remove the boundary's influence on the profiles.

In conclusion, the average zero-plane displacement normalized by roughness height of 0.41 is of the same order of magnitude as those for the sediment- and vegetation-scale roughness experiments, 0.20 and 0.26, respectively, as well as for the indoor bedform-scale experiment, 0.34, and for those found in the literature for static, rough beds (Table 2). The discrepancy could be attributed to the fact that flow through the meander was generally three-dimensional in nature, violating one assumption necessary when applying the log law; however, the logarithmic profiles did fit the measured streamwise velocities well when removing profiles located within two depths of either bank ($y/H < 0.2$).

4.5 Summary

The resulting zero-plane displacement for all four experiments is between 20 to 40% of the respective roughness height. The results indicate that the smaller, sediment-scale roughness elements make up the lower end of the range, while the larger, bedform roughness elements may encompass the higher end. This similarity in ratios of zero-plane displacement to roughness height for static beds and for mobile beds helps confirm the hypothesis that the method described in the literature for locating a profile origin in the presence of small, sediment-scale roughness elements may also be applicable for defining a profile origin in the presence of larger roughness elements such as large scale fluctuations in bed elevation caused by bedforms. It is also suggested that the analysis be kept to the inner flow region when possible, although adequate results may be obtained from considering a larger portion of the flow, even the entire flow depth in some cases. The average results for all four data sets are summarized in Table 3. Tabulated values for individual experiments can be found in Appendix C.

Table 3: Average zero-plane displacements normalized by roughness coefficient for four data sets with constant roughness packing density.

Data Set	**Roughness Type**	***Packing Density***	**k_s (cm)**	**Average d_h (cm)**	**Average d_h/k_s**	**Comment**
Fully Packed (Kanellopoulos, 1998)	Sediment	0.7[a]	0.8	0.16	0.20	k_s = sphere diameter
Vegetation (Liu et al., 2008)	Vegetation	0.12[a]	7.62	2.00	0.26	k_s = dowel height
Mobile bed – flume	Bedform	0.5[b]	2.34	0.80	0.34	k_s = bedform height
Mobile bed – outdoor	Bedform	N/A[c]	5	2.04	0.41	k_s = avg bedform height

[a] Calculated using λ
[b] Calculated as the height to spacing ratio (assuming a bedform height of 0.5 m and wavelength of 1 m)
[c] Only one bedform was present

Chapter 5: Discussion

5.1 Relationship Between Zero Velocity Plane and Original Datum

Since it is rarely known at what stage of the oscillation the bed is in when taking measurements in the field, it is important to explore the relationship between the profile origin and the reference datum. The investigation involved locating the plane of zero velocity using the minimum and the maximum bed locations as the original reference elevations in the flume bedform-scale experiment. The location of the velocity profile origin was 0.37 cm above the average bed elevation and 1.54 cm above the minimum bed elevation, or bedform trough, resulting in negative values (Table 4). Negative values simply mean that the plane of zero velocity is located above the original datum. For all three reference bed elevations selected (minimum, maximum, and average), the origin displacement was located at virtually the same elevation (4.47 cm); therefore, the location of the profile origin can be considered constant and independent of the reference bed elevation. These findings indicate that the profile origin location remains the same, no matter at what stage in the fluctuation the actual bed is located. However, it should be noted that the velocity record should be sufficient to capture at least one, preferably multiple, full oscillation cycles in bed elevation, or the migration of several full bedforms, so as to have a minimally biased velocity measurement that is representative of the long-term average.

Table 4: Zero-plane displacement (d_h) and profile origin location above an arbitrary datum for mobile bed flume experiment using three different reference bed elevations. Negative zero-plane displacements indicate that the plane of zero velocity is located above the reference bed elevation and vice-versa for positive values; therefore the profile origin elevation is equal to the difference between the reference elevation and d_h.

Bed Reference	Reference Bed Elevation (cm)	d_h (cm)	Profile Origin Elevation (cm)
Average	4.1 cm	-0.37	4.47
Minimum	2.9 cm	-1.54	4.44
Maximum	5.3 cm	0.80	4.50

5.2 Effect of Packing Density on Zero-plane Displacement

The fifth data source (Balakrishnan, 1997) was used in order to supplement the already discussed results by assessing the influence of packing density on zero-plane displacement. Data from Balakrishnan (1997), encompassing packing densities of 2%, 20%, 35%, and 50%, along with data from the literature (Raupach et al., 1986 and Raupach, 1988) and two experiments discussed previously (Kanellopoulos, 1998; Liu et al., 1998), is shown in Figure 14. In order to determine a threshold value, two major assumptions were made: (1) there must exist a threshold for λ, as discussed by Jackson (1981), and (2) there is no zero-plane displacement for smooth surfaces ($\lambda = 0$). It is reasonable to expect that a threshold does exist by considering that at low packing densities (below the threshold) the roughness elements are so sparse that they have virtually no effect on the overall boundary roughness. As packing density increases, however, the roughness elements begin to interact, eventually creating a new rough surface.

By assuming no zero-plane displacement for smooth surfaces and using the data point with the lowest packing density, a relationship between zero-plane displacement and packing density can be found for low packing densities (Equation 10a). By using all other data points, a weak relationship between zero-plane displacement and packing density can be found for high packing densities (Equation 10b). The intercept of these two functions indicates that the threshold value may lie somewhere near $\lambda = 4\%$ (Figure 14).

$$d_h/k_s = 5.72 \cdot \lambda \qquad \text{for } \lambda \leq 0.04 \qquad (10a)$$

$$d_h/k_s = -0.11 \cdot \lambda + 0.24 \qquad \text{for } \lambda > 0.04 \qquad (10b)$$

The relatively flat line in Figure 14 for λ values above the threshold supports the conclusion in Jackson (1981) that above the threshold, zero-plane displacement is independent of packing density. This could be explained physically by considering that as packing density increases, flow near the boundary becomes "smoother" as each roughness element moves within the wake of the upstream roughness elements, displacing the flow upward again, effectively decreasing the penetration depth (albeit probably not completely to zero). Results indicate that zero-plane displacement can range up to 0.23 below the threshold, and from 0.13 to 0.23 above the threshold. It is also worth noting that the results favor the conclusion drawn by Jackson (1981). The results tend to not support the conclusion drawn by Nepf & Ghisablerti (2008) that as

packing density increases toward a maximum of unity, penetration depth decreases to zero and therefore zero-plane displacement decreases to zero (Equation 5).

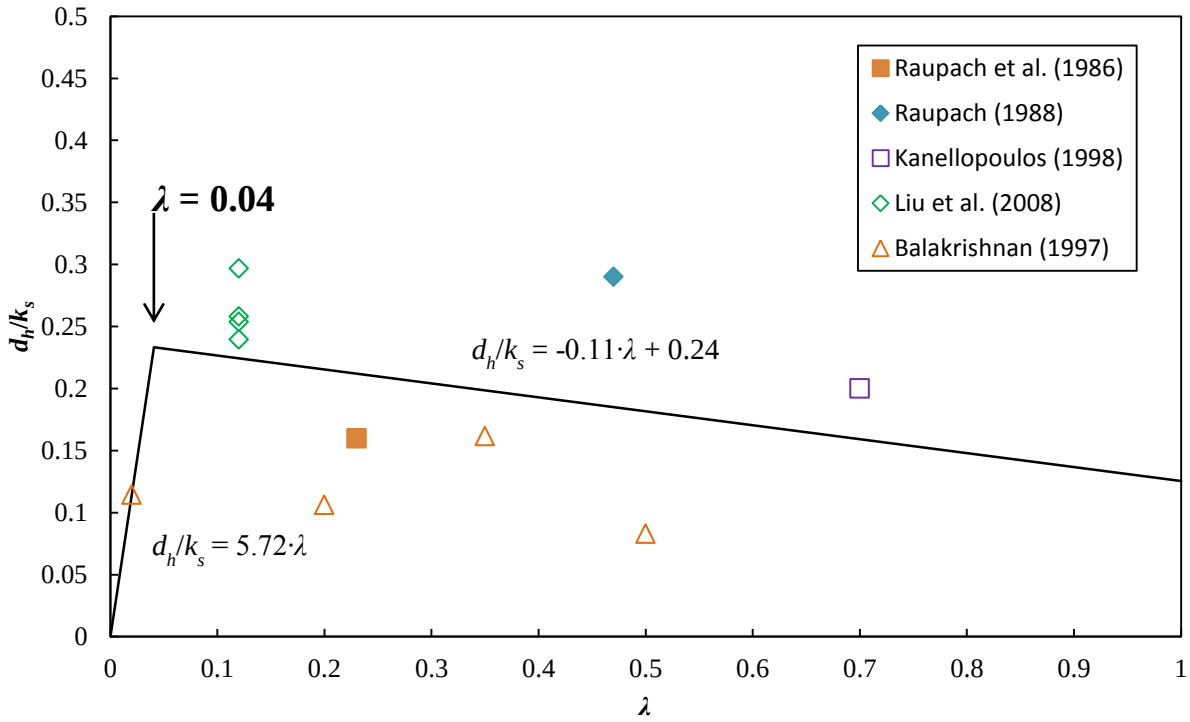

Figure 14: Effects of packing density, λ, on normalized zero-plane displacement for data found in the literature (solid symbols) and analyses described here (open symbols) over fixed roughness elements.

More evidence pointing to the existence of a packing density threshold near 4% comes from comparing the zero-plane displacements, as well as the shear velocities, from measurements found in Balakrishnan (1997). If zero-plane displacement is truly independent of packing density for high packing densities then the bed should have the properties of a contiguous roughness above the threshold, meaning that the local variations in flow around the protruding roughness elements are insignificant. Consequently, the behavior above the threshold should be identical to the case of a closely packed bed and velocities taken at any single point should be equivalent to spatially averaged velocities at the same elevation, granted that the elevation is above the roughness sublayer, so that the profiles should theoretically be indistinguishable. For indistinguishable profiles, the parameters describing the two profiles, such as zero-plane displacement and shear velocity, should also be identical. The differences between zero-plane

displacements and shear velocities obtained from a single velocity profile above a spherical roughness element and ones obtained from spatially averaged streamwise velocities (Balakrishnan, 1997) are shown in Figure 15. For the cases with packing densities of 20% and greater, the difference in zero-plane displacements are marginal and the values nearly identical. For the case with a packing density of only 2%, the difference is much larger suggesting that the threshold where point measurements deviate from spatial averages may lie somewhere between 2% and 20%. A similar, perhaps less evident, trend can be seen in the percent differences in shear velocities between profiles of spatially averaged, streamwise velocities and a single profile above an individual roughness element for different packing densities (Figure 15). There is a larger discrepancy in shear velocities for the 2% packing density than for the 20%, 35%, and 50% cases. The less evident trend in shear velocities could be explained by the fact that the method used collapses shear velocities to a tight distribution, as described previously, dampening the amount of spread among values. Note that shear velocities used were the result of fitting a log profile to the bottom 20% of the flow depth and using the calculated zero-plane displacement.

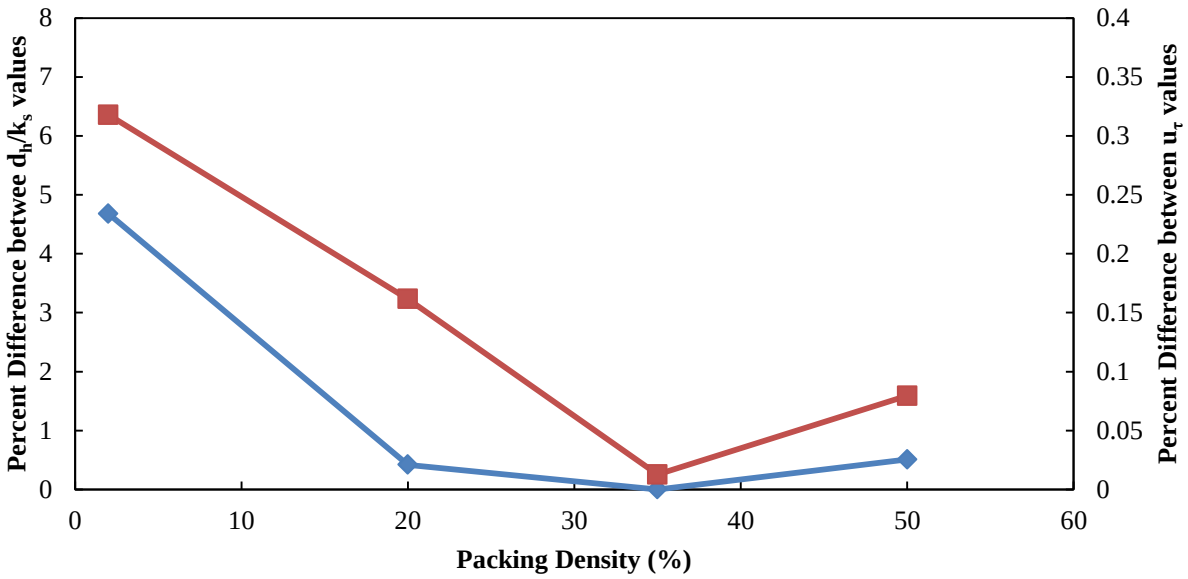

Figure 15: Percent difference between d_h/k_s values (diamonds, left axis) and u_τ (squares, right axis) values obtained from spatial averages and point measurements on top of spherical roughness elements (Location A). Raw data obtained from Balakrishnan (1997) experiment.

A similar indicator of a threshold has can be seen by considering the mean drag coefficient on individual roughness elements. According to results found in Marshall (1971), the threshold is dependent on the ratio of roughness element diameter to height, d/h. As d/h increases, the λ threshold for drag coefficient increases (Figure 16). For the d/h ratios studied in Marshall (1971), the λ threshold ranges from 0.012 to 0.022 ($6.8 < \lambda^{-0.5} < 9$), slightly smaller than the threshold determined using data discussed here and considering d_h/k_s as the determining factor instead of drag coefficient. It should also be noted that the diameter to height ratio, d/h, for the vegetation experiment described here is 0.083, an order of magnitude lower than those considered in Marshall (1971). According to the trend shown in Figure 16, the threshold for d/h = 0.083 would be lower than 0.012, assuming the thresholds determined considering drag coefficient and d_h/k_s are equivalent. The similarity with the threshold of 0.04 found herein is remarkable considering the wide range of roughness element sizes and shapes used.

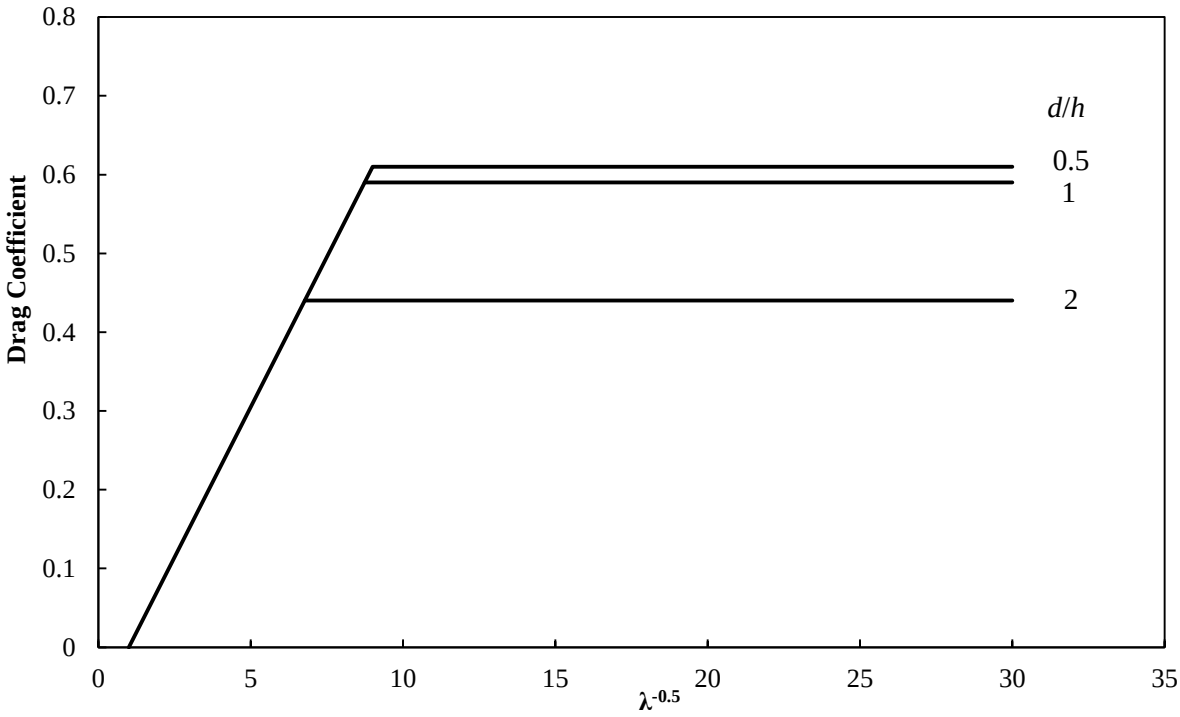

Figure 16: Regression showing the variation of mean drag coefficient on individual roughness elements. Redrawn from Marshall (1971).

The effects of packing density on zero-plane displacement were also hypothesized by Raupach (1992). For that investigation, zero-plane displacement was estimated as the centroid of the drag

force profile. It was estimated that the ratio of zero-plane displacement to roughness height increased from a value of 0.0 at $\lambda = 0.001$, to 1.0 at $\lambda = 10$. For the data shown in Figure 14, the maximum theoretical value for d_h/k_s is 0.23, occurring at the threshold value of 0.04. No threshold for λ was considered in the analysis of Raupach (1992), although it was postulated that stress partition, considering the stress as the sum of the stresses imparted on the individual roughness element and the surface below, becomes unnecessary for $\lambda > 0.03$ to 0.10 due to the decrease in shear on individual roughness elements caused by sheltering. This could also help explain the mild slope of the line in Figure 14 for $\lambda > 0.04$. As packing density increases and, consequently, sheltering increases, the flow is not allowed to penetrate down as far in between roughness elements and therefore, according to Equation 5, the zero-plane displacement decreases slightly.

5.3 Bedform-scale Roughness and Their Dependence on Wavelength

It is acknowledged that for bedforms, the roughness effects are probably dependent on wavelength as well as amplitude as shown in Smith and McLean (1977). However, for the purpose of simplicity the analyses used herein only considered amplitude. It is reasonable to expect that for large wavelengths, the sediment scale roughness elements dominate, whereas for short wavelengths the bedforms themselves make up the majority of the roughness effects. The precise relationship between roughness height and wavelength would require further research outside of the objectives of this document.

5.4 Differences Between Profiles of Spatial Averages and Point Measurements

It is also necessary to comment on the differences in considering spatially averaged velocities instead of point measurements. Spatially averaged quantities give a better representation of a channel's overall flow characteristics and allow for the calculation of global flow parameters, such as zero-plane displacement and shear velocity that describe the overall behavior of the flow. The zero-plane displacement could be used to represent the channel's roughness characteristics, such as roughness element size, shape, and spacing, in a single quantity. Global flow parameters are often used to describe large-scale flow parameters such as flow resistance and discharge.

Heterogeneous flow conditions are often encountered above a bed of fully packed spheres in a prismatic channel. Dancey et al. (2000) demonstrated longitudinal heterogeneity in 25

measurements of the local average vertical velocity component located 0.51 mm above four closely packed, 8 mm diameter spherical roughness elements (Figure 17). The same pattern of spherical roughness elements in a fully packed configuration made up the entire bed. Their results indicate that flow penetrates down into the void between the upstream roughness element and the two adjacent roughness elements (Figure 17), and continues to penetrate until reaching the upstream face of the final sphere where it is forced upward only to, presumably, repeat the process on the downstream face. As fluid flows over and around the spherical roughness elements, many local variations in velocities occur rapidly, driven by the changes in the local topography. Spatially averaged quantities should be necessary in order to account for the inhomogeneity described, where the local values vary quickly and may not describe the behavior of the entire flow. Spatial averages allow for the calculation of global flow parameters, which describe that macro-scale behavior. Local values based on near bed velocity measurements may not describe the overall flow pattern well and therefore are not adequate to describe the global parameters.

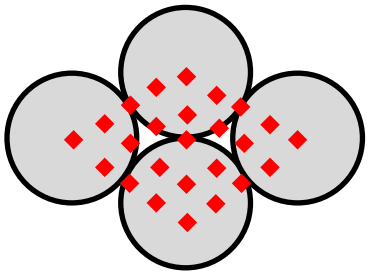

Figure 17: Location of velocity measurements in Dancey et al. (2000). Black circles represent spherical roughness elements. Red diamonds represent locations of velocity measurements 0.51 mm above the top of the layer of spheres.

It has also been postulated that the velocity profile over large-scale, sinusoidal roughness elements on a sandy bed is composed of two separate regions controlled by the different roughness elements present (Smith and McLean, 1977). Near the bed, the profile is governed by the smaller roughness scale composed of individual sediment grains or, in the case of bedload, the height of the bedload transport layer. Further away from the bed, the profile is governed by the larger roughness elements made of wave-like structures. In the near bed section, the profile is related to the local skin friction, while away from the bed the profile is related to overall boundary shear (Smith and McLean, 1977) described by spatially averaged quantities.

It has been demonstrated that spatially averaged quantities are theoretically necessary; however, it can be shown using results obtained from the vegetation-scale experiment ($\lambda = 0.12$) that they are not always required. Profiles of point measurements are shown in Figure 18a, while profiles of spatially averaged velocities are shown in Figure 18b. Notice how the profiles of point velocities at each of the six measurement locations are scattered below the top of the dowels, but surprisingly collapse to a single profile above the dowel array where the flow is unaffected by the individual roughness elements so that the boundary exhibits a quasi-averaged behavior (Figure 18a). On the other hand, the profiles of spatially averaged velocities (Figure 18b) are similar at all elevations. Therefore the aforementioned assumption that flow conditions are identical for experiments L1, L2, L3, and L4 is supported. Since the methodology discussed in this paper applies to the inner flow region, where the point measurement profiles collapse to a single profile, it is the case that the results obtained from using point measurements will be similar to those obtained from using spatial averages (Table 5). For this reason, it may be safe to assume that one profile of velocity point measurements may be representative of the spatial average and used to determine global flow parameters when dealing with the inner flow region if the packing density is sufficiently high so that the individual roughness elements make up a rough surface; in other words, if the individual roughness elements lose their own distinct identity and instead behave as parts of a whole. It is conjectured here that using point measurements in the vicinity of the boundary, in place of spatial averages, may be valid for packing densities above the threshold, although this has not been fully demonstrated. This assumption may be utilized to cut down on the length of experiments, especially when global flow parameters are of interest.

Table 5: Normalized zero-plane displacement and shear velocity for vegetation-scale experiments. Values obtained for point measurements are from each of the six individual profiles for each experiment.

Experiment	d_h/k_s for point measurements	d_h/k_s for spatial averages	Percent Difference	u_τ (m/s) for point measurements	u_τ (m/s) for spatial averages	Percent Difference
L1	0.25	0.26	3.2	0.072	0.072	0.0
	0.30		15.4	0.069		3.1
	0.24		7.3	0.072		0.0
	0.22		14.1	0.075		4.0
	0.23		9.5	0.073		2.4
	0.28		6.6	0.072		0.3
L2	0.28	0.25	9.8	0.070	0.069	0.8
	0.25		0.6	0.068		1.6
	0.22		12.4	0.071		3.1
	0.23		9.1	0.071		2.6
	0.24		4.9	0.069		0.2
	0.27		6.6	0.068		1.9
L3	0.27	0.24	10.8	0.072	0.072	0.5
	0.20		15.4	0.073		1.0
	0.25		4.0	0.074		3.4
	0.26		7.0	0.070		2.7
	0.22		6.5	0.071		0.8
	0.23		4.7	0.072		0.3
L4	0.33	0.30	9.6	0.069	0.069	0.2
	0.27		8.1	0.070		0.6
	0.30		1.6	0.068		1.2
	0.27		10.0	0.071		2.2
	0.30		0.7	0.069		0.3
	0.28		7.5	0.071		2.8

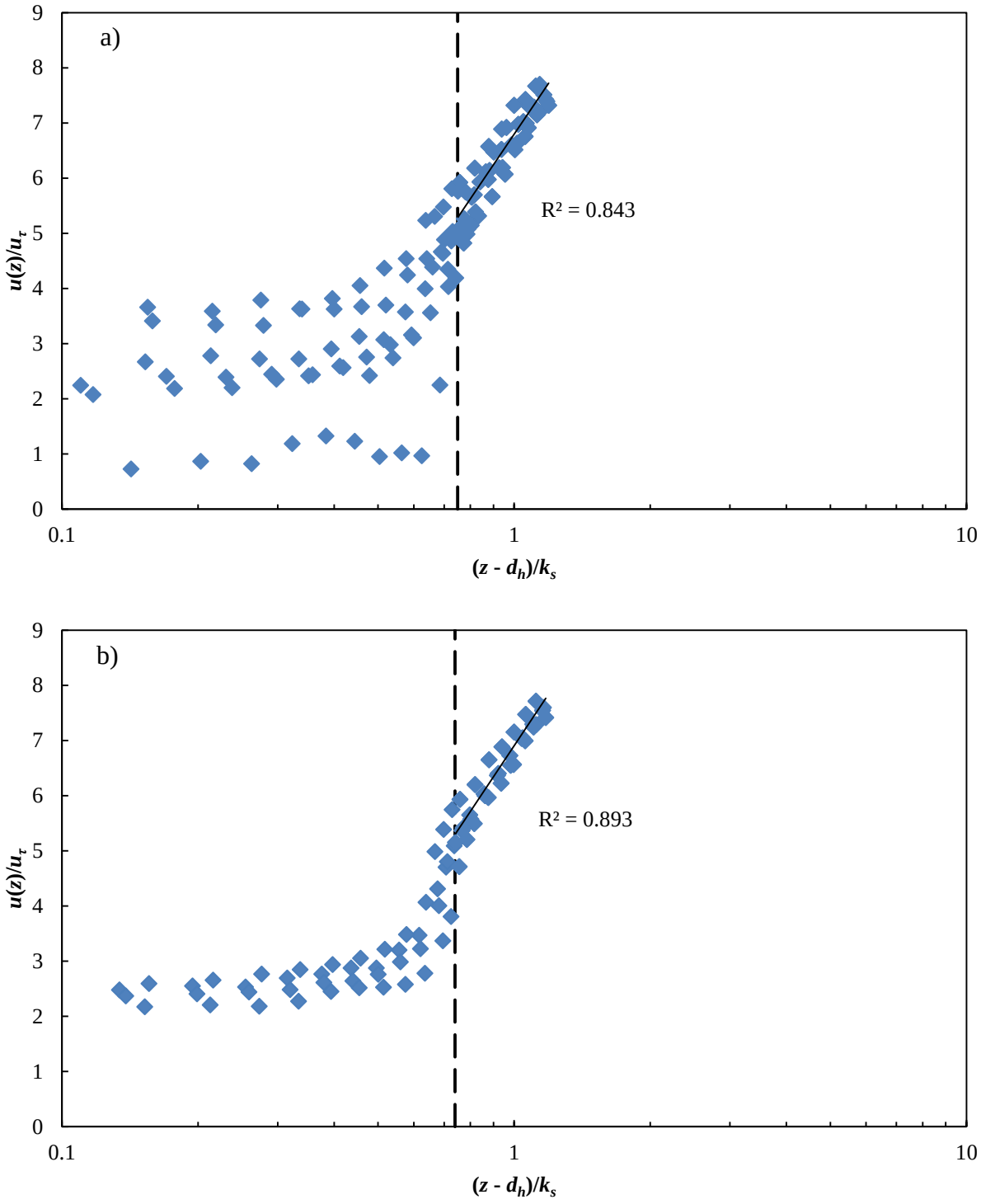

Figure 18: (a) Velocity profiles of point measurements at all six locations for experiment L1. Notice that all profiles collapse to a single profile above the top of the dowel array. (b) Profiles of spatially averaged velocities for all four experiments L1, L2, L3, and L4. Notice how all profiles are nearly identical at all depths. Vertical, dashed lines represent top of dowel array.

Chapter 6: Conclusion

Data from five separate experiments were used in order to assess the validity of the methodology typically employed for determining the zero-plane displacement for a wide range of roughness types and sizes ranging from static, sediment-scale roughnesses to mobile, bed-form scale roughness elements. It was determined that the concept is valid for all roughness types, even mobile bedforms. Results also suggest that zero-plane displacements ranging from 0.2 to 0.4 times the roughness height are generally good estimates for all roughness types and sizes. It may be necessary to use the lower end of the range when dealing with smaller, sediment-scale roughness types and using the higher end of the range when considering the larger, bar-like roughness elements. The method should be applied to the inner flow region; however, it has been shown in the past that the logarithmic law is applicable for as much as the entire flow depth. The range of zero-plane displacement values was derived from both actual velocity measurements and when considering the theoretical depth of penetration of vortices into the array of roughness elements. During the process, it was also determined that the zero velocity plane location is independent of the reference bed elevation chosen so that it does not matter whether data is being collected over the crest or trough or in between.

The effect of packing density on zero-plane displacement was also explored. Results point to the possible existence of a packing density threshold of around 4%, above which zero-plane displacement is much less dependent on roughness element density. Below the threshold, zero-plane displacement has a direct relationship with packing density. In the case of a bed made of a series of neighboring protrusions acting together as a single, continuous rough surface, the spatially averaged velocity profile is identical to a profile at a single location. Therefore, the parameters used to describe the profile, namely zero-plane displacement and shear velocity, should be identical. It was found that for packing densities of 20%, 35%, and 50%, and using a single profile, this was the case. The shear velocity and zero-plane displacement for a single profile and the spatial average profile at a 2% packing density differed much more drastically, pointing to a threshold value between 2% and 20%.

It was also determined that it may not be necessary to consider spatially averaged velocities when fitting profiles within the inner flow region. It was shown that only minor differences in the values of zero-plane displacement and shear velocity occurred when using profiles made of

spatially averaged velocities and single point velocities. Since it requires more time and effort to measure spatially averaged quantities, the ability to use point measurements to obtain the same results could drastically reduce the amount of experimental resources needed.

References

1. Afzalimehr, H. and C. D. Rennie (2009), Determination of bed shear stress in gravel-bed rivers using boundary-layer parameters, *Hydrological Sciences Journal*, 54(1), 147-159, doi:10.1623/hysj.54.1.147.
2. Balakrishnan, M. (1997), The Role of Turbulence on the Entrainment of a Single Sphere and the Effects of Roughness on Fluid-Solid Interaction, Ph. D Thesis, Dep. of Mech. Eng., Virginia Tech, Blacksburg, Virginia.
3. Buffin-Belanger, T. and A. G. Roy (2005), 1 min in the life of a river: selecting the optimal record length for the measurement of turbulence in fluvial boundary layers, *Geomorphology*, 68(1), 77-94, doi: 10.1016/j.geomorph.2004.09.032.
4. Chang, H. H. (1988), *Fluvial Processes in River Engineering*, John Wiley & Sons, Inc.
5. Church, D. G., D. G. McLean, and J. F. Wolcott (1987), River bed gravels: sampling and analysis, *Sediment Transport in Gravel Bed Rivers.*
6. Dancey, C. L., M. Balakrishnan, P. Diplas, and A. N. Papanicolaou (2000), The spatial inhomogeneity of turbulence above a fully rough, packed bed in open channel flow, *Experiments in Fluids*, 29, 402-410.
7. Einstein, H. A. and E. A. El-Samni (1949), Hydrodynamic forces on a rough wall, *Reviews of Modern Physics*, 21, 520-524.
8. Fairbanks, J. (1998), Velocity and Turbulence Characteristics in Flows Through Rigid Vegetation, M. S. Thesis, Dept. of Civil Eng., Virginia Tech, Blacksburg, Virginia.
9. Goring, D. G. and V. I. Nikora (2002), Despiking acoustic Doppler velocimeter data, *Journal of Hydraulic Engineering*, 128(1), 117-126.

10. Jackson, P. S. (1981), On the displacement height in the logarithmic velocity profile, *J. Fluid Mech.*, 111, 15-25.
11. Jarvis, P. G., G. B. James, and J. J. Landsberg (1976), Coniferous Forest, in *Vegetation and the Atmosphere Vol. 2*, edited by Monteith, J. L., pp. 171-240, Academic Press, London, England.
12. Kanellopoulos, P. M. (1998), Incipient motion under shallow flow conditions, Ph. D Thesis, Dep. of Civil Eng., Virginia Tech, Blacksburg, Virginia.
13. Kironoto, B. A., and W. H. Graf (1995), Turbulence characteristics in rough non-uniform open-channel flow, *Proceedings of the Institution of Civil Engineers, Water, Maritime, and Energy*, 112, 336-348.
14. Lee, B. E. and B. F. Soliman (1977), An Investigation of the Forces on Three Dimensional Bluff Bodies in in Rough Wall Turbulent Boundary Layers, *Fluids Engineering, Transactions of the ASME*, 99, 503-510.
15. Liu, D., P. Diplas, J. D. Fairbanks, and C. C. Hodges (2008), An experimental study of flow through rigid vegetation, *J. Geophys. Res.*, 113, doi:10.1029/2008JF001042.
16. Marshall, J. K. (1971), Drag Measurements in Roughness Arrays of Varying Density and Distribution, *Agricultural Meteorology*, 8, 269-292.
17. Murphy, E., M. Ghisalberti, and H. Nepf (2007), Model and laboratory study of dispersion in flows with submerged vegetation, *Water Resources Research*, 43, doi:10.1029/2006WR005229.
18. Nepf, H. and M. Ghisalberti (2008), Flow and transport in channels with submerged vegetation, *Acta Geophysica*, 56(3), 753-777, doi:10.2478/s11600-008-0017-y.

19. Parsheh, M., F. Sotiropoulos, and F. Porte-Angel (2010), Estimation of power spectra of acoustic Doppler velocimetry data contaminated with intermittent spikes, *Journal of Hydraulic Engineering*, 136(6), 368-378, doi:10.1061/(ASCE)HY.1943-7900.0000202.
20. Perry, A. E. and P. N. Joubert (1963), Rough-wall boundary layers in adverse pressure gradients, *J. Fluid Mech.*, 17, 193-211.
21. Raupach, M. R. (1988), Canopy Transport Processes, in *Flow and Transport in the Natural Environment*, Steffen, edited by W. L. and O. T. Denmean, Springer, Berlin.
22. Raupach, M. R. (1992), Drag and Drag Partition on Rough Surfaces, *Boundary-Layer Meteorology*, 60, 375-395.
23. Raupach, M. R., R. A. Antonia, and S. Rajagopalan (1991), Roughwall turbulent boundary layers, *Appl. Mech. Rev.*, 44(1), 1–25.
24. Raupach, M. R., P. A. Coppin, and B. J. Legg (1986), Experiments on Scalar Dispersion Within a Plant Canopy, Part I: The Turbulence Structure, *Boundary-Layer Meteorology*, 35, 21-52.
25. Recking, A. (2009), Theoretical Development on the effects of changing flow hydraulics on incipient bed load motion, *Water Resour. Res.*, 45(4) doi: 10.1029/2008WR006826.
26. Schlichting, H., and K. Gersten (2000), *Boundary Layer Theory 8th Ed.*, Springer, New York.
27. Smart, G. M. (1999), Turbulent velocity profiles and boundary shear in gravel bed rivers, *Journal of Hydraulic Engineering*, 125 (2), 106-116.
28. Smith, J. D., and S. R. McLean (1977), Spatially Averaged Flow Over a Wavy Surface, *Journal of Hydraulic Eng.*, 82(12), 1735-1746.

Appendix A: Sample Spreadsheet Used to Calculate d_h

Each cross section is made up of velocity point measurements within up to eight vertical profiles. Velocity points (circles in Figure A1) are numbered beginning at the river right water surface, increasing toward the bed and across the stream. Note that profiles within two stream depths of either bank were not considered in the analyses, but they are shown in the Figure A1 and Table A1. Also note that Table A1 only contains a sample of the first five profiles in the cross section.

Measurements elevations and bathymetry elevations are referenced differently and are not brought to the same reference until the column 'z_plot' in Table A1. Also note that only measurements within 20 cm of the stream bed were considered in any regression (Table A1; Figure A2). Measurements above 20 cm are indicated with a diagonal slash through the cells in Table A1.

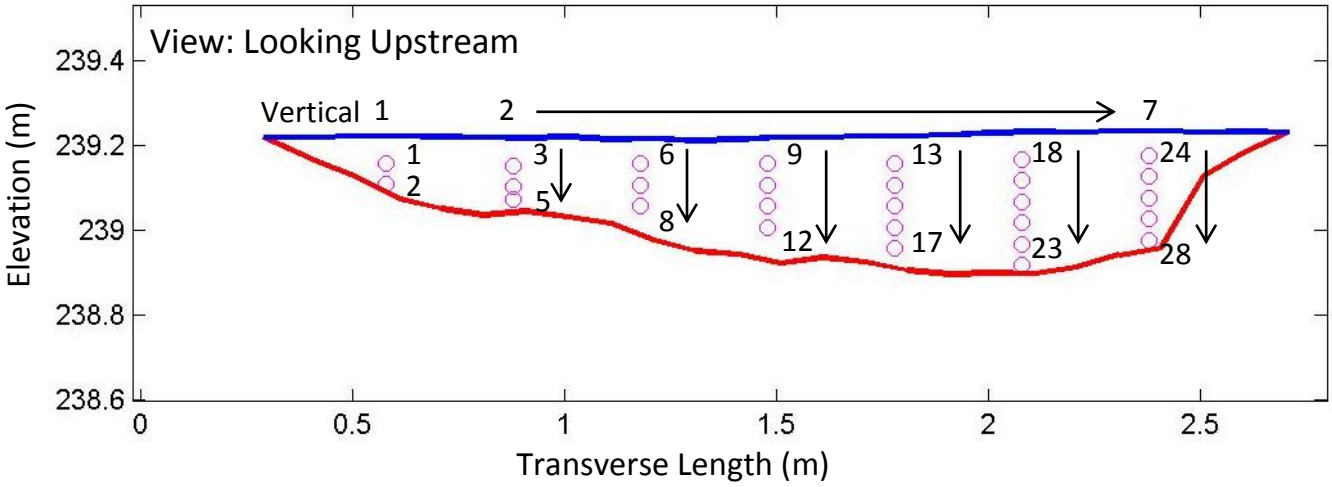

Figure A1: Velocity measurements within a cross section showing point numbering and profile numbering.

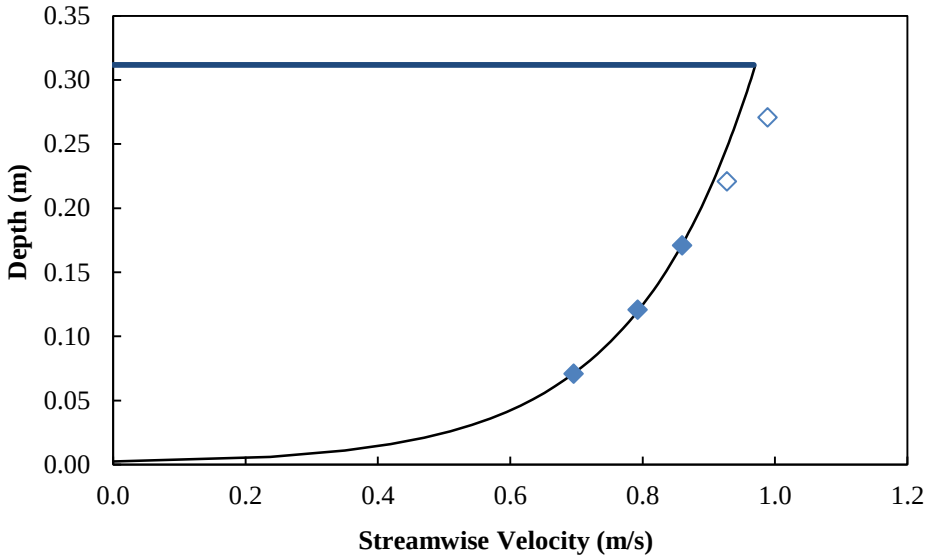

Figure A2: Regression fit to vertical profile number 5 in table below. Solid symbols are within 20 cm of the bed; open symbols above 20 cm and not considered in the regression. Profile parameters are: u_τ = 0.07 m/s, Γ = 8.5, R^2 = 1.000.

Table A1: Spreadsheet used to calculate d_h for five sample profiles.

Vertical	Point	z_abs[a] (cm)	WS elev (cm)	Bed elev (cm)	Depth (m)	Shift[b] (cm)	d_h[c] (cm)	z_plot[d] (cm)	z_rel[e] (m)	z_force[f] (m)	Regression Stats[g]		u_τ^h (m/s)	Γ^i
1	1	73	61.30	48.03	0.1327	16.70	0.27	56.18	0.08	0.08	11.95	-6.40	0.033	8.5
	2	68						51.18	0.03	0.03	1.000			
2	3	72.5	61.03	43.43	0.1760	16.47	1.35	55.68	0.12	0.14	6.66	-6.40	0.060	8.5
	4	67.5						50.68	0.07	0.09	0.754			
	5	64.5						47.68	0.04	0.06				
3	6	73	60.77	38.00	0.2277	17.23	1.35	56.18	0.18	0.20	5.28	-6.40	0.076	8.5
	7	68						51.18	0.13	0.15	0.943			
	8	63						46.18	0.08	0.10				
4	~~9~~[j]	~~73~~	60.95	32.06	0.2889	17.05	-0.63	~~56.18~~	~~0.24~~	~~0.23~~	5.73	-6.40	0.070	8.5
	10	68						51.18	0.19	0.18	0.971			
	11	63						46.18	0.14	0.13				
	12	58						41.18	0.09	0.08				
5	~~13~~	~~73~~	61.50	30.33	0.3117	16.50	1.22	~~56.18~~	~~0.26~~	~~0.27~~	5.39	-6.40	0.074	8.5
	~~14~~	~~68~~						~~51.18~~	~~0.21~~	~~0.22~~	1.000			
	15	63						46.18	0.16	0.17				
	16	58						41.18	0.11	0.12				
	17	53						36.18	0.06	0.07				

[a] z-coordinate relative to the absolute reference (read from the scale on the ADV)

[b] Shift required to cause the top-most measurement to be 5 cm from the water surface. All profiles are shifted by the average of all values, NOT each individual value. Shift = z_abs – WS_elev + 5.

[c] Zero-plane displacement varied until $\Gamma = 8.5$

[d] z-coordinate after applying the average shift. z_plot = z_abs – Average[Shift].

[e] z-coordinate relative to the bed. z_rel = z_plot – Bed_elev.

[f] z-coordinate relative to the bed after applying the zero-plane displacement. z_force = z_rel - d_h.

[g] Regression statistics slope, m_r, (top left), intercept, b_r, (top right), and R^2 (bottom)

[h] Shear velocity = κ/m_r

[i] $\Gamma = -1/\kappa \cdot (\exp(b_r)/(k_s \cdot 100))$; also used as the iteration objective

[j] Cells crossed out indicate that they were not used in the regression because they are outside the inner region (z_force > 0.2 m)

Appendix B: OSL Data

There are two coordinate systems used here. The first is OSL_x, OSL_y, and OSL_z. These refer to the coordinates in the Outdoor StreamLab and are used to locate all measurements within the stream. The vertical OSL_z coordinate is referenced to sea level. A second set of coordinates are the x, y, and z local coordinates used to designate the local streamwise, lateral, and vertical directions. They are defined based on the local stream geometry and are in different orientations at each cross section in the stream. In general, if a coordinate is given as 'x, y, or z' it is representing the local coordinate system where x is the streamwise direction (parallel to the stream banks), y is the lateral direction (perpendicular to the stream banks), and z is the vertical direction. The x coordinate is measured from the center of the traverse holding the ADV and positive is in the downstream direction (the actual ADV is offset from the traverse slightly). The y coordinate is measured from the river right and positive is in the direction from right bank to left bank. The z coordinate is measured from an arbitrary datum and positive is in the direction from the bed to the surface.

The table headings are described as:

- *Point* – Denotes the point number in the cross section. Points were numbered beginning at the surface along the river right bank and increasing towards the bed and then towards the opposite bank. Note that for cross sections 1 and 2 in Baseline1, numbering was started at the bottom along the river right bank and increasing towards the opposite bank; however they are sorted to match the rest of the cross sections.
- *Q* – Contains the discharge measured during measurements at each point. Discharge was attempted to be measured each time a velocity measurement was taken; however, it wasn't always done and therefore there are some 'NaN' entries.
- *OSL x-coordinate* – The coordinate in the OSL x-direction for each point. Useful for mapping measurements throughout the stream.
- *OSL y-coordinate* – The coordinate in the OSL y-direction for each point. Useful for mapping measurements throughout the stream.
- *OSL z-coordinate* – The coordinate in the OSL z-direction for each point. Useful for mapping measurements throughout the stream.

- *u_raw* – The time averaged streamwise (local x-direction) velocity measurement measured by the ADV. The average of approximately 48,000 individual measurements. Raw data should not be used in calculations because it contains erroneous measurements that will skew the results.
- *v_raw* – The time averaged streamwise (local y-direction) velocity measurement measured by the ADV. The average of approximately 48,000 individual measurements. Raw data should not be used in calculations because it contains erroneous measurements that will skew the results.
- *w_raw* –The time averaged streamwise (local z-direction) velocity measurement measured by the ADV. The average of approximately 48,000 individual measurements. Raw data should not be used in calculations because it contains erroneous measurements that will skew the results.
- *U_raw* – The average velocity magnitude of the 48,000 values calculated using the 3 raw components at each time step. Raw data should not be used in calculations because it contains erroneous measurements that will skew the results
- *u_filt* – The time averaged streamwise (local x-direction) velocity of the filtered data. The average of approximately 48,000 individual measurements, less the measurements removed by the filter. Filtering is essential and removes erroneous measurements.
- *v_filt* – The time averaged streamwise (local y-direction) velocity of the filtered data. The average of approximately 48,000 individual measurements, less the measurements removed by the filter. Filtering is essential and removes erroneous measurements.
- *w_filt* – The time averaged streamwise (local z-direction) velocity of the filtered data. The average of approximately 48,000 individual measurements, less the measurements removed by the filter. Filtering is essential and removes erroneous measurements.
- *U_filt* – The average velocity magnitude of the approximately 48,000 values calculated using the 3 filtered components at each time step. Filtering is essential and removes erroneous measurements.
- *u_rot* – The time averaged, filtered streamwise velocity component rotated into OSL coordinates from the local x, y, and z coordinates. These measurements are not necessarily parallel to the streambanks.

- *v_rot* – The time averaged, filtered lateral velocity component rotated into OSL coordinates from the local x, y, and z coordinates. These measurements are not necessarily perpendicular to the streambanks.
- *w_rot* – The time averaged, filtered vertical velocity component rotated into OSL coordinates from the local x, y, and z coordinates. These values are identical to 'w_filt' because vertical orientation is the same in the OSL and local coordinates.
- *U_rot* – The time averaged, filtered, velocity magnitude rotated into OSL coordinates from the local x, y, and z coordinates. The magnitude is not changed when rotated into OSL coordinates from local coordinates.

Table B1: Data collected from two experiments conducted in the OSL.

Baseline 1 – Cross Section 1								
Point	***Q*** **(L/s)**	**OSL x-coordinate (m)**	**OSL y-coordinate (m)**	**OSL z-coordinate[a] (m)**	***u*_raw[b] (m/s)**	***v*_raw[b] (m/s)**	***w*_raw[b] (m/s)**	***U*_raw[b] (m/s)**
1	281	13.411	11.898	239.14	0.064	-0.023	-0.016	0.186
2	281	13.411	11.898	239.14	0.263	0.006	-0.040	0.433
3	283	13.411	11.898	239.15	0.786	0.175	-0.043	0.870
4	284	13.081	12.124	239.11	0.974	0.121	-0.079	1.336
5	284	13.081	12.124	239.12	1.115	0.235	0.011	1.202
6	283	13.081	12.124	239.16	1.408	0.030	0.108	1.435
7	284	12.717	12.372	239.08	0.663	0.042	-0.066	0.705
8	283	12.717	12.372	239.09	0.832	0.012	-0.047	1.051
9	284	12.717	12.372	239.14	1.234	0.068	0.101	1.320
10	287	12.354	12.621	239.10	0.490	0.125	0.042	0.689
11	280	12.354	12.621	239.11	0.914	0.116	-0.077	1.058
12	286	12.354	12.621	239.16	1.358	0.119	0.036	1.405
13	286	11.929	12.912	239.12	0.818	-0.080	-0.075	0.920
14	284	11.929	12.912	239.13	0.815	0.007	-0.060	0.845
15	286	11.929	12.912	239.15	0.907	-0.052	-0.017	0.939
Point	***u*_filt[c] (m/s)**	***v*_filt[c] (m/s)**	***w*_filt[c] (m/s)**	***U*_filt[c] (m/s)**	***u*_rot[d] (m/s)**	***v*_rot[d] (m/s)**	***w*_rot[d] (m/s)**	***U*_rot[d] (m/s)**
1	0.064	-0.023	-0.014	0.140	0.055	0.040	-0.014	0.140
2	0.264	0.007	-0.037	0.413	0.143	0.221	-0.037	0.413
3	0.787	0.174	-0.044	0.852	0.300	0.748	-0.044	0.852
4	0.964	0.121	-0.079	1.264	0.444	0.863	-0.079	1.264
5	1.117	0.218	0.011	1.190	0.451	1.045	0.011	1.190
6	1.412	0.030	0.108	1.421	0.773	1.182	0.108	1.421
7	0.666	0.042	-0.066	0.695	0.341	0.573	-0.066	0.695
8	0.837	0.014	-0.048	0.865	0.461	0.699	-0.048	0.865
9	1.236	0.066	0.102	1.319	0.644	1.057	0.102	1.319
10	0.490	0.125	0.043	0.673	0.174	0.475	0.043	0.673
11	0.919	0.119	-0.086	1.027	0.421	0.826	-0.086	1.027
12	1.361	0.119	0.036	1.372	0.671	1.191	0.037	1.372
13	0.819	-0.080	-0.072	0.849	0.529	0.631	-0.072	0.849
14	0.817	0.007	-0.060	0.843	0.456	0.678	-0.060	0.843
15	0.908	-0.054	-0.017	0.937	0.557	0.719	-0.017	0.937
Baseline 1 – Cross Section 2								
Point	***Q*** **(L/s)**	**OSL x-coordinate (m)**	**OSL y-coordinate (m)**	**OSL z-coordinate[a] (m)**	***u*_raw[b] (m/s)**	***v*_raw[b] (m/s)**	***w*_raw[b] (m/s)**	***U*_raw[b] (m/s)**
1	276	14.554	14.786	239.08	-0.141	0.012	-0.009	0.181
2	275	14.554	14.786	239.09	-0.198	0.001	-0.019	0.228
3	275	14.554	14.786	239.10	-0.221	-0.009	-0.022	0.242
4	276	14.554	14.786	239.11	-0.211	-0.014	-0.022	0.235
5	274	14.554	14.786	239.12	-0.224	-0.018	-0.025	0.247
6	270	14.416	14.867	238.91	0.213	0.023	0.000	0.290
7	275	14.416	14.867	238.95	0.349	0.134	-0.041	0.549
8	283	14.416	14.867	239.00	0.413	0.064	-0.051	0.597
9	280	14.416	14.867	239.05	0.417	0.114	-0.024	0.595
10	288	14.416	14.867	239.12	0.169	0.088	0.012	0.372

11	283	14.278	14.948	238.90	0.226	0.043	-0.056	0.275
12	280	14.278	14.948	238.95	0.591	0.140	-0.034	0.713
13	272	14.278	14.948	239.00	0.787	0.112	-0.036	0.914
14	273	14.278	14.948	239.05	1.024	0.167	-0.025	1.153
15	274	14.278	14.948	239.11	1.226	-0.259	0.097	1.444
16	275	14.140	15.029	238.93	0.470	-0.006	-0.060	0.506
17	279	14.140	15.029	238.96	0.598	0.035	-0.076	0.698
18	276	14.140	15.029	239.01	0.841	0.096	-0.032	0.912
19	279	14.140	15.029	239.06	1.031	0.101	0.020	1.092
20	272	14.140	15.029	239.12	1.064	0.084	0.111	1.213
21	275	14.002	15.110	238.97	0.440	-0.024	-0.036	0.505
22	275	14.002	15.110	238.99	0.492	-0.004	-0.018	0.617
23	275	14.002	15.110	239.02	0.728	0.041	-0.018	0.819
24	276	14.002	15.110	239.06	0.992	0.038	-0.015	1.076
25	275	14.002	15.110	239.11	1.175	0.019	0.106	1.294
26	277	14.002	15.110	239.14	1.314	0.158	0.140	1.445
27	270	13.864	15.191	238.92	0.043	-0.014	-0.004	0.086
28	278	13.864	15.191	238.95	0.505	-0.093	-0.087	0.584
29	274	13.864	15.191	239.00	0.660	-0.053	-0.096	0.878
30	277	13.864	15.191	239.05	0.887	-0.005	-0.066	1.058
31	275	13.864	15.191	239.12	1.225	0.080	0.141	1.345
32	271	13.726	15.272	238.94	0.478	-0.145	-0.043	0.530
33	276	13.726	15.272	238.97	0.599	-0.132	-0.052	0.691
34	272	13.726	15.272	239.02	0.837	-0.004	-0.049	0.919
35	276	13.726	15.272	239.07	1.008	-0.030	-0.042	1.099
36	273	13.726	15.272	239.12	1.197	0.082	0.112	1.300
37	274	13.588	15.353	238.94	0.436	-0.086	-0.034	0.504
38	279	13.588	15.353	238.97	0.576	-0.101	-0.044	0.710
39	278	13.588	15.353	239.02	0.774	-0.066	-0.051	0.852
40	276	13.588	15.353	239.07	0.902	-0.048	-0.024	0.962
41	269	13.588	15.353	239.12	1.005	0.001	0.003	1.055
42	279	13.450	15.434	238.94	0.149	-0.054	-0.027	0.253
43	271	13.450	15.434	238.97	0.258	-0.046	-0.036	0.435
44	275	13.450	15.434	239.02	0.438	0.007	-0.033	0.518
45	272	13.450	15.434	239.07	0.657	0.026	-0.021	0.744
46	276	13.450	15.434	239.13	0.683	0.013	0.002	0.741
47	269	13.286	15.530	238.98	-0.026	0.019	-0.010	0.136
48	277	13.286	15.530	239.00	-0.029	-0.014	-0.018	0.161
49	258	13.286	15.530	239.04	-0.051	-0.014	0.008	0.150
50	270	13.286	15.530	239.08	-0.073	-0.061	-0.013	0.196
51	269	13.286	15.530	239.13	-0.022	-0.018	0.002	0.193

Point	***u*_filt[c] (m/s)**	***v*_filt[c] (m/s)**	***w*_filt[c] (m/s)**	***U*_filt[c] (m/s)**	***u*_rot[d] (m/s)**	***v*_rot[d] (m/s)**	***w*_rot[d] (m/s)**	***U*_rot[d] (m/s)**
1	-0.141	0.012	-0.009	0.174	-0.082	-0.115	-0.009	0.174
2	-0.198	0.001	-0.019	0.223	-0.101	-0.171	-0.019	0.223
3	-0.221	-0.009	-0.022	0.238	-0.105	-0.195	-0.022	0.238
4	-0.211	-0.013	-0.022	0.229	-0.095	-0.189	-0.022	0.229
5	-0.224	-0.018	-0.025	0.243	-0.098	-0.202	-0.025	0.243
6	0.211	0.024	0.001	0.279	0.086	0.194	0.001	0.279
7	0.347	0.135	-0.043	0.441	0.059	0.367	-0.042	0.441
8	0.414	0.064	-0.049	0.509	0.155	0.390	-0.049	0.509
9	0.422	0.113	-0.023	0.545	0.116	0.422	-0.023	0.545
10	0.166	0.089	0.011	0.338	0.007	0.188	0.011	0.338

11	0.223	0.043	-0.055	0.267	0.076	0.214	-0.055	0.267
12	0.591	0.135	-0.034	0.649	0.182	0.579	-0.034	0.649
13	0.790	0.111	-0.035	0.838	0.304	0.737	-0.034	0.838
14	1.027	0.165	-0.025	1.065	0.378	0.969	-0.024	1.065
15	1.228	-0.326	0.102	1.353	0.903	0.894	0.100	1.353
16	0.469	-0.006	-0.059	0.497	0.242	0.401	-0.059	0.497
17	0.598	0.038	-0.074	0.637	0.270	0.535	-0.074	0.637
18	0.842	0.092	-0.031	0.881	0.347	0.773	-0.031	0.881
19	1.033	0.099	0.020	1.065	0.438	0.941	0.020	1.065
20	1.066	0.088	0.111	1.119	0.464	0.964	0.111	1.119
21	0.438	-0.024	-0.035	0.482	0.242	0.366	-0.035	0.482
22	0.491	0.004	-0.016	0.552	0.245	0.425	-0.016	0.552
23	0.734	0.039	-0.017	0.783	0.337	0.653	-0.017	0.783
24	0.995	0.036	-0.015	1.025	0.473	0.876	-0.015	1.025
25	1.178	0.004	0.108	1.226	0.593	1.017	0.108	1.226
26	1.316	0.158	0.144	1.337	0.531	1.215	0.144	1.337
27	0.044	-0.013	-0.004	0.074	0.033	0.031	-0.004	0.074
28	0.503	-0.093	-0.086	0.553	0.335	0.387	-0.086	0.553
29	0.662	-0.056	-0.094	0.726	0.383	0.542	-0.095	0.726
30	0.890	-0.010	-0.066	0.925	0.459	0.762	-0.066	0.925
31	1.227	0.080	0.141	1.241	0.553	1.098	0.142	1.241
32	0.478	-0.144	-0.042	0.520	0.366	0.339	-0.042	0.520
33	0.599	-0.127	-0.050	0.638	0.413	0.452	-0.051	0.638
34	0.838	-0.028	-0.049	0.866	0.448	0.709	-0.049	0.866
35	1.010	-0.032	-0.041	1.033	0.539	0.855	-0.041	1.033
36	1.199	0.082	0.112	1.212	0.537	1.076	0.112	1.212
37	0.435	-0.086	-0.034	0.489	0.294	0.332	-0.034	0.489
38	0.576	-0.088	-0.043	0.626	0.367	0.453	-0.043	0.626
39	0.775	-0.071	-0.050	0.817	0.454	0.633	-0.050	0.817
40	0.903	-0.055	-0.024	0.934	0.504	0.751	-0.024	0.934
41	1.006	-0.015	0.002	1.033	0.523	0.860	0.002	1.033
42	0.147	-0.054	-0.026	0.246	0.121	0.100	-0.026	0.246
43	0.256	-0.044	-0.032	0.338	0.167	0.198	-0.032	0.338
44	0.437	0.006	-0.033	0.494	0.216	0.380	-0.033	0.494
45	0.658	0.024	-0.021	0.704	0.313	0.579	-0.020	0.704
46	0.684	0.010	0.001	0.721	0.338	0.595	0.001	0.721
47	-0.026	0.018	-0.010	0.133	-0.029	-0.013	-0.010	0.133
48	-0.029	-0.014	-0.016	0.139	-0.002	-0.032	-0.016	0.139
49	-0.051	-0.014	0.007	0.142	-0.014	-0.051	0.007	0.142
50	-0.073	-0.061	-0.013	0.190	0.016	-0.094	-0.013	0.190
51	-0.023	-0.018	0.003	0.189	0.004	-0.030	0.003	0.189

Baseline 1 – Cross Section 3								
Point	***Q*** **(L/s)**	**OSL x-coordinate (m)**	**OSL y-coordinate (m)**	**OSL z-coordinate[a] (m)**	***u*_raw[b] (m/s)**	***v*_raw[b] (m/s)**	***w*_raw[b] (m/s)**	***U*_raw[b] (m/s)**
1	283	15.996	16.543	239.13	0.257	0.049	-0.044	0.276
2	286	15.801	16.699	239.13	0.503	-0.012	-0.002	0.520
3	279	15.801	16.699	239.08	0.390	0.079	-0.015	0.415
4	286	15.591	16.869	239.13	0.667	-0.047	0.027	0.706
5	287	15.591	16.869	239.08	0.629	-0.089	0.017	0.691
6	277	15.381	17.038	239.13	0.871	0.054	0.038	0.924
7	287	15.381	17.038	239.08	0.813	-0.032	0.039	0.855
8	281	15.381	17.038	239.05	0.776	-0.020	0.038	0.820

9	281	15.170	17.208	239.13	1.200	0.086	0.096	1.278
10	285	15.170	17.208	239.08	1.099	0.130	0.029	1.130
11	277	15.170	17.208	239.03	0.916	0.058	0.030	0.946
12	282	15.170	17.208	238.98	0.817	0.024	0.042	0.861
13	283	15.170	17.208	238.95	0.704	-0.068	0.026	0.775
14	291	15.170	17.208	238.93	0.646	-0.075	0.016	0.684
15	283	14.960	17.377	239.13	1.021	0.111	0.019	1.057
16	282	14.960	17.377	239.08	0.998	0.108	-0.012	1.032
17	280	14.960	17.377	239.03	0.885	0.134	-0.007	0.924
18	280	14.960	17.377	238.98	0.771	0.055	-0.010	0.832
19	280	14.960	17.377	238.93	0.673	0.040	-0.001	0.727
20	287	14.960	17.377	238.90	0.614	-0.042	0.009	0.665
21	288	14.750	17.547	239.14	0.350	0.020	0.005	0.414
22	286	14.750	17.547	239.09	0.458	0.073	-0.006	0.513
23	284	14.750	17.547	239.04	0.540	0.118	-0.013	0.602
24	286	14.750	17.547	238.99	0.537	0.125	-0.006	0.607
25	284	14.750	17.547	238.94	0.543	0.136	-0.003	0.611
26	290	14.750	17.547	238.90	0.473	0.053	-0.011	0.570
27	290	14.750	17.547	238.87	0.376	0.052	0.008	0.410
28	283	14.540	17.716	239.14	-0.036	-0.030	-0.003	0.160
29	287	14.540	17.716	239.09	-0.013	-0.025	-0.005	0.155
30	289	14.540	17.716	239.04	-0.007	-0.029	-0.003	0.137
31	287	14.540	17.716	238.99	-0.001	-0.007	-0.011	0.086

Point	***u*_filt[c] (m/s)**	***v*_filt[c] (m/s)**	***w*_filt[c] (m/s)**	***U*_filt[c] (m/s)**	***u*_rot[d] (m/s)**	***v*_rot[d] (m/s)**	***w*_rot[d] (m/s)**	***U*_rot[d] (m/s)**
1	0.256	0.049	-0.044	0.276	0.123	0.230	-0.044	0.276
2	0.503	-0.011	-0.002	0.517	0.324	0.385	-0.002	0.517
3	0.390	0.079	-0.015	0.414	0.183	0.353	-0.015	0.414
4	0.667	-0.050	0.026	0.689	0.457	0.487	0.026	0.689
5	0.629	-0.086	0.018	0.649	0.461	0.436	0.018	0.649
6	0.871	0.039	0.037	0.901	0.516	0.703	0.037	0.901
7	0.813	-0.037	0.039	0.844	0.539	0.610	0.039	0.844
8	0.777	-0.037	0.037	0.799	0.516	0.581	0.037	0.799
9	1.200	0.063	0.096	1.256	0.704	0.974	0.096	1.256
10	1.099	0.125	0.029	1.128	0.593	0.934	0.029	1.128
11	0.916	0.056	0.030	0.942	0.531	0.749	0.030	0.942
12	0.817	0.010	0.042	0.840	0.505	0.643	0.042	0.840
13	0.704	-0.067	0.026	0.732	0.494	0.506	0.026	0.732
14	0.646	-0.074	0.016	0.673	0.464	0.457	0.016	0.673
15	1.021	0.107	0.019	1.055	0.557	0.863	0.019	1.055
16	0.999	0.104	-0.012	1.030	0.546	0.843	-0.012	1.030
17	0.885	0.132	-0.007	0.923	0.453	0.772	-0.007	0.923
18	0.771	0.051	-0.009	0.803	0.445	0.632	-0.009	0.803
19	0.673	0.041	0.001	0.700	0.390	0.549	0.001	0.700
20	0.614	-0.038	0.010	0.643	0.415	0.454	0.010	0.643
21	0.349	0.020	0.005	0.407	0.204	0.284	0.005	0.407
22	0.457	0.072	-0.007	0.507	0.230	0.401	-0.007	0.507
23	0.539	0.118	-0.013	0.589	0.247	0.494	-0.013	0.589
24	0.537	0.125	-0.006	0.588	0.240	0.497	-0.006	0.588
25	0.543	0.135	-0.004	0.590	0.236	0.507	-0.004	0.590
26	0.472	0.054	-0.008	0.505	0.254	0.401	-0.008	0.505
27	0.375	0.052	0.009	0.408	0.195	0.324	0.009	0.408
28	-0.038	-0.030	-0.003	0.133	0.000	-0.049	-0.003	0.133

29	-0.013	-0.026	-0.005	0.124	0.012	-0.026	-0.005	0.124
30	-0.007	-0.030	-0.003	0.108	0.019	-0.024	-0.003	0.108
31	-0.002	-0.007	-0.011	0.061	0.004	-0.005	-0.011	0.061
Baseline 1 – Cross Section 4								
Point	***Q*** **(L/s)**	**OSL x-coordinate (m)**	**OSL y-coordinate (m)**	**OSL z-coordinate[a] (m)**	***u*_raw[b] (m/s)**	***v*_raw[b] (m/s)**	***w*_raw[b] (m/s)**	***U*_raw[b] (m/s)**
1	283	17.318	17.652	239.14	0.137	-0.035	0.023	0.161
2	283	17.132	17.887	239.06	0.449	-0.011	0.014	0.459
3	285	17.132	17.887	239.11	0.513	0.098	0.020	0.657
4	285	17.132	17.887	239.16	0.539	0.129	0.025	0.721
5	286	16.946	18.122	239.09	0.679	-0.030	0.021	0.716
6	284	16.946	18.122	239.15	0.733	-0.004	0.020	0.754
7	285	16.760	18.358	239.05	0.382	-0.016	-0.024	0.430
8	288	16.760	18.358	239.10	0.753	-0.005	0.020	0.781
9	284	16.760	18.358	239.15	0.846	0.031	0.024	0.879
10	290	16.574	18.593	239.01	0.623	-0.118	0.046	0.689
11	287	16.574	18.593	239.05	0.811	0.017	0.050	0.875
12	284	16.574	18.593	239.10	0.849	0.086	0.037	0.890
13	284	16.574	18.593	239.15	0.911	0.177	0.044	0.964
14	285	16.388	18.828	238.90	0.524	-0.081	0.020	0.569
15	289	16.388	18.828	238.95	0.685	0.030	-0.007	0.731
16	284	16.388	18.828	239.00	0.773	0.065	-0.014	0.848
17	288	16.388	18.828	239.05	0.851	0.109	-0.017	0.929
18	283	16.388	18.828	239.10	0.913	0.161	-0.003	0.984
19	289	16.388	18.828	239.15	0.916	0.122	0.009	0.981
20	286	16.202	19.064	238.87	0.164	0.000	-0.016	0.194
21	286	16.202	19.064	238.90	0.247	0.010	-0.022	0.287
22	282	16.202	19.064	238.95	0.376	0.063	0.006	0.430
23	288	16.202	19.064	239.00	0.401	0.082	0.007	0.461
24	286	16.202	19.064	239.05	0.317	0.069	0.012	0.378
25	284	16.202	19.064	239.10	0.339	0.056	0.017	0.391
26	282	16.202	19.064	239.15	0.358	0.060	0.022	0.412
27	286	16.016	19.299	239.10	0.000	-0.001	-0.001	0.002
28	292	16.016	19.299	239.15	0.029	-0.053	-0.019	0.175
Point	***u*_filt[c] (m/s)**	***v*_filt[c] (m/s)**	***w*_filt[c] (m/s)**	***U*_filt[c] (m/s)**	***u*_rot[d] (m/s)**	***v*_rot[d] (m/s)**	***w*_rot[d] (m/s)**	***U*_rot[d] (m/s)**
1	0.137	-0.034	0.023	0.160	0.129	0.058	0.023	0.160
2	0.449	-0.012	0.014	0.458	0.360	0.269	0.014	0.458
3	0.513	0.097	0.011	0.531	0.343	0.394	0.011	0.531
4	0.539	0.130	0.026	0.566	0.342	0.436	0.026	0.566
5	0.679	-0.032	0.021	0.696	0.553	0.396	0.021	0.696
6	0.734	-0.007	0.019	0.749	0.580	0.449	0.019	0.749
7	0.383	-0.015	-0.023	0.419	0.310	0.226	-0.023	0.419
8	0.753	-0.012	0.019	0.776	0.598	0.458	0.019	0.776
9	0.846	0.028	0.024	0.877	0.647	0.547	0.024	0.877
10	0.624	-0.119	0.047	0.669	0.563	0.293	0.047	0.669
11	0.812	-0.003	0.050	0.845	0.639	0.501	0.050	0.845
12	0.850	0.082	0.037	0.883	0.616	0.591	0.037	0.883
13	0.912	0.173	0.043	0.957	0.608	0.701	0.043	0.957
14	0.524	-0.084	0.020	0.559	0.463	0.259	0.020	0.559
15	0.685	0.019	-0.007	0.716	0.525	0.440	-0.007	0.716

16	0.774	0.062	-0.013	0.816	0.568	0.529	-0.013	0.816
17	0.851	0.105	-0.016	0.894	0.603	0.610	-0.016	0.894
18	0.913	0.155	-0.003	0.958	0.621	0.688	-0.003	0.958
19	0.917	0.119	0.009	0.964	0.646	0.662	0.009	0.964
20	0.163	0.000	-0.016	0.192	0.128	0.101	-0.016	0.192
21	0.247	0.009	-0.022	0.281	0.188	0.160	-0.022	0.281
22	0.375	0.062	0.006	0.412	0.256	0.282	0.006	0.412
23	0.401	0.081	0.007	0.450	0.264	0.312	0.007	0.450
24	0.316	0.069	0.013	0.370	0.205	0.250	0.013	0.370
25	0.337	0.055	0.017	0.386	0.230	0.253	0.017	0.386
26	0.357	0.059	0.022	0.405	0.243	0.268	0.022	0.405
27	0.000	-0.001	-0.001	0.002	0.000	-0.001	-0.001	0.002
28	0.029	-0.053	-0.015	0.143	0.055	-0.024	-0.015	0.143

Baseline 1 – Cross Section 5

Point	***Q*** **(L/s)**	**OSL x-coordinate (m)**	**OSL y-coordinate (m)**	**OSL z-coordinate[a] (m)**	***u*_raw[b] (m/s)**	***v*_raw[b] (m/s)**	***w*_raw[b] (m/s)**	***U*_raw[b] (m/s)**
1	280	18.512	18.094	239.10	0.311	0.049	0.016	0.321
2	283	18.512	18.094	239.14	0.291	0.037	0.009	0.302
3	277	18.488	18.393	239.10	0.502	0.015	0.049	0.511
4	279	18.488	18.393	239.14	0.556	0.096	-0.008	0.610
5	282	18.465	18.692	239.11	0.558	0.118	0.024	0.580
6	274	18.465	18.692	239.14	0.609	0.158	0.023	0.637
7	281	18.441	18.992	239.06	0.476	-0.087	0.027	0.516
8	286	18.441	18.992	239.09	0.555	0.053	-0.002	0.608
9	283	18.441	18.992	239.14	0.605	0.161	0.011	0.673
10	279	18.418	19.291	239.02	0.640	-0.052	-0.025	0.682
11	281	18.418	19.291	239.04	0.616	-0.012	-0.034	0.643
12	283	18.418	19.291	239.09	0.618	0.014	0.001	0.645
13	274	18.418	19.291	239.14	0.639	0.082	0.003	0.666
14	278	18.394	19.590	238.97	0.719	-0.148	0.080	0.796
15	283	18.394	19.590	238.99	0.716	-0.098	0.035	0.765
16	275	18.394	19.590	239.04	0.681	0.040	0.037	0.713
17	280	18.394	19.590	239.09	0.698	0.100	0.027	0.729
18	279	18.394	19.590	239.14	0.693	0.148	0.013	0.724
19	280	18.371	19.889	238.77	0.005	-0.007	-0.001	0.029
20	272	18.371	19.889	238.79	0.403	-0.114	0.016	0.456
21	282	18.371	19.889	238.84	0.600	-0.057	-0.009	0.650
22	276	18.371	19.889	238.89	0.667	-0.066	-0.032	0.725
23	273	18.371	19.889	238.94	0.679	0.019	-0.016	0.732
24	272	18.371	19.889	238.99	0.743	0.038	-0.022	0.794
25	273	18.371	19.889	239.04	0.748	0.055	-0.030	0.788
26	275	18.371	19.889	239.09	0.749	0.096	-0.029	0.789
27	273	18.371	19.889	239.14	0.748	0.136	-0.016	0.782
28	271	18.355	20.088	238.87	0.158	-0.019	-0.075	0.252
29	275	18.355	20.088	238.89	0.291	0.007	-0.049	0.370
30	271	18.355	20.088	238.94	0.384	0.062	-0.098	0.516
31	272	18.355	20.088	238.99	0.431	0.049	-0.100	0.564
32	273	18.355	20.088	239.04	0.470	0.049	-0.069	0.562
33	276	18.355	20.088	239.09	0.576	0.060	-0.052	0.634
34	274	18.355	20.088	239.14	0.660	0.076	-0.029	0.701
35	274	18.394	19.590	238.92	0.635	-0.209	0.056	0.737

Point	*u*_filt[c] (m/s)	*v*_filt[c] (m/s)	*w*_filt[c] (m/s)	*U*_filt[c] (m/s)	*u*_rot[d] (m/s)	*v*_rot[d] (m/s)	*w*_rot[d] (m/s)	*U*_rot[d] (m/s)
1	0.311	0.049	0.016	0.321	0.306	0.073	0.016	0.321
2	0.290	0.037	0.009	0.301	0.287	0.059	0.009	0.301
3	0.502	0.015	0.049	0.511	0.499	0.054	0.049	0.511
4	0.556	0.096	-0.006	0.571	0.547	0.140	-0.006	0.571
5	0.558	0.118	0.024	0.579	0.547	0.162	0.024	0.579
6	0.609	0.157	0.023	0.636	0.595	0.205	0.024	0.636
7	0.477	-0.088	0.027	0.507	0.482	-0.050	0.027	0.507
8	0.555	0.053	-0.001	0.568	0.549	0.096	-0.001	0.568
9	0.605	0.160	0.008	0.640	0.591	0.207	0.008	0.640
10	0.641	-0.057	-0.025	0.665	0.643	-0.007	-0.025	0.665
11	0.616	-0.014	-0.034	0.642	0.615	0.034	-0.034	0.642
12	0.619	0.012	0.000	0.644	0.616	0.061	0.000	0.644
13	0.640	0.081	0.003	0.659	0.632	0.131	0.003	0.659
14	0.719	-0.155	0.079	0.778	0.729	-0.098	0.079	0.778
15	0.716	-0.104	0.034	0.758	0.722	-0.048	0.034	0.758
16	0.681	0.037	0.036	0.710	0.676	0.090	0.037	0.710
17	0.698	0.098	0.027	0.727	0.688	0.153	0.027	0.727
18	0.693	0.147	0.013	0.724	0.679	0.201	0.014	0.724
19	0.004	-0.007	-0.001	0.024	0.005	-0.007	-0.001	0.024
20	0.402	-0.115	0.017	0.442	0.410	-0.083	0.016	0.442
21	0.600	-0.061	-0.009	0.646	0.603	-0.014	-0.009	0.646
22	0.668	-0.067	-0.032	0.718	0.671	-0.015	-0.032	0.718
23	0.679	0.016	-0.016	0.722	0.675	0.069	-0.016	0.722
24	0.744	0.035	-0.022	0.784	0.739	0.093	-0.022	0.784
25	0.749	0.051	-0.031	0.784	0.742	0.110	-0.030	0.784
26	0.749	0.093	-0.029	0.783	0.740	0.151	-0.029	0.783
27	0.748	0.134	-0.016	0.781	0.736	0.192	-0.016	0.781
28	0.159	-0.019	-0.074	0.237	0.160	-0.006	-0.074	0.237
29	0.291	0.007	-0.048	0.347	0.289	0.030	-0.048	0.347
30	0.383	0.060	-0.097	0.445	0.377	0.090	-0.097	0.445
31	0.431	0.050	-0.098	0.487	0.426	0.084	-0.098	0.487
32	0.470	0.046	-0.068	0.517	0.465	0.083	-0.068	0.517
33	0.576	0.055	-0.051	0.612	0.570	0.100	-0.051	0.612
34	0.661	0.067	-0.029	0.691	0.653	0.119	-0.028	0.691
35	0.635	-0.211	0.056	0.720	0.650	-0.160	0.056	0.720

Baseline 1 – Cross Section 6

Point	*Q* (L/s)	OSL x-coordinate (m)	OSL y-coordinate (m)	OSL z-coordinate[a] (m)	*u*_raw[b] (m/s)	*v*_raw[b] (m/s)	*w*_raw[b] (m/s)	*U*_raw[b] (m/s)
1	287	19.907	17.939	239.13	0.006	-0.018	0.032	0.080
2	287	19.983	18.198	239.13	0.549	0.072	-0.012	0.562
3	287	19.983	18.198	239.08	0.519	-0.198	0.003	0.588
4	283	20.059	18.457	239.13	0.573	0.025	-0.019	0.589
5	282	20.059	18.457	239.08	0.546	-0.118	0.039	0.593
6	280	20.059	18.457	239.03	0.484	-0.186	-0.014	0.582
7	282	20.136	18.716	239.13	0.637	-0.049	0.003	0.661
8	284	20.136	18.716	239.08	0.673	-0.127	0.011	0.717
9	288	20.136	18.716	239.03	0.668	-0.288	0.032	0.766
10	285	20.212	18.975	239.13	0.691	-0.009	0.041	0.717
11	285	20.212	18.975	239.08	0.691	-0.090	0.035	0.733

12	282	20.212	18.975	239.03	0.655	-0.149	0.054	0.724
13	278	20.212	18.975	239.00	0.645	-0.209	0.039	0.724
14	281	20.212	18.975	238.97	0.453	-0.096	-0.017	0.540
15	281	20.289	19.234	239.13	0.713	0.043	0.026	0.736
16	286	20.289	19.234	239.08	0.775	-0.024	0.040	0.808
17	286	20.289	19.234	239.03	0.768	-0.057	0.026	0.804
18	287	20.289	19.234	238.98	0.778	-0.097	0.047	0.823
19	284	20.289	19.234	238.93	0.741	-0.136	0.028	0.799
20	280	20.289	19.234	238.91	0.585	-0.193	0.044	0.716
21	285	20.393	19.589	239.13	0.759	0.008	0.019	0.786
22	285	20.393	19.589	239.08	0.767	0.027	0.027	0.795
23	285	20.393	19.589	239.03	0.759	0.010	0.014	0.788
24	284	20.393	19.589	238.98	0.651	0.012	0.026	0.686
25	285	20.393	19.589	238.93	0.481	-0.055	0.009	0.580
26	283	20.393	19.589	238.89	0.381	-0.048	0.008	0.460
Point	***u*_filt[c] (m/s)**	***v*_filt[c] (m/s)**	***w*_filt[c] (m/s)**	***U*_filt[c] (m/s)**	***u*_rot[d] (m/s)**	***v*_rot[d] (m/s)**	***w*_rot[d] (m/s)**	***U*_rot[d] (m/s)**
1	0.006	-0.018	0.032	0.072	0.001	-0.019	0.032	0.072
2	0.550	0.072	-0.012	0.561	0.547	-0.086	-0.012	0.561
3	0.519	-0.202	0.002	0.577	0.441	-0.341	0.002	0.577
4	0.573	0.024	-0.019	0.589	0.557	-0.139	-0.019	0.589
5	0.546	-0.121	0.038	0.583	0.489	-0.271	0.037	0.583
6	0.485	-0.195	-0.015	0.556	0.410	-0.325	-0.015	0.556
7	0.637	-0.052	0.002	0.660	0.596	-0.230	0.002	0.660
8	0.673	-0.132	0.010	0.716	0.608	-0.317	0.010	0.716
9	0.669	-0.299	0.032	0.755	0.557	-0.476	0.031	0.755
10	0.692	-0.013	0.041	0.715	0.660	-0.208	0.041	0.715
11	0.691	-0.092	0.034	0.731	0.637	-0.284	0.034	0.731
12	0.656	-0.159	0.053	0.712	0.585	-0.338	0.053	0.712
13	0.646	-0.226	0.038	0.707	0.555	-0.399	0.038	0.707
14	0.453	-0.091	-0.015	0.510	0.409	-0.215	-0.015	0.510
15	0.713	0.041	0.025	0.735	0.695	-0.163	0.025	0.735
16	0.775	-0.026	0.039	0.807	0.736	-0.245	0.039	0.807
17	0.768	-0.059	0.026	0.802	0.720	-0.274	0.026	0.802
18	0.778	-0.103	0.046	0.817	0.717	-0.319	0.046	0.817
19	0.743	-0.145	0.027	0.794	0.671	-0.349	0.027	0.794
20	0.587	-0.188	0.046	0.674	0.510	-0.346	0.046	0.674
21	0.759	0.004	0.019	0.784	0.729	-0.211	0.019	0.784
22	0.768	0.023	0.026	0.793	0.743	-0.196	0.026	0.793
23	0.759	0.007	0.014	0.786	0.730	-0.209	0.014	0.786
24	0.652	0.009	0.026	0.684	0.627	-0.176	0.026	0.684
25	0.481	-0.053	0.009	0.518	0.446	-0.187	0.009	0.518
26	0.379	-0.047	0.011	0.410	0.350	-0.152	0.011	0.410
Baseline 1 – Cross Section 7								
Point	***Q* (L/s)**	**OSL x-coordinate (m)**	**OSL y-coordinate (m)**	**OSL z-coordinate[a] (m)**	***u*_raw[b] (m/s)**	***v*_raw[b] (m/s)**	***w*_raw[b] (m/s)**	***U*_raw[b] (m/s)**
1	281	20.949	17.227	239.13	0.062	-0.144	0.068	0.304
2	281	21.102	17.462	239.13	0.561	-0.008	0.016	0.576
3	281	21.102	17.462	239.08	0.605	-0.042	-0.036	0.636
4	281	21.102	17.462	239.03	0.577	-0.019	-0.069	0.618
5	285	21.102	17.462	239.01	0.355	-0.022	0.034	0.374

6	285	21.255	17.696	239.13	0.620	-0.042	0.007	0.644
7	286	21.255	17.696	239.08	0.647	-0.031	0.000	0.678
8	289	21.255	17.696	239.03	0.646	-0.108	-0.047	0.697
9	281	21.408	17.931	239.13	0.772	-0.050	0.012	0.817
10	284	21.408	17.931	239.08	0.753	-0.027	0.020	0.808
11	286	21.408	17.931	239.03	0.709	-0.028	0.021	0.738
12	281	21.408	17.931	238.99	0.540	-0.110	0.040	0.587
13	286	21.561	18.165	239.13	0.769	0.004	0.021	0.793
14	282	21.561	18.165	239.08	0.783	-0.038	0.035	0.825
15	288	21.561	18.165	239.03	0.727	-0.099	0.002	0.766
16	288	21.561	18.165	239.00	0.628	-0.170	-0.005	0.689
17	286	21.714	18.400	239.13	0.797	0.051	0.011	0.819
18	286	21.714	18.400	239.08	0.857	-0.012	0.013	0.884
19	285	21.714	18.400	239.03	0.803	-0.001	0.052	0.848
20	286	21.714	18.400	238.99	0.717	-0.084	0.011	0.781
21	284	21.714	18.400	238.96	0.661	-0.142	0.028	0.719
22	284	21.867	18.634	239.13	0.828	0.064	0.017	0.851
23	284	21.867	18.634	239.08	0.860	0.031	0.029	0.886
24	284	21.867	18.634	239.03	0.849	0.038	0.029	0.874
25	284	21.867	18.634	238.98	0.762	-0.009	0.034	0.792
26	284	21.867	18.634	238.93	0.529	-0.041	0.031	0.557
27	281	22.020	18.869	239.13	0.791	0.081	0.002	0.820
28	287	22.020	18.869	239.08	0.841	0.098	-0.021	0.869
29	284	22.020	18.869	239.03	0.732	0.050	-0.031	0.764
30	279	22.020	18.869	239.00	0.383	-0.074	-0.033	0.519

Point	***u*_filt**[c] **(m/s)**	***v*_filt**[c] **(m/s)**	***w*_filt**[c] **(m/s)**	***U*_filt**[c] **(m/s)**	***u*_rot**[d] **(m/s)**	***v*_rot**[d] **(m/s)**	***w*_rot**[d] **(m/s)**	***U*_rot**[d] **(m/s)**
1	0.062	-0.144	0.075	0.198	-0.027	-0.155	0.075	0.198
2	0.561	-0.009	0.016	0.575	0.465	-0.314	0.016	0.575
3	0.605	-0.043	-0.038	0.626	0.483	-0.367	-0.038	0.626
4	0.577	-0.021	-0.071	0.602	0.472	-0.332	-0.071	0.602
5	0.355	-0.023	0.034	0.370	0.285	-0.213	0.034	0.370
6	0.620	-0.044	0.007	0.643	0.495	-0.375	0.007	0.643
7	0.647	-0.034	-0.001	0.673	0.524	-0.382	-0.001	0.673
8	0.647	-0.111	-0.047	0.686	0.481	-0.446	-0.047	0.686
9	0.772	-0.051	0.012	0.808	0.619	-0.465	0.012	0.808
10	0.753	-0.032	0.020	0.787	0.613	-0.438	0.020	0.787
11	0.709	-0.031	0.020	0.732	0.577	-0.413	0.020	0.732
12	0.541	-0.112	0.040	0.579	0.392	-0.390	0.040	0.579
13	0.769	0.003	0.020	0.793	0.646	-0.418	0.020	0.793
14	0.783	-0.043	0.033	0.816	0.633	-0.464	0.032	0.816
15	0.728	-0.104	0.002	0.764	0.553	-0.485	0.001	0.764
16	0.629	-0.185	-0.005	0.678	0.426	-0.498	-0.005	0.678
17	0.797	0.049	0.010	0.818	0.694	-0.394	0.010	0.818
18	0.858	-0.015	0.012	0.883	0.710	-0.481	0.012	0.883
19	0.804	-0.006	0.050	0.839	0.670	-0.444	0.050	0.839
20	0.719	-0.084	0.011	0.757	0.556	-0.464	0.011	0.757
21	0.662	-0.142	0.028	0.710	0.477	-0.480	0.028	0.710
22	0.828	0.063	0.016	0.850	0.728	-0.400	0.016	0.850
23	0.860	0.031	0.027	0.885	0.737	-0.445	0.027	0.885
24	0.849	0.036	0.029	0.873	0.731	-0.433	0.029	0.873
25	0.763	-0.012	0.033	0.791	0.633	-0.427	0.033	0.791
26	0.529	-0.046	0.031	0.551	0.417	-0.328	0.031	0.551

27	0.792	0.079	0.002	0.819	0.706	-0.366	0.003	0.819
28	0.842	0.097	-0.021	0.867	0.758	-0.379	-0.021	0.867
29	0.734	0.049	-0.031	0.760	0.641	-0.360	-0.031	0.760
30	0.380	-0.068	-0.030	0.422	0.281	-0.264	-0.030	0.422
Baseline 1 – Cross Section 8								
Point	***Q*** **(L/s)**	**OSL x-coordinate (m)**	**OSL y-coordinate (m)**	**OSL z-coordinate[a] (m)**	***u*_raw[b] (m/s)**	***v*_raw[b] (m/s)**	***w*_raw[b] (m/s)**	***U*_raw[b] (m/s)**
1	275	22.170	16.342	239.10	0.657	-0.029	0.011	0.703
2	275	22.170	16.342	239.07	0.652	-0.144	0.011	0.786
3	277	22.317	16.477	239.10	0.779	-0.015	0.000	0.800
4	279	22.317	16.477	239.07	0.776	-0.010	0.018	0.800
5	278	22.317	16.477	239.04	0.797	-0.084	0.014	0.875
6	278	22.317	16.477	239.01	0.738	-0.074	-0.020	0.771
7	277	22.317	16.477	238.99	0.620	-0.012	-0.037	0.687
8	279	22.464	16.613	239.10	0.758	-0.012	0.020	0.781
9	280	22.464	16.613	239.07	0.730	-0.050	-0.001	0.754
10	277	22.464	16.613	239.04	0.792	-0.013	0.005	0.841
11	275	22.464	16.613	239.01	0.715	-0.051	-0.041	0.778
12	277	22.464	16.613	239.00	0.705	-0.092	0.011	0.748
13	277	22.611	16.749	239.10	0.807	-0.038	0.010	0.847
14	277	22.611	16.749	239.07	0.793	-0.065	0.023	0.831
15	280	22.611	16.749	239.04	0.663	-0.002	0.002	0.700
16	279	22.611	16.749	239.01	0.732	-0.090	0.012	0.771
17	277	22.611	16.749	239.00	0.670	-0.045	0.010	0.691
18	279	22.758	16.884	239.10	0.798	-0.102	0.010	0.826
19	281	22.758	16.884	239.07	0.838	-0.093	0.009	0.878
20	279	22.758	16.884	239.04	0.782	-0.099	-0.028	0.839
21	286	22.758	16.884	239.01	0.657	-0.174	0.022	0.722
22	286	22.758	16.884	239.00	0.660	-0.139	0.019	0.723
23	282	22.905	17.020	239.11	0.883	-0.097	0.016	0.913
24	282	22.905	17.020	239.08	0.841	-0.109	0.010	0.873
25	286	22.905	17.020	239.05	0.756	-0.073	0.033	0.792
26	282	22.905	17.020	239.02	0.677	-0.217	0.018	0.798
27	286	22.905	17.020	238.99	0.566	-0.198	0.017	0.661
28	279	23.052	17.155	239.11	0.892	-0.039	0.026	0.915
29	288	23.052	17.155	239.08	0.871	-0.115	0.023	0.904
30	283	23.052	17.155	239.05	0.852	-0.103	0.015	0.898
31	285	23.052	17.155	239.02	0.787	-0.145	0.033	0.834
32	280	23.052	17.155	238.99	0.715	-0.261	0.009	0.789
33	286	23.052	17.155	238.97	0.646	-0.288	0.022	0.737
34	286	23.199	17.291	239.11	0.929	-0.038	0.007	0.954
35	275	23.199	17.291	239.08	0.885	-0.046	0.008	0.907
36	275	23.199	17.291	239.05	0.858	-0.059	0.014	0.888
37	275	23.199	17.291	239.02	0.790	-0.075	0.032	0.824
38	279	23.199	17.291	238.99	0.690	-0.228	0.028	0.811
39	283	23.199	17.291	238.96	0.521	-0.167	0.042	0.581
40	279	23.346	17.427	239.11	0.851	0.037	0.023	0.872
41	279	23.346	17.427	239.08	0.905	0.032	0.024	0.925
42	279	23.346	17.427	239.05	0.890	0.044	0.021	0.910
43	283	23.346	17.427	239.02	0.847	0.012	0.034	0.871
44	279	23.346	17.427	238.99	0.706	-0.062	0.033	0.782
45	281	23.346	17.427	238.96	0.410	0.043	0.041	0.480

46	276	23.493	17.562	239.11	0.108	0.007	0.018	0.208
47	282	23.493	17.562	239.09	0.106	0.007	0.008	0.213
48	277	23.493	17.562	239.07	0.129	0.011	0.010	0.223
49	282	23.493	17.562	239.05	0.188	0.021	0.028	0.263
50	274	23.493	17.562	239.03	0.254	0.051	0.037	0.317
51	279	23.493	17.562	239.01	0.311	0.090	0.046	0.374
52	279	23.493	17.562	238.99	0.345	0.138	0.054	0.409

Point	***u*_filt[c] (m/s)**	***v*_filt[c] (m/s)**	***w*_filt[c] (m/s)**	***U*_filt[c] (m/s)**	***u*_rot[d] (m/s)**	***v*_rot[d] (m/s)**	***w*_rot[d] (m/s)**	***U*_rot[d] (m/s)**
1	0.658	-0.029	0.012	0.670	0.424	-0.503	0.012	0.670
2	0.654	-0.142	0.011	0.740	0.339	-0.578	0.011	0.740
3	0.780	-0.016	-0.002	0.796	0.517	-0.584	-0.002	0.796
4	0.776	-0.011	0.016	0.795	0.518	-0.578	0.016	0.795
5	0.797	-0.088	0.014	0.827	0.476	-0.646	0.014	0.827
6	0.738	-0.079	-0.020	0.766	0.443	-0.596	-0.021	0.766
7	0.620	-0.012	-0.036	0.640	0.412	-0.464	-0.036	0.640
8	0.759	-0.015	0.020	0.779	0.503	-0.568	0.020	0.779
9	0.731	-0.055	-0.001	0.752	0.455	-0.574	-0.002	0.752
10	0.793	-0.015	0.002	0.815	0.527	-0.593	0.002	0.815
11	0.716	-0.055	-0.042	0.743	0.446	-0.563	-0.042	0.743
12	0.705	-0.094	0.012	0.730	0.409	-0.582	0.011	0.730
13	0.807	-0.040	0.007	0.824	0.518	-0.620	0.007	0.824
14	0.793	-0.073	0.022	0.820	0.484	-0.633	0.022	0.820
15	0.665	-0.005	0.001	0.691	0.447	-0.492	0.001	0.691
16	0.732	-0.094	0.012	0.760	0.428	-0.602	0.012	0.760
17	0.670	-0.048	0.010	0.690	0.419	-0.525	0.010	0.690
18	0.798	-0.104	0.010	0.820	0.465	-0.658	0.010	0.820
19	0.839	-0.095	0.006	0.857	0.499	-0.681	0.005	0.857
20	0.783	-0.103	-0.031	0.809	0.455	-0.645	-0.031	0.809
21	0.657	-0.177	0.023	0.698	0.316	-0.603	0.022	0.698
22	0.660	-0.141	0.021	0.696	0.344	-0.581	0.020	0.696
23	0.884	-0.098	0.013	0.901	0.527	-0.716	0.012	0.901
24	0.842	-0.111	0.008	0.862	0.489	-0.694	0.008	0.862
25	0.756	-0.081	0.032	0.782	0.453	-0.611	0.031	0.782
26	0.677	-0.224	0.017	0.733	0.294	-0.650	0.017	0.733
27	0.566	-0.182	0.019	0.618	0.250	-0.539	0.018	0.618
28	0.892	-0.040	0.022	0.905	0.576	-0.683	0.022	0.905
29	0.872	-0.117	0.021	0.892	0.505	-0.720	0.020	0.892
30	0.852	-0.106	0.011	0.872	0.500	-0.698	0.010	0.872
31	0.788	-0.158	0.032	0.829	0.418	-0.686	0.032	0.829
32	0.715	-0.264	0.009	0.783	0.290	-0.705	0.008	0.783
33	0.647	-0.298	0.021	0.735	0.220	-0.677	0.020	0.735
34	0.929	-0.039	0.005	0.939	0.601	-0.709	0.005	0.939
35	0.885	-0.048	0.007	0.902	0.565	-0.683	0.007	0.902
36	0.859	-0.064	0.013	0.882	0.535	-0.675	0.013	0.882
37	0.791	-0.083	0.031	0.817	0.475	-0.637	0.031	0.817
38	0.691	-0.223	0.028	0.757	0.305	-0.659	0.027	0.757
39	0.521	-0.174	0.042	0.579	0.225	-0.501	0.041	0.579
40	0.851	0.034	0.023	0.870	0.602	-0.603	0.023	0.870
41	0.906	0.029	0.023	0.921	0.636	-0.646	0.023	0.921
42	0.891	0.042	0.020	0.906	0.635	-0.626	0.020	0.906
43	0.848	0.011	0.034	0.863	0.583	-0.616	0.034	0.863
44	0.711	-0.060	0.032	0.749	0.438	-0.564	0.032	0.749

45	0.411	0.045	0.041	0.465	0.311	-0.272	0.041	0.465
46	0.106	0.007	0.017	0.202	0.077	-0.073	0.017	0.202
47	0.105	0.006	0.008	0.207	0.076	-0.073	0.008	0.207
48	0.127	0.010	0.010	0.217	0.094	-0.087	0.010	0.217
49	0.187	0.020	0.028	0.257	0.141	-0.123	0.028	0.257
50	0.251	0.050	0.036	0.309	0.207	-0.151	0.036	0.309
51	0.310	0.090	0.046	0.366	0.276	-0.167	0.046	0.366
52	0.343	0.137	0.054	0.405	0.334	-0.160	0.054	0.405
Baseline 1 – Cross Section 9								
Point	***Q*** **(L/s)**	**OSL x-coordinate (m)**	**OSL y-coordinate (m)**	**OSL z-coordinate[a] (m)**	***u*_raw[b] (m/s)**	***v*_raw[b] (m/s)**	***w*_raw[b] (m/s)**	***U*_raw[b] (m/s)**
1	282	23.461	14.427	239.08	0.426	0.083	0.068	0.580
2	282	23.461	14.427	239.06	0.388	-0.078	0.027	0.519
3	282	23.461	14.427	239.05	0.328	0.045	-0.005	0.381
4	282	23.839	14.651	239.08	1.159	0.216	0.051	1.210
5	280	23.839	14.651	239.07	1.127	0.156	0.045	1.173
6	284	23.839	14.651	239.05	1.074	0.162	0.026	1.100
7	283	23.839	14.651	239.04	1.118	0.158	0.020	1.138
8	283	24.218	14.876	239.08	1.253	0.510	0.025	1.395
9	285	24.218	14.876	239.06	1.100	0.277	0.059	1.190
10	280	24.218	14.876	239.04	1.048	0.034	-0.027	1.075
11	291	24.596	15.100	239.09	1.246	0.523	0.077	1.389
12	284	24.596	15.100	239.06	1.184	0.327	0.065	1.280
13	286	24.596	15.100	239.04	1.085	0.091	-0.005	1.140
14	286	24.975	15.324	239.09	0.695	0.067	0.015	0.726
15	284	24.975	15.324	239.06	0.718	0.053	0.001	0.753
16	284	24.975	15.324	239.04	0.615	0.001	-0.020	0.648
Point	***u*_filt[c] (m/s)**	***v*_filt[c] (m/s)**	***w*_filt[c] (m/s)**	***U*_filt[c] (m/s)**	***u*_rot[d] (m/s)**	***v*_rot[d] (m/s)**	***w*_rot[d] (m/s)**	***U*_rot[d] (m/s)**
1	0.426	0.084	0.066	0.466	0.288	-0.324	0.067	0.466
2	0.387	-0.073	0.030	0.423	0.134	-0.371	0.030	0.423
3	0.328	0.048	-0.005	0.370	0.209	-0.258	-0.005	0.370
4	1.160	0.216	0.051	1.195	0.777	-0.888	0.052	1.195
5	1.130	0.156	0.045	1.162	0.710	-0.893	0.046	1.162
6	1.076	0.162	0.026	1.099	0.688	-0.843	0.027	1.099
7	1.121	0.158	0.019	1.140	0.707	-0.884	0.020	1.140
8	1.258	0.515	0.025	1.397	1.084	-0.820	0.028	1.397
9	1.102	0.277	0.058	1.188	0.800	-0.807	0.060	1.188
10	1.049	0.032	-0.028	1.067	0.562	-0.887	-0.027	1.068
11	1.248	0.530	0.077	1.388	1.092	-0.804	0.080	1.388
12	1.186	0.342	0.065	1.281	0.898	-0.846	0.067	1.281
13	1.087	0.087	-0.008	1.133	0.628	-0.891	-0.007	1.133
14	0.695	0.066	0.015	0.726	0.411	-0.564	0.015	0.726
15	0.718	0.051	0.001	0.748	0.410	-0.592	0.001	0.748
16	0.615	0.000	-0.020	0.646	0.313	-0.529	-0.020	0.646
Baseline 2 – Cross Section 1								
Point	***Q*** **(L/s)**	**OSL x-coordinate (m)**	**OSL y-coordinate (m)**	**OSL z-coordinate[a] (m)**	***u*_raw[b] (m/s)**	***v*_raw[b] (m/s)**	***w*_raw[b] (m/s)**	***U*_raw[b] (m/s)**
1	283	13.372	11.839	239.16	1.003	0.169	-0.030	1.161
2	286	13.372	11.839	239.14	0.694	0.232	-0.054	0.797

3	282	13.125	12.008	239.17	1.232	0.128	0.078	1.440
4	286	13.125	12.008	239.15	1.257	0.487	0.006	1.456
5	285	13.125	12.008	239.13	0.980	0.301	-0.085	1.152
6	286	13.125	12.008	239.12	0.640	0.073	-0.118	0.954
7	286	12.877	12.177	239.16	0.585	-0.301	0.223	1.067
8	285	12.877	12.177	239.14	1.181	0.254	-0.040	1.325
9	286	12.877	12.177	239.12	1.079	0.193	-0.020	1.156
10	284	12.877	12.177	239.10	0.922	0.041	-0.047	1.022
11	283	12.629	12.347	239.17	1.147	0.094	0.121	1.262
12	288	12.629	12.347	239.15	1.179	0.029	0.077	1.288
13	294	12.629	12.347	239.13	1.059	0.070	0.058	1.110
14	287	12.629	12.347	239.11	0.969	0.015	0.019	1.030
15	287	12.382	12.516	239.16	1.344	0.412	-0.016	1.647
16	288	12.382	12.516	239.14	1.274	0.405	-0.007	1.541
17	287	12.382	12.516	239.12	1.177	0.394	-0.029	1.353
18	285	12.382	12.516	239.10	0.946	0.035	-0.118	1.053
19	288	12.134	12.685	239.15	1.336	0.429	-0.002	1.540
20	NaN[e]	12.134	12.685	239.13	1.342	0.497	-0.033	1.532
21	NaN[e]	12.134	12.685	239.11	1.156	0.403	-0.044	1.272
22	289	12.134	12.685	239.09	0.935	0.092	-0.089	1.200
23	288	11.886	12.855	239.17	1.002	-0.089	-0.021	1.113
24	291	11.886	12.855	239.15	0.938	-0.113	-0.053	1.023
25	289	11.886	12.855	239.13	0.852	-0.084	-0.087	0.875
26	285	11.886	12.855	239.11	0.740	-0.062	-0.124	0.794
Point	***u*_filt[c] (m/s)**	***v*_filt[c] (m/s)**	***w*_filt[c] (m/s)**	***U*_filt[c] (m/s)**	***u*_rot[d] (m/s)**	***v*_rot[d] (m/s)**	***w*_rot[d] (m/s)**	***U*_rot[d] (m/s)**
1	1.005	0.168	-0.030	1.125	0.429	0.924	-0.030	1.125
2	0.695	0.232	-0.053	0.791	0.201	0.705	-0.053	0.791
3	1.241	0.128	0.078	1.406	0.595	1.097	0.078	1.406
4	1.266	0.487	0.006	1.463	0.312	1.320	0.006	1.463
5	0.982	0.302	-0.088	1.144	0.305	0.981	-0.087	1.144
6	0.642	0.073	-0.118	0.900	0.302	0.571	-0.118	0.900
7	0.584	-0.308	0.224	1.039	0.585	0.308	0.223	1.039
8	1.187	0.198	-0.040	1.247	0.506	1.092	-0.039	1.247
9	1.083	0.195	-0.021	1.141	0.450	1.004	-0.020	1.141
10	0.926	0.037	-0.046	0.951	0.492	0.785	-0.046	0.951
11	1.155	0.093	0.118	1.198	0.575	1.006	0.118	1.198
12	1.190	0.029	0.075	1.288	0.648	0.998	0.075	1.288
13	1.062	0.054	0.058	1.091	0.555	0.907	0.058	1.091
14	0.970	0.015	0.019	1.011	0.535	0.809	0.019	1.011
15	1.347	0.412	-0.016	1.637	0.420	1.345	-0.016	1.637
16	1.278	0.405	-0.007	1.530	0.387	1.284	-0.006	1.530
17	1.184	0.403	-0.029	1.330	0.336	1.205	-0.029	1.330
18	0.951	0.035	-0.120	0.975	0.507	0.805	-0.120	0.975
19	1.338	0.429	-0.002	1.526	0.401	1.346	-0.001	1.526
20	1.347	0.497	-0.033	1.535	0.350	1.392	-0.032	1.535
21	1.158	0.443	-0.044	1.270	0.288	1.206	-0.043	1.270
22	0.939	0.092	-0.089	0.970	0.454	0.827	-0.089	0.970
23	1.004	-0.089	-0.021	1.107	0.640	0.778	-0.021	1.107
24	0.939	-0.162	-0.051	1.013	0.663	0.684	-0.051	1.013
25	0.852	-0.084	-0.087	0.874	0.550	0.656	-0.088	0.874
26	0.742	-0.062	-0.123	0.770	0.470	0.578	-0.123	0.770
Baseline 2 – Cross Section 2								

Point	*Q* (L/s)	OSL x-coordinate (m)	OSL y-coordinate (m)	OSL z-coordinate[a] (m)	*u*_raw[b] (m/s)	*v*_raw[b] (m/s)	*w*_raw[b] (m/s)	*U*_raw[b] (m/s)
1	281	14.519	14.725	239.13	-0.269	-0.005	-0.019	0.290
2	277	14.519	14.725	239.10	-0.207	0.006	-0.016	0.233
3	281	14.519	14.725	239.07	-0.068	0.019	-0.002	0.133
4	280	14.329	14.837	239.13	1.027	0.245	-0.006	1.143
5	281	14.329	14.837	239.10	1.263	0.261	-0.047	1.325
6	281	14.329	14.837	239.07	1.223	0.232	-0.092	1.277
7	282	14.329	14.837	239.04	1.157	0.214	-0.123	1.214
8	280	14.329	14.837	239.01	1.057	0.195	-0.139	1.120
9	279	14.329	14.837	238.98	0.923	0.170	-0.147	0.992
10	279	14.329	14.837	238.95	0.719	0.104	-0.114	0.779
11	281	14.329	14.837	238.93	0.623	0.103	-0.113	0.699
12	282	14.140	14.948	239.13	1.260	0.122	0.136	1.298
13	283	14.140	14.948	239.10	1.200	0.139	0.097	1.246
14	281	14.140	14.948	239.07	1.059	0.132	0.056	1.086
15	281	14.140	14.948	239.04	0.955	0.134	0.003	0.988
16	281	14.140	14.948	239.01	0.835	0.125	-0.028	0.876
17	282	14.140	14.948	238.99	0.723	0.078	-0.047	0.765
18	282	13.950	15.059	239.15	1.016	0.159	0.062	1.108
19	280	13.950	15.059	239.12	0.911	0.159	0.039	0.980
20	282	13.950	15.059	239.09	0.797	0.064	0.039	0.834
21	278	13.950	15.059	239.06	0.701	0.050	0.018	0.741
22	282	13.950	15.059	239.03	0.638	0.004	-0.007	0.678
23	284	13.950	15.059	239.02	0.510	0.007	0.003	0.562
24	282	13.760	15.171	239.13	1.308	0.254	0.056	1.456
25	283	13.760	15.171	239.10	1.245	0.281	0.023	1.394
26	285	13.760	15.171	239.07	1.082	0.020	-0.037	1.103
27	283	13.760	15.171	239.04	0.981	0.013	-0.067	1.007
28	281	13.760	15.171	239.01	0.737	-0.035	-0.051	0.775
29	279	13.760	15.171	239.12	1.116	0.286	0.056	1.249
30	285	13.570	15.282	239.09	0.994	0.029	-0.005	1.025
31	277	13.570	15.282	239.06	0.823	0.012	0.001	0.845
32	275	13.570	15.282	239.03	0.723	-0.006	-0.013	0.749
33	281	13.570	15.282	239.00	0.672	-0.045	-0.027	0.701
34	283	13.570	15.282	238.99	0.620	-0.048	-0.026	0.662
35	284	13.381	15.393	239.13	0.418	-0.034	-0.004	0.505
36	279	13.381	15.393	239.10	0.560	-0.014	-0.012	0.630
37	283	13.381	15.393	239.07	0.661	-0.001	-0.035	0.716
38	285	13.381	15.393	239.04	0.681	0.023	-0.051	0.728
39	281	13.381	15.393	239.01	0.642	0.021	-0.070	0.686
40	280	13.381	15.393	238.98	0.513	0.004	-0.047	0.560
41	281	13.191	15.505	239.14	-0.084	-0.016	0.036	0.172
42	281	13.191	15.505	239.11	-0.047	-0.020	0.041	0.144
43	281	13.191	15.505	239.08	-0.013	0.001	0.020	0.216

Point	*u*_filt[c] (m/s)	*v*_filt[c] (m/s)	*w*_filt[c] (m/s)	*U*_filt[c] (m/s)	*u*_rot[d] (m/s)	*v*_rot[d] (m/s)	*w*_rot[d] (m/s)	*U*_rot[d] (m/s)
1	-0.269	-0.005	-0.019	0.288	-0.132	-0.235	-0.019	0.288
2	-0.207	0.006	-0.016	0.232	-0.110	-0.175	-0.016	0.232
3	-0.068	0.019	-0.002	0.132	-0.051	-0.049	-0.002	0.132
4	1.041	0.245	-0.005	1.111	0.316	1.022	-0.004	1.111
5	1.267	0.249	-0.047	1.314	0.427	1.219	-0.045	1.314

6	1.226	0.228	-0.092	1.270	0.423	1.173	-0.090	1.270
7	1.159	0.212	-0.123	1.207	0.403	1.107	-0.121	1.207
8	1.058	0.195	-0.139	1.112	0.367	1.012	-0.138	1.112
9	0.923	0.171	-0.147	0.981	0.319	0.883	-0.146	0.981
10	0.719	0.104	-0.114	0.775	0.274	0.673	-0.113	0.775
11	0.623	0.105	-0.113	0.691	0.225	0.591	-0.112	0.691
12	1.261	0.121	0.136	1.289	0.535	1.149	0.137	1.289
13	1.201	0.146	0.097	1.239	0.483	1.109	0.098	1.239
14	1.060	0.132	0.056	1.086	0.423	0.981	0.057	1.086
15	0.957	0.134	0.003	0.987	0.368	0.893	0.004	0.987
16	0.836	0.125	-0.028	0.874	0.315	0.784	-0.028	0.874
17	0.723	0.078	-0.047	0.762	0.299	0.664	-0.046	0.762
18	1.023	0.160	0.062	1.101	0.380	0.963	0.063	1.101
19	0.912	0.157	0.039	0.968	0.326	0.866	0.040	0.968
20	0.798	0.064	0.039	0.831	0.349	0.720	0.039	0.831
21	0.701	0.051	0.018	0.736	0.311	0.631	0.018	0.736
22	0.638	0.004	-0.007	0.672	0.319	0.553	-0.007	0.672
23	0.509	0.007	0.003	0.555	0.252	0.442	0.003	0.555
24	1.309	0.254	0.056	1.457	0.444	1.257	0.057	1.457
25	1.247	0.281	0.023	1.387	0.388	1.217	0.024	1.387
26	1.083	0.019	-0.037	1.102	0.532	0.944	-0.037	1.102
27	0.982	0.013	-0.067	1.004	0.485	0.853	-0.067	1.004
28	0.737	-0.035	-0.050	0.771	0.404	0.618	-0.050	0.771
29	1.117	0.286	0.056	1.247	0.319	1.108	0.057	1.247
30	0.994	0.024	-0.005	1.015	0.482	0.870	-0.004	1.015
31	0.823	0.013	0.001	0.843	0.406	0.716	0.001	0.843
32	0.723	-0.006	-0.012	0.747	0.371	0.620	-0.012	0.747
33	0.672	-0.045	-0.026	0.699	0.379	0.557	-0.027	0.699
34	0.620	-0.048	-0.024	0.646	0.355	0.510	-0.024	0.646
35	0.417	-0.035	-0.004	0.499	0.241	0.342	-0.004	0.499
36	0.560	-0.015	-0.012	0.625	0.296	0.475	-0.012	0.625
37	0.661	-0.001	-0.035	0.713	0.336	0.570	-0.035	0.713
38	0.681	0.024	-0.051	0.724	0.324	0.599	-0.051	0.724
39	0.642	0.020	-0.070	0.681	0.307	0.564	-0.070	0.681
40	0.513	0.003	-0.046	0.555	0.257	0.444	-0.046	0.555
41	-0.084	-0.016	0.036	0.158	-0.029	-0.081	0.036	0.158
42	-0.047	-0.020	0.041	0.134	-0.006	-0.051	0.041	0.134
43	-0.016	0.000	0.021	0.156	-0.008	-0.014	0.021	0.156
Baseline 2 – Cross Section 3								
Point	***Q*** **(L/s)**	**OSL x-coordinate (m)**	**OSL y-coordinate (m)**	**OSL z-coordinate[a] (m)**	***u*_raw[b] (m/s)**	***v*_raw[b] (m/s)**	***w*_raw[b] (m/s)**	***U*_raw[b] (m/s)**
1	280	15.956	16.488	239.14	0.150	0.018	-0.011	0.178
2	276	15.745	16.656	239.14	0.504	-0.020	0.000	0.517
3	NaN[e]	15.745	16.656	239.09	0.532	-0.050	-0.004	0.549
4	278	15.745	16.656	239.06	0.426	-0.027	-0.014	0.440
5	283	15.534	16.824	239.14	0.836	-0.056	0.006	0.862
6	281	15.534	16.824	239.09	0.725	-0.050	0.017	0.752
7	279	15.534	16.824	239.06	0.671	-0.052	0.010	0.696
8	278	15.323	16.993	239.14	0.972	0.013	0.004	1.122
9	286	15.323	16.993	239.09	0.908	0.003	-0.023	0.926
10	280	15.323	16.993	239.04	0.755	-0.044	0.034	0.781
11	281	15.323	16.993	238.99	0.548	-0.007	-0.038	0.591

12	279	15.112	17.161	239.14	0.933	0.139	0.014	0.975
13	277	15.112	17.161	239.09	0.889	0.071	-0.010	0.907
14	279	15.112	17.161	239.04	0.851	0.022	0.004	0.868
15	NaN[e]	15.112	17.161	238.99	0.750	-0.013	0.006	0.773
16	281	15.112	17.161	238.96	0.630	-0.034	-0.020	0.656
17	285	14.901	17.330	239.14	0.991	0.128	0.015	1.027
18	283	14.901	17.330	239.09	0.916	0.102	-0.006	0.938
19	283	14.901	17.330	239.04	0.812	0.103	-0.008	0.836
20	281	14.901	17.330	238.99	0.683	0.046	-0.005	0.704
21	NaN[e]	14.901	17.330	238.94	0.578	-0.008	-0.013	0.627
22	283	14.690	17.498	239.14	0.462	0.041	0.003	0.497
23	282	14.690	17.498	239.09	0.527	0.064	-0.007	0.568
24	278	14.690	17.498	239.04	0.577	0.083	-0.018	0.617
25	286	14.690	17.498	238.99	0.553	0.075	-0.027	0.596
26	278	14.690	17.498	238.94	0.485	0.035	-0.020	0.514
27	280	14.690	17.498	238.91	0.441	0.021	-0.020	0.466
28	283	14.479	17.666	239.14	0.031	-0.015	0.009	0.157
29	284	14.479	17.666	239.09	0.035	-0.014	0.013	0.171
30	282	14.479	17.666	239.04	0.073	0.007	0.007	0.172
Point	***u*_filt[c] (m/s)**	***v*_filt[c] (m/s)**	***w*_filt[c] (m/s)**	***U*_filt[c] (m/s)**	***u*_rot[d] (m/s)**	***v*_rot[d] (m/s)**	***w*_rot[d] (m/s)**	***U*_rot[d] (m/s)**
1	0.150	0.018	-0.011	0.174	0.079	0.129	-0.011	0.174
2	0.504	-0.019	0.000	0.517	0.330	0.382	0.000	0.517
3	0.532	-0.050	-0.003	0.544	0.370	0.385	-0.003	0.544
4	0.426	-0.027	-0.013	0.439	0.286	0.316	-0.014	0.439
5	0.837	-0.059	0.006	0.854	0.568	0.617	0.006	0.854
6	0.725	-0.050	0.017	0.743	0.491	0.536	0.017	0.743
7	0.671	-0.052	0.011	0.690	0.459	0.493	0.011	0.690
8	0.974	0.017	0.004	1.093	0.594	0.771	0.004	1.093
9	0.908	0.003	-0.023	0.921	0.564	0.712	-0.023	0.921
10	0.755	-0.044	0.035	0.771	0.505	0.562	0.035	0.771
11	0.549	-0.007	-0.037	0.575	0.348	0.425	-0.037	0.575
12	0.933	0.147	0.014	0.962	0.467	0.821	0.014	0.962
13	0.889	0.071	-0.010	0.904	0.499	0.739	-0.010	0.904
14	0.851	0.022	0.004	0.865	0.514	0.679	0.004	0.865
15	0.751	-0.013	0.006	0.766	0.479	0.579	0.006	0.766
16	0.630	-0.034	-0.020	0.651	0.420	0.472	-0.020	0.651
17	0.991	0.136	0.015	1.021	0.512	0.859	0.015	1.021
18	0.916	0.102	-0.006	0.938	0.492	0.780	-0.006	0.938
19	0.812	0.103	-0.008	0.836	0.426	0.699	-0.008	0.836
20	0.683	0.045	-0.005	0.703	0.391	0.562	-0.005	0.703
21	0.578	-0.008	-0.012	0.599	0.367	0.447	-0.012	0.599
22	0.461	0.040	0.003	0.495	0.256	0.386	0.003	0.495
23	0.527	0.064	-0.007	0.563	0.279	0.452	-0.007	0.563
24	0.577	0.083	-0.018	0.610	0.295	0.502	-0.018	0.610
25	0.553	0.075	-0.027	0.587	0.286	0.479	-0.027	0.587
26	0.484	0.035	-0.019	0.510	0.275	0.400	-0.019	0.510
27	0.440	0.020	-0.020	0.465	0.259	0.357	-0.020	0.465
28	0.031	-0.016	0.009	0.143	0.031	0.014	0.009	0.143
29	0.034	-0.015	0.012	0.149	0.033	0.017	0.012	0.149
30	0.072	0.006	0.006	0.156	0.040	0.060	0.006	0.156
Baseline 2 – Cross Section 4								
Point	***Q***	**OSL x-**	**OSL y-**	**OSL z-**	***u*_raw[b]**	***v*_raw[b]**	***w*_raw[b]**	***U*_raw[b]**

	(L/s)	coordinate (m)	coordinate (m)	coordinate[a] (m)	(m/s)	(m/s)	(m/s)	(m/s)
1	286	17.262	17.610	239.14	0.209	-0.056	0.013	0.228
2	283	17.070	17.854	239.14	0.503	-0.077	-0.004	0.513
3	277	17.070	17.854	239.09	0.458	-0.086	-0.006	0.474
4	279	17.070	17.854	239.07	0.395	-0.077	0.017	0.410
5	285	16.878	18.097	239.14	0.666	-0.082	0.004	0.677
6	283	16.878	18.097	239.09	0.614	-0.122	0.016	0.634
7	279	16.878	18.097	239.04	0.545	-0.136	0.017	0.571
8	284	16.686	18.341	239.14	0.752	-0.048	0.020	0.765
9	286	16.686	18.341	239.09	0.669	-0.064	0.010	0.687
10	279	16.686	18.341	239.04	0.555	-0.119	0.028	0.585
11	275	16.495	18.584	239.14	0.778	0.032	0.021	0.794
12	281	16.495	18.584	239.09	0.721	-0.020	0.027	0.739
13	280	16.495	18.584	239.04	0.680	-0.088	0.005	0.704
14	281	16.495	18.584	238.99	0.360	-0.071	0.005	0.392
15	283	16.303	18.828	239.14	0.869	0.130	0.004	0.904
16	281	16.303	18.828	239.09	0.821	0.070	-0.001	0.839
17	279	16.303	18.828	239.04	0.774	0.010	0.014	0.791
18	276	16.303	18.828	238.99	0.699	-0.070	0.018	0.721
19	282	16.303	18.828	238.94	0.645	-0.141	0.039	0.680
20	278	16.111	19.071	239.14	0.681	0.029	0.004	0.706
21	278	16.111	19.071	239.09	0.597	0.017	-0.003	0.625
22	280	16.111	19.071	239.04	0.566	-0.004	-0.026	0.598
23	282	16.111	19.071	238.99	0.507	-0.028	-0.031	0.545
24	276	16.111	19.071	238.94	0.351	-0.058	-0.050	0.400
25	282	15.938	19.291	239.15	0.160	-0.015	-0.015	0.203

Point	*u*_filt[c] (m/s)	*v*_filt[c] (m/s)	*w*_filt[c] (m/s)	*U*_filt[c] (m/s)	*u*_rot[d] (m/s)	*v*_rot[d] (m/s)	*w*_rot[d] (m/s)	*U*_rot[d] (m/s)
1	0.209	-0.056	0.013	0.227	0.198	0.085	0.013	0.227
2	0.503	-0.077	-0.004	0.513	0.443	0.250	-0.004	0.513
3	0.458	-0.086	-0.006	0.471	0.412	0.216	-0.006	0.471
4	0.395	-0.077	0.017	0.409	0.358	0.184	0.017	0.409
5	0.666	-0.082	0.004	0.676	0.574	0.347	0.004	0.676
6	0.614	-0.122	0.015	0.633	0.558	0.284	0.015	0.633
7	0.545	-0.136	0.018	0.571	0.513	0.230	0.017	0.571
8	0.753	-0.049	0.020	0.765	0.622	0.428	0.019	0.765
9	0.669	-0.064	0.010	0.686	0.565	0.364	0.010	0.686
10	0.555	-0.119	0.028	0.584	0.510	0.250	0.028	0.584
11	0.778	0.032	0.021	0.793	0.592	0.507	0.021	0.793
12	0.721	-0.020	0.027	0.739	0.579	0.431	0.027	0.739
13	0.680	-0.088	0.005	0.703	0.589	0.352	0.004	0.703
14	0.360	-0.071	0.005	0.390	0.327	0.167	0.005	0.390
15	0.870	0.130	0.004	0.899	0.603	0.641	0.005	0.899
16	0.822	0.070	-0.001	0.839	0.602	0.563	-0.001	0.839
17	0.774	0.010	0.014	0.791	0.602	0.487	0.014	0.791
18	0.699	-0.070	0.018	0.721	0.593	0.377	0.017	0.721
19	0.645	-0.141	0.039	0.679	0.594	0.288	0.039	0.679
20	0.681	0.029	0.004	0.702	0.517	0.444	0.004	0.702
21	0.597	0.017	-0.003	0.622	0.459	0.383	-0.003	0.622
22	0.566	-0.003	-0.026	0.593	0.447	0.347	-0.026	0.593
23	0.507	-0.028	-0.031	0.539	0.415	0.292	-0.031	0.539
24	0.350	-0.058	-0.050	0.396	0.311	0.171	-0.050	0.396

25	0.159	-0.015	-0.015	0.201	0.134	0.087	-0.015	0.201
Baseline 2 – Cross Section 5								
Point	***Q*** **(L/s)**	**OSL x-coordinate (m)**	**OSL y-coordinate (m)**	**OSL z-coordinate[a] (m)**	***u*_raw[b] (m/s)**	***v*_raw[b] (m/s)**	***w*_raw[b] (m/s)**	***U*_raw[b] (m/s)**
1	279	18.427	18.117	239.13	0.356	0.024	-0.006	0.362
2	280	18.404	18.416	239.14	0.627	0.055	0.010	0.635
3	277	18.404	18.416	239.09	0.340	0.055	0.014	0.396
4	283	18.381	18.716	239.14	0.672	0.153	-0.007	0.694
5	278	18.381	18.716	239.11	0.614	0.070	0.001	0.634
6	278	18.357	19.015	239.14	0.677	0.175	-0.014	0.714
7	277	18.357	19.015	239.09	0.556	0.025	-0.049	0.590
8	278	18.357	19.015	239.06	0.433	-0.087	0.031	0.493
9	276	18.334	19.314	239.14	0.758	0.192	0.004	0.796
10	279	18.334	19.314	239.09	0.692	0.094	0.010	0.714
11	279	18.334	19.314	239.04	0.696	-0.032	0.022	0.715
12	283	18.334	19.314	239.01	0.601	-0.064	-0.001	0.644
13	282	18.311	19.613	239.15	0.731	0.195	0.013	0.770
14	283	18.311	19.613	239.10	0.739	0.133	0.020	0.765
15	280	18.311	19.613	239.05	0.711	0.060	0.006	0.728
16	281	18.311	19.613	239.00	0.773	-0.104	-0.014	0.794
17	279	18.311	19.613	238.97	0.705	-0.073	0.080	0.731
18	284	18.311	19.613	238.95	0.660	-0.164	-0.001	0.700
19	279	18.288	19.912	239.15	0.757	0.149	-0.015	0.783
20	276	18.288	19.912	239.10	0.756	0.101	-0.026	0.775
21	279	18.288	19.912	239.05	0.743	0.056	-0.038	0.762
22	279	18.288	19.912	239.00	0.711	0.010	-0.043	0.734
23	280	18.288	19.912	238.95	0.682	-0.049	-0.043	0.717
24	280	18.288	19.912	238.90	0.622	-0.091	-0.063	0.666
25	279	18.288	19.912	238.87	0.584	-0.127	-0.066	0.644
26	284	18.288	19.912	238.85	0.497	-0.120	-0.057	0.553
27	284	18.288	19.912	238.82	0.464	-0.163	-0.055	0.545
28	279	18.288	19.912	238.80	0.402	-0.173	-0.037	0.470
29	281	18.264	20.211	239.16	0.354	0.031	-0.034	0.419
Point	***u*_filt[c] (m/s)**	***v*_filt[c] (m/s)**	***w*_filt[c] (m/s)**	***U*_filt[c] (m/s)**	***u*_rot[d] (m/s)**	***v*_rot[d] (m/s)**	***w*_rot[d] (m/s)**	***U*_rot[d] (m/s)**
1	0.355	0.024	-0.006	0.362	0.352	0.052	-0.006	0.362
2	0.628	0.055	0.010	0.634	0.621	0.104	0.010	0.634
3	0.341	0.056	0.016	0.377	0.336	0.082	0.016	0.377
4	0.672	0.153	-0.008	0.694	0.658	0.205	-0.007	0.694
5	0.615	0.070	0.001	0.631	0.608	0.118	0.001	0.631
6	0.677	0.176	-0.014	0.714	0.662	0.228	-0.014	0.714
7	0.556	0.026	-0.050	0.587	0.552	0.069	-0.050	0.587
8	0.432	-0.086	0.031	0.488	0.438	-0.052	0.031	0.488
9	0.758	0.192	0.003	0.794	0.741	0.250	0.004	0.794
10	0.692	0.094	0.010	0.713	0.683	0.148	0.010	0.713
11	0.697	-0.032	0.022	0.713	0.697	0.022	0.022	0.713
12	0.602	-0.064	-0.001	0.637	0.605	-0.017	-0.001	0.637
13	0.731	0.196	0.013	0.769	0.713	0.252	0.013	0.769
14	0.740	0.133	0.020	0.764	0.727	0.190	0.020	0.764
15	0.711	0.060	0.006	0.728	0.704	0.115	0.006	0.728
16	0.773	-0.104	-0.014	0.792	0.779	-0.043	-0.014	0.792

17	0.706	-0.073	0.080	0.729	0.709	-0.018	0.080	0.729
18	0.660	-0.164	-0.001	0.698	0.671	-0.113	-0.002	0.698
19	0.757	0.149	-0.015	0.783	0.744	0.207	-0.015	0.783
20	0.756	0.101	-0.026	0.775	0.746	0.159	-0.026	0.775
21	0.744	0.056	-0.038	0.761	0.737	0.114	-0.038	0.761
22	0.711	0.010	-0.043	0.732	0.708	0.066	-0.043	0.732
23	0.683	-0.049	-0.043	0.710	0.684	0.004	-0.043	0.710
24	0.622	-0.091	-0.063	0.661	0.627	-0.043	-0.063	0.661
25	0.584	-0.127	-0.066	0.634	0.593	-0.081	-0.066	0.634
26	0.497	-0.120	-0.056	0.550	0.505	-0.081	-0.057	0.550
27	0.463	-0.163	-0.054	0.529	0.475	-0.126	-0.054	0.529
28	0.402	-0.173	-0.037	0.468	0.414	-0.141	-0.037	0.468
29	0.353	0.031	-0.034	0.411	0.350	0.058	-0.034	0.411

Baseline 2 – Cross Section 6

Point	*Q* (L/s)	OSL x-coordinate (m)	OSL y-coordinate (m)	OSL z-coordinate[a] (m)	*u*_raw[b] (m/s)	*v*_raw[b] (m/s)	*w*_raw[b] (m/s)	*U*_raw[b] (m/s)
1	283	19.834	17.990	239.13	0.246	-0.005	-0.004	0.259
2	281	19.916	18.279	239.13	0.500	-0.036	-0.001	0.513
3	282	19.916	18.279	239.08	0.345	-0.169	0.002	0.398
4	281	19.998	18.567	239.14	0.536	0.007	0.007	0.543
5	281	19.998	18.567	239.09	0.496	-0.080	-0.044	0.520
6	280	19.998	18.567	239.04	0.444	-0.160	0.025	0.494
~~7~~[f]	~~279~~	~~19.998~~	~~18.567~~	~~238.99~~	~~0.187~~	~~-0.141~~	~~-0.035~~	~~0.311~~
8	281	20.080	18.856	239.14	0.561	0.023	0.016	0.572
9	281	20.080	18.856	239.09	0.559	-0.064	0.013	0.577
10	282	20.080	18.856	239.04	0.612	-0.160	-0.001	0.646
11	278	20.080	18.856	238.99	0.535	-0.190	-0.018	0.595
12	281	20.080	18.856	238.96	0.498	-0.226	-0.042	0.591
~~13~~[f]	~~280~~	~~20.163~~	~~19.144~~	~~239.14~~	~~0.592~~	~~0.072~~	~~0.005~~	~~0.605~~
14	284	20.163	19.144	239.09	0.610	0.004	0.025	0.622
15	281	20.163	19.144	239.04	0.641	-0.090	0.053	0.662
16	281	20.163	19.144	238.99	0.672	-0.184	0.076	0.713
17	278	20.163	19.144	238.94	0.711	-0.260	0.103	0.774
18	281	20.163	19.144	238.92	0.601	-0.239	0.107	0.670
19	284	20.245	19.433	239.14	0.656	0.014	0.001	0.663
20	281	20.245	19.433	239.09	0.673	-0.013	-0.004	0.681
21	281	20.245	19.433	239.04	0.709	-0.044	0.009	0.717
22	282	20.245	19.433	238.99	0.732	-0.081	0.013	0.744
23	285	20.245	19.433	238.94	0.768	-0.106	0.026	0.784
24	280	20.245	19.433	238.89	0.737	-0.126	0.045	0.759
25	282	20.245	19.433	238.84	0.494	-0.119	0.049	0.528
26	283	20.327	19.721	239.14	0.662	-0.022	-0.010	0.678
27	284	20.327	19.721	239.09	0.735	-0.029	-0.027	0.750
28	282	20.327	19.721	239.04	0.732	-0.040	-0.055	0.750
29	281	20.327	19.721	238.99	0.659	-0.026	-0.063	0.681
30	277	20.327	19.721	238.94	0.470	-0.054	-0.054	0.511

Point	*u*_filt[c] (m/s)	*v*_filt[c] (m/s)	*w*_filt[c] (m/s)	*U*_filt[c] (m/s)	*u*_rot[d] (m/s)	*v*_rot[d] (m/s)	*w*_rot[d] (m/s)	*U*_rot[d] (m/s)
1	0.246	-0.005	-0.004	0.251	0.235	-0.072	-0.004	0.251
2	0.501	-0.036	-0.001	0.508	0.472	-0.171	-0.001	0.508
3	0.345	-0.169	0.002	0.398	0.285	-0.257	0.002	0.398

4	0.536	0.007	0.007	0.543	0.517	-0.140	0.007	0.543
5	0.496	-0.080	-0.044	0.520	0.455	-0.213	-0.044	0.520
6	0.444	-0.160	0.025	0.493	0.383	-0.276	0.025	0.493
~~7~~[f]	~~0.186~~	~~-0.141~~	~~-0.034~~	~~0.288~~	~~0.141~~	~~-0.186~~	~~-0.034~~	~~0.288~~
8	0.561	0.023	0.016	0.571	0.546	-0.132	0.016	0.571
9	0.559	-0.063	0.013	0.577	0.520	-0.214	0.013	0.577
10	0.613	-0.160	-0.001	0.646	0.545	-0.321	-0.001	0.646
11	0.535	-0.191	-0.018	0.593	0.463	-0.330	-0.018	0.593
12	0.499	-0.226	-0.042	0.572	0.418	-0.354	-0.042	0.572
~~13~~[f]	~~0.592~~	~~0.072~~	~~0.005~~	~~0.604~~	~~0.589~~	~~-0.093~~	~~0.005~~	~~0.604~~
14	0.610	0.004	0.025	0.621	0.588	-0.163	0.025	0.621
15	0.641	-0.090	0.053	0.661	0.591	-0.262	0.053	0.661
16	0.672	-0.184	0.076	0.711	0.596	-0.361	0.076	0.711
17	0.711	-0.260	0.103	0.771	0.613	-0.445	0.102	0.771
18	0.602	-0.240	0.107	0.669	0.514	-0.396	0.107	0.669
19	0.656	0.014	0.001	0.663	0.634	-0.166	0.001	0.663
20	0.673	-0.013	-0.004	0.680	0.644	-0.197	-0.004	0.680
21	0.709	-0.044	0.009	0.717	0.669	-0.237	0.009	0.717
22	0.732	-0.081	0.013	0.743	0.682	-0.279	0.013	0.743
23	0.769	-0.106	0.026	0.784	0.710	-0.312	0.026	0.784
24	0.738	-0.126	0.045	0.759	0.675	-0.323	0.045	0.759
25	0.494	-0.120	0.049	0.527	0.443	-0.251	0.049	0.527
26	0.663	-0.021	-0.010	0.677	0.631	-0.202	-0.010	0.677
27	0.736	-0.028	-0.027	0.748	0.700	-0.229	-0.027	0.748
28	0.733	-0.039	-0.056	0.748	0.694	-0.239	-0.056	0.748
29	0.660	-0.026	-0.064	0.679	0.627	-0.206	-0.064	0.679
30	0.470	-0.054	-0.054	0.505	0.437	-0.180	-0.054	0.505

Baseline 2 – Cross Section 7

Point	*Q* (L/s)	OSL x-coordinate (m)	OSL y-coordinate (m)	OSL z-coordinate[a] (m)	*u*_raw[b] (m/s)	*v*_raw[b] (m/s)	*w*_raw[b] (m/s)	*U*_raw[b] (m/s)
1	281	20.921	17.309	239.13	0.101	-0.027	0.025	0.137
2	279	21.079	17.552	239.13	0.563	-0.102	-0.002	0.579
3	286	21.079	17.552	239.08	0.569	-0.118	-0.001	0.592
4	283	21.079	17.552	239.03	0.459	-0.152	-0.121	0.523
5	279	21.237	17.795	239.13	0.598	-0.086	0.017	0.619
6	282	21.232	17.787	239.08	0.645	-0.118	-0.036	0.671
7	287	21.237	17.795	239.06	0.571	-0.129	-0.048	0.606
8	286	21.395	18.039	239.13	0.703	-0.096	0.004	0.717
9	280	21.395	18.039	239.08	0.724	-0.106	0.014	0.742
10	277	21.395	18.039	239.03	0.531	-0.115	0.016	0.592
11	283	21.553	18.282	239.13	0.752	-0.047	0.014	0.760
12	282	21.553	18.282	239.08	0.825	-0.123	0.014	0.842
13	282	21.553	18.282	239.03	0.753	-0.084	0.034	0.773
14	281	21.553	18.282	238.98	0.475	-0.076	0.005	0.544
15	280	21.711	18.525	239.13	0.800	-0.020	0.012	0.807
16	285	21.711	18.525	239.08	0.843	-0.053	0.023	0.852
17	283	21.711	18.525	239.03	0.835	-0.079	0.029	0.845
18	282	21.711	18.525	238.98	0.771	-0.140	-0.006	0.795
19	285	21.711	18.525	238.96	0.627	-0.161	0.012	0.661
20	283	21.869	18.769	239.14	0.824	-0.015	-0.014	0.829
21	283	21.869	18.769	239.09	0.819	-0.009	-0.019	0.824
22	281	21.869	18.769	239.04	0.832	-0.021	-0.003	0.836

23	NaN[e]	21.869	18.769	238.99	0.832	-0.071	-0.005	0.840
24	279	21.869	18.769	238.94	0.716	-0.126	0.024	0.745
25	283	21.869	18.769	238.91	0.578	-0.190	0.018	0.624
26	282	21.999	18.970	239.15	0.591	-0.023	0.018	0.624
27	282	21.999	18.970	239.10	0.517	-0.005	-0.019	0.557
28	279	21.999	18.970	239.07	0.421	0.036	-0.005	0.473
Point	***u*_filt[c] (m/s)**	***v*_filt[c] (m/s)**	***w*_filt[c] (m/s)**	***U*_filt[c] (m/s)**	***u*_rot[d] (m/s)**	***v*_rot[d] (m/s)**	***w*_rot[d] (m/s)**	***U*_rot[d] (m/s)**
1	0.100	-0.026	0.025	0.135	0.070	-0.077	0.025	0.135
2	0.563	-0.102	-0.003	0.579	0.417	-0.392	-0.003	0.579
3	0.569	-0.118	-0.001	0.591	0.413	-0.409	-0.001	0.591
4	0.460	-0.152	-0.121	0.520	0.303	-0.378	-0.122	0.520
5	0.599	-0.086	0.016	0.618	0.456	-0.399	0.016	0.618
6	0.645	-0.118	-0.035	0.669	0.477	-0.450	-0.036	0.669
7	0.572	-0.129	-0.048	0.604	0.409	-0.419	-0.048	0.604
8	0.703	-0.096	0.004	0.717	0.538	-0.463	0.004	0.717
9	0.725	-0.106	0.013	0.741	0.550	-0.484	0.013	0.741
10	0.533	-0.115	0.017	0.582	0.384	-0.387	0.017	0.582
11	0.752	-0.046	0.013	0.760	0.606	-0.448	0.013	0.760
12	0.825	-0.123	0.014	0.842	0.626	-0.552	0.014	0.842
13	0.754	-0.084	0.035	0.768	0.586	-0.481	0.035	0.768
14	0.475	-0.076	0.006	0.532	0.357	-0.323	0.006	0.532
15	0.800	-0.020	0.012	0.806	0.660	-0.452	0.012	0.806
16	0.844	-0.052	0.023	0.852	0.679	-0.503	0.023	0.852
17	0.835	-0.079	0.029	0.845	0.658	-0.521	0.028	0.845
18	0.771	-0.140	-0.005	0.791	0.571	-0.537	-0.006	0.791
19	0.627	-0.162	0.012	0.658	0.438	-0.477	0.012	0.658
20	0.824	-0.014	-0.014	0.828	0.683	-0.460	-0.014	0.828
21	0.819	-0.009	-0.019	0.824	0.682	-0.453	-0.019	0.824
22	0.832	-0.021	-0.003	0.836	0.686	-0.471	-0.003	0.836
23	0.832	-0.071	-0.006	0.840	0.660	-0.512	-0.006	0.840
24	0.717	-0.126	0.024	0.739	0.532	-0.496	0.024	0.739
25	0.578	-0.190	0.018	0.623	0.382	-0.474	0.018	0.623
26	0.592	-0.023	0.018	0.617	0.484	-0.341	0.018	0.617
27	0.517	-0.004	-0.020	0.549	0.432	-0.285	-0.020	0.549
28	0.421	0.037	-0.005	0.465	0.374	-0.198	-0.005	0.465
Baseline 2 – Cross Section 8								
Point	***Q* (L/s)**	**OSL x-coordinate (m)**	**OSL y-coordinate (m)**	**OSL z-coordinate[a] (m)**	***u*_raw[b] (m/s)**	***v*_raw[b] (m/s)**	***w*_raw[b] (m/s)**	***U*_raw[b] (m/s)**
1	284	22.091	16.375	239.12	0.673	-0.054	-0.007	0.684
2	281	22.091	16.375	239.09	0.601	-0.097	0.006	0.625
3	278	22.091	16.375	239.07	0.411	-0.060	-0.012	0.453
4	285	22.264	16.534	239.12	0.763	-0.067	-0.003	0.770
5	282	22.264	16.534	239.09	0.718	-0.069	-0.028	0.728
6	279	22.264	16.534	239.06	0.683	-0.089	-0.022	0.699
7	283	22.264	16.534	239.03	0.674	-0.080	-0.011	0.691
8	276	22.264	16.534	239.01	0.619	-0.114	0.006	0.635
9	284	22.437	16.693	239.12	0.778	-0.096	-0.006	0.790
10	280	22.437	16.693	239.09	0.787	-0.075	-0.023	0.796
11	277	22.437	16.693	239.06	0.713	-0.044	0.003	0.726
12	279	22.437	16.693	239.03	0.660	-0.037	-0.040	0.678

13	277	22.609	16.852	239.12	0.835	-0.109	-0.002	0.848
14	278	22.609	16.852	239.09	0.762	-0.080	-0.005	0.776
15	280	22.609	16.852	239.06	0.805	-0.153	-0.018	0.838
16	278	22.609	16.852	239.03	0.708	-0.147	-0.020	0.756
17	280	22.782	17.012	239.12	0.817	-0.086	0.005	0.826
18	280	22.782	17.012	239.09	0.844	-0.095	-0.015	0.855
19	285	22.782	17.012	239.06	0.820	-0.126	-0.013	0.837
20	282	22.782	17.012	239.03	0.732	-0.103	-0.042	0.752
21	279	22.782	17.012	239.02	0.478	-0.102	0.012	0.531
22	274	22.955	17.171	239.12	0.845	-0.092	0.006	0.854
23	280	22.955	17.171	239.09	0.828	-0.106	0.002	0.839
24	285	22.955	17.171	239.06	0.897	-0.156	-0.006	0.915
25	280	22.955	17.171	239.03	0.834	-0.168	0.005	0.856
26	278	22.955	17.171	239.02	0.751	-0.210	-0.006	0.788
27	280	23.128	17.330	239.12	0.883	-0.069	0.002	0.889
28	281	23.128	17.330	239.09	0.886	-0.094	0.012	0.894
29	282	23.128	17.330	239.06	0.875	-0.082	0.011	0.883
30	279	23.128	17.330	239.03	0.848	-0.115	0.012	0.860
31	281	23.128	17.330	239.00	0.802	-0.174	0.007	0.828
32	286	23.128	17.330	238.97	0.649	-0.170	0.049	0.687
33	285	23.128	17.330	238.96	0.497	-0.202	0.054	0.578
34	283	23.301	17.489	239.14	0.803	-0.078	-0.008	0.814
35	284	23.301	17.489	239.11	0.844	-0.016	-0.012	0.850
36	283	23.301	17.489	239.08	0.873	-0.009	-0.006	0.878
37	285	23.301	17.489	239.05	0.847	0.001	0.009	0.853
38	283	23.301	17.489	239.02	0.788	-0.011	-0.006	0.797
39	285	23.301	17.489	238.99	0.680	-0.035	0.014	0.711
40	284	23.474	17.648	239.14	-0.038	-0.030	-0.020	0.153
41	278	23.474	17.648	239.11	0.015	-0.003	0.024	0.163
42	283	23.474	17.648	239.08	0.060	0.023	0.049	0.217
43	281	23.474	17.648	239.05	0.073	0.031	0.074	0.278

Point	***u*_filt[c] (m/s)**	***v*_filt[c] (m/s)**	***w*_filt[c] (m/s)**	***U*_filt[c] (m/s)**	***u*_rot[d] (m/s)**	***v*_rot[d] (m/s)**	***w*_rot[d] (m/s)**	***U*_rot[d] (m/s)**
1	0.673	-0.054	-0.006	0.684	0.416	-0.532	-0.007	0.684
2	0.602	-0.098	0.006	0.618	0.336	-0.509	0.006	0.618
3	0.412	-0.060	-0.012	0.442	0.235	-0.343	-0.012	0.442
4	0.763	-0.066	-0.003	0.770	0.468	-0.606	-0.003	0.770
5	0.718	-0.068	-0.028	0.728	0.436	-0.575	-0.029	0.728
6	0.684	-0.089	-0.023	0.699	0.398	-0.564	-0.024	0.699
7	0.675	-0.080	-0.010	0.690	0.398	-0.551	-0.011	0.690
8	0.619	-0.113	0.006	0.635	0.336	-0.532	0.005	0.635
9	0.779	-0.096	-0.006	0.789	0.457	-0.638	-0.007	0.789
10	0.788	-0.075	-0.023	0.796	0.478	-0.630	-0.023	0.796
11	0.714	-0.045	0.003	0.725	0.451	-0.555	0.003	0.725
12	0.661	-0.036	-0.040	0.676	0.421	-0.510	-0.040	0.676
13	0.836	-0.109	-0.002	0.848	0.486	-0.689	-0.003	0.848
14	0.763	-0.080	-0.005	0.775	0.458	-0.615	-0.006	0.775
15	0.806	-0.153	-0.018	0.827	0.433	-0.696	-0.019	0.827
16	0.708	-0.147	-0.018	0.735	0.372	-0.621	-0.019	0.735
17	0.817	-0.086	0.005	0.826	0.490	-0.659	0.005	0.826
18	0.845	-0.095	-0.015	0.855	0.503	-0.685	-0.015	0.855
19	0.821	-0.126	-0.013	0.837	0.463	-0.689	-0.014	0.837
20	0.733	-0.103	-0.042	0.751	0.421	-0.608	-0.043	0.751

21	0.479	-0.102	0.012	0.527	0.249	-0.421	0.012	0.527
22	0.845	-0.092	0.005	0.854	0.505	-0.684	0.005	0.854
23	0.828	-0.106	0.002	0.839	0.483	-0.681	0.002	0.839
24	0.898	-0.156	-0.006	0.915	0.493	-0.766	-0.007	0.915
25	0.834	-0.168	0.005	0.856	0.441	-0.727	0.004	0.856
26	0.751	-0.209	-0.007	0.788	0.355	-0.695	-0.008	0.788
27	0.883	-0.069	0.002	0.889	0.547	-0.697	0.002	0.889
28	0.886	-0.093	0.012	0.894	0.531	-0.715	0.011	0.894
29	0.875	-0.082	0.010	0.883	0.533	-0.700	0.010	0.883
30	0.848	-0.115	0.012	0.860	0.490	-0.702	0.011	0.860
31	0.802	-0.173	0.007	0.828	0.416	-0.708	0.006	0.828
32	0.649	-0.170	0.049	0.687	0.315	-0.593	0.048	0.687
33	0.497	-0.202	0.055	0.561	0.188	-0.503	0.053	0.561
34	0.804	-0.077	-0.007	0.814	0.488	-0.643	-0.008	0.814
35	0.844	-0.015	-0.011	0.849	0.560	-0.631	-0.012	0.849
36	0.873	-0.009	-0.006	0.878	0.585	-0.649	-0.006	0.878
37	0.848	0.001	0.009	0.854	0.575	-0.623	0.009	0.854
38	0.788	-0.010	-0.007	0.796	0.527	-0.587	-0.007	0.796
39	0.683	-0.034	0.011	0.704	0.438	-0.526	0.011	0.704
40	-0.038	-0.031	-0.021	0.140	-0.049	0.008	-0.021	0.140
41	0.014	-0.003	0.023	0.139	0.007	-0.012	0.023	0.139
42	0.060	0.022	0.048	0.166	0.057	-0.029	0.049	0.166
43	0.073	0.031	0.076	0.187	0.072	-0.032	0.076	0.187
Baseline 2 – Cross Section 9								
Point	***Q*** **(L/s)**	**OSL x-coordinate (m)**	**OSL y-coordinate (m)**	**OSL z-coordinate[a] (m)**	***u*_raw[b] (m/s)**	***v*_raw[b] (m/s)**	***w*_raw[b] (m/s)**	***U*_raw[b] (m/s)**
1	284	23.414	14.486	239.09	0.086	-0.005	0.010	0.224
2	277	23.414	14.486	239.06	0.138	0.006	0.003	0.263
3	280	23.414	14.486	239.03	0.084	0.014	-0.010	0.184
4	277	23.724	14.670	239.09	0.974	0.131	0.024	0.991
5	281	23.724	14.670	239.06	1.002	0.118	0.016	1.015
6	279	23.724	14.670	239.03	0.918	0.103	0.017	0.931
7	282	23.724	14.670	239.02	0.893	0.104	0.004	0.907
8	277	24.034	14.853	239.09	1.036	0.069	0.053	1.063
9	280	24.034	14.853	239.06	0.901	0.078	0.000	0.913
10	283	24.034	14.853	239.03	0.925	0.079	0.004	0.938
11	284	24.034	14.853	239.01	0.849	0.046	0.005	0.863
12	278	24.343	15.037	239.08	1.208	0.164	-0.043	1.334
13	283	24.343	15.037	239.05	1.127	0.110	-0.024	1.151
14	283	24.343	15.037	239.02	1.071	0.043	-0.036	1.081
15	284	24.343	15.037	238.99	0.891	0.003	-0.002	0.904
16	283	24.653	15.220	239.09	1.151	0.038	0.002	1.193
17	282	24.653	15.220	239.06	1.070	0.004	0.002	1.081
18	281	24.653	15.220	239.03	0.929	-0.003	-0.015	0.946
19	282	24.653	15.220	239.00	0.774	-0.019	-0.024	0.798
20	280	24.653	15.220	238.98	0.712	0.006	-0.036	0.738
21	278	24.963	15.404	239.09	0.516	0.011	0.010	0.541
22	277	24.963	15.404	239.06	0.467	0.003	0.004	0.495
23	281	24.963	15.404	239.03	0.369	-0.025	-0.008	0.405
24	277	24.963	15.404	239.01	0.289	-0.025	0.001	0.344
Point	***u*_filt[c]**	***v*_filt[c]**	***w*_filt[c]**	***U*_filt[c]**	***u*_rot[d]**	***v*_rot[d]**	***w*_rot[d]**	***U*_rot[d]**

	(m/s)	(m/s)	(m/s)	(m/s)	(m/s)	(m/s)	(m/s)	(m/s)
1	0.084	-0.006	0.008	0.184	0.038	-0.075	0.008	0.184
2	0.138	0.007	0.002	0.223	0.076	-0.115	0.002	0.223
3	0.080	0.015	-0.010	0.161	0.054	-0.061	-0.010	0.161
4	0.975	0.131	0.024	0.988	0.610	-0.772	0.024	0.988
5	1.004	0.118	0.015	1.015	0.614	-0.803	0.016	1.015
6	0.918	0.103	0.017	0.930	0.557	-0.737	0.017	0.930
7	0.894	0.104	0.004	0.906	0.546	-0.715	0.004	0.906
8	1.038	0.070	0.051	1.048	0.589	-0.858	0.051	1.048
9	0.901	0.078	0.000	0.912	0.527	-0.735	0.000	0.912
10	0.925	0.079	0.004	0.937	0.540	-0.755	0.004	0.937
11	0.850	0.046	0.005	0.862	0.473	-0.707	0.005	0.862
12	1.209	0.164	-0.043	1.333	0.758	-0.956	-0.042	1.333
13	1.131	0.110	-0.025	1.142	0.671	-0.917	-0.024	1.142
14	1.072	0.043	-0.036	1.081	0.584	-0.900	-0.036	1.081
15	0.892	0.003	-0.001	0.902	0.457	-0.766	-0.001	0.902
16	1.153	0.056	0.000	1.182	0.636	-0.963	0.001	1.182
17	1.072	0.005	0.001	1.081	0.551	-0.920	0.001	1.082
18	0.930	-0.002	-0.015	0.946	0.472	-0.801	-0.015	0.946
19	0.775	-0.019	-0.024	0.797	0.379	-0.676	-0.024	0.797
20	0.713	0.006	-0.036	0.737	0.369	-0.610	-0.036	0.737
21	0.515	0.011	0.010	0.539	0.272	-0.438	0.010	0.539
22	0.467	0.003	0.005	0.493	0.240	-0.400	0.005	0.493
23	0.368	-0.025	-0.008	0.401	0.166	-0.329	-0.008	0.401
24	0.288	-0.026	0.003	0.323	0.124	-0.261	0.003	0.323

[a] Elevation relative to sea level

[b] Raw data, unfiltered and in coordinates relative to the ADV (local coordinates)

[c] Data filtered using the modified PST technique

[d] Data filtered an rotated into OSL x, y, and z coordinates

[e] Not reported/measured

[f] Record suspected to be corrupt and therefore omitted from analysis

Appendix C: Results From All Experiments

The results from each individual profile are contained in Appendix C. Results from individual profiles were averaged and reported in this thesis, except for data obtained by Balakrishnan (1997) in which case each profile was analyzed separately.

Table C1: Results from Baseline1 experiment in the OSL.

Cross Section	Vertical Profile	k_s (cm)	z_0 (cm)	d_h (cm)	d_h/k_s	R^2
3	3	5	0.17	8.98	1.80	1.000
3	4	5	0.17	2.02	0.40	0.997
3	5	5	0.17	-0.84	-0.17	0.908
4	3	5	0.17	8.62	1.72	1.000
4	4	5	0.17	-0.87	-0.17	0.996
4	5	5	0.17	1.68	0.34	0.950
4	6	5	0.17	-1.04	-0.21	0.991
5	3	5	0.17	5.14	1.03	1.000
5	4	5	0.17	8.45	1.69	1.000
5	6	5	0.17	4.23	0.85	0.939
6	2	5	0.17	3.74	0.75	1.000
6	3	5	0.17	2.70	0.54	0.988
6	5	5	0.17	-2.71	-0.54	0.868
7	4	5	0.17	4.02	0.80	0.920
7	5	5	0.17	2.66	0.53	0.966
7	6	5	0.17	3.32	0.66	0.991
8	3	5	0.17	1.01	0.20	0.920
8	4	5	0.17	-0.43	-0.09	0.575
8	5	5	0.17	-0.91	-0.18	0.913
8	6	5	0.17	-2.42	-0.48	0.985
			Average	2.37	0.47	0.945

Table C2: Results from Baseline2 experiment in the OSL.

Cross Section	Vertical Profile	k_s (cm)	z_0 (cm)	d_h (cm)	d_h/k_s	R^2
3	3	5	0.17	2.88	0.58	0.967
3	4	5	0.17	2.15	0.43	0.988
3	5	5	0.17	6.77	1.35	0.985
4	2	5	0.17	4.13	0.83	0.975
4	3	5	0.17	8.94	1.79	1.000
4	4	5	0.17	3.79	0.76	0.995
4	5	5	0.17	9.30	1.86	0.968
4	6	5	0.17	5.49	1.10	0.972
5	2	5	0.17	0.92	0.18	1.000
5	3	5	0.17	1.39	0.28	1.000
5	4	5	0.17	0.17	0.03	1.000
5	5	5	0.17	5.21	1.04	0.819
5	6	5	0.17	-0.31	-0.06	0.960
5	7	5	0.17	-0.35	-0.07	0.973
6	2	5	0.17	-0.24	-0.05	1.000
6	3	5	0.17	3.68	0.74	0.998
6	4	5	0.17	0.04	0.01	0.084
6	6	5	0.17	1.37	0.27	0.652
7	3	5	0.17	1.81	0.36	1.000
7	4	5	0.17	1.16	0.23	1.000
7	5	5	0.17	6.91	1.38	1.000
7	6	5	0.17	3.84	0.77	0.866
7	7	5	0.17	-0.32	-0.06	0.941
8	3	5	0.17	0.34	0.07	0.962
8	4	5	0.17	0.73	0.15	0.658
8	5	5	0.17	-4.84	-0.97	0.894
8	6	5	0.17	-7.04	-1.41	0.969
8	7	5	0.17	-5.91	-1.18	0.956
			Average	1.86	0.37	0.916

Table C3: Results from bedform flume experiment.

k_s (cm)	z_0 (cm)	d_h (cm)	d_h/k_s	R^2	Comments
2.34	0.08	0.80	0.34	0.955	k_s = bedform height = 2.3 cm

Table C4: Results from analysis using data collected by Kanellopoulos (1998).

k_s (cm)	z_0 (cm)	d_h (cm)	d_h/k_s	R^2	Comments
0.8	0.03	0.16	0.20	0.996	k_s = sphere diameter = 8 mm

Table C5: Results from analysis using data collected by Liu et al. (2008).

Experiment	k_s (cm)	z_0 (cm)	d_h (cm)	d_h/k_s	R^2	Comments
L1 (3.1)	7.62	0.25	1.97	0.26	0.999	ks = dowel height = 7.62 cm
L2 (3.2)	7.62	0.25	1.93	0.25	0.988	ks = dowel height = 7.62 cm
L3 (3.3)	7.62	0.25	1.83	0.24	0.995	ks = dowel height = 7.62 cm
L4 (3.4)	7.62	0.25	2.26	0.30	0.993	ks = dowel height = 7.62 cm
		Average	2.00	0.26	0.994	

Table C6: Results from analysis using data collected by Balakrishnan (1997).

Experiment	k_s (cm)	z_0 (cm)	d_h (cm)	d_h/k_s	R^2	Comments
2%	0.8	0.03	0.09	0.11	0.666	ks = sphere diameter = 8 mm
20%	0.8	0.03	0.09	0.11	0.569	ks = sphere diameter = 8 mm
35%	0.8	0.03	0.13	0.16	0.926	ks = sphere diameter = 8 mm
50%	0.8	0.03	0.07	0.08	0.407	ks = sphere diameter = 8 mm

Appendix D: MATLAB Codes

Code calculates the depth at each vertical as well as the value of y/H (depthCalc_jrp.m).

```
function [output1,output2,output3] = depthCalc_jrp(yz_data,wsbed_prof)

%%%% matrix 'wsbed_mod' contains bed and water surface profile data shifted
%%%% to account for the offset of the point gauge from the ADV
wsbed_mod = zeros(length(wsbed_prof),2);
wsbed_mod(:,1) = (wsbed_prof(:,1) + 110)/10;  % COL1: shifted x-coordinate (cm)
wsbed_mod(:,2) = wsbed_prof(:,3) - wsbed_prof(:,2);  % COL2: depth (cm)

%%%% matrix 'meas_pts' contains measurement locations such that the
%%%% y-coordinate is the measurement elevation above the bed
meas_pts = zeros(length(yz_data),2);
meas_pts(:,1) = yz_data(:,1)/10;  % COL1: x-coordinate of velocity measurement (cm)

%%%% Determine the number of vertical profiles and save what point they start at (if more than 22 profiles,
%%%% changes will be needed)
num_verts = 1;
temp_begin_pt = zeros(22,1);
temp_begin_pt(1) = 1;
m=2;
for j=2:length(yz_data),
   if abs(yz_data(j-1,1) - yz_data(j,1)) > 0,
      num_verts = num_verts + 1;
      if temp_begin_pt(m) <= j && m <= length(temp_begin_pt),
         temp_begin_pt(m) = j;
         m=m+1;
      else
         m=m+1;
      end
   end
end
vert_begin_pt = zeros(num_verts,1);
for n=1:num_verts,
   vert_begin_pt(n)=temp_begin_pt(n);
end
clear j m n temp_begin_pt

%%%% Determine the index of the ws and bed profiles to the right of the
%%%% velocity measurements.  Used to interpolate and shift velocity
%%%% measurements.
wsbed_indices = zeros(length(yz_data),1);
for j=1:length(yz_data),
   for k=1:length(wsbed_mod),
      if wsbed_mod(k,1) > yz_data(j,1)/10,
         wsbed_indices(j,1) = k;
         break
      end
   end
end
clear j k

%%% Interpolate water surface elevations at each vertical
```

```
ws_interp = zeros(num_verts,1);
for i=1:num_verts,
   ws_interp(i,1) = wsbed_prof(wsbed_indices(vert_begin_pt(i)),3) –
   (wsbed_mod(wsbed_indices(vert_begin_pt(i)),1)-
   (yz_data(vert_begin_pt(i),1))/10)/(wsbed_mod(wsbed_indices(vert_begin_pt(i)),1)-
   wsbed_mod(wsbed_indices(vert_begin_pt(i))-1,1))*(wsbed_prof(wsbed_indices(vert_begin_pt(i)),3)-
   wsbed_prof(wsbed_indices(vert_begin_pt(i))-1,3));
end
clear i

%%% Interpolate bed elevations at each vertical
bed_interp = zeros(num_verts,1);
for j=1:num_verts,
   bed_interp(j,1) = wsbed_prof(wsbed_indices(vert_begin_pt(j)),2) –
   (wsbed_mod(wsbed_indices(vert_begin_pt(j)),1)-
   (yz_data(vert_begin_pt(j),1))/10)/(wsbed_mod(wsbed_indices(vert_begin_pt(j)),1)-
   wsbed_mod(wsbed_indices(vert_begin_pt(j))-1,1))*(wsbed_prof(wsbed_indices(vert_begin_pt(j)),2)-
   wsbed_prof(wsbed_indices(vert_begin_pt(j))-1,2));
end
clear j

%%% Calculate the depth at each vertical
depths = zeros(num_verts,1);
for k=1:num_verts,
   depths(k,1) = ws_interp(k,1) - bed_interp(k,1);
end
clear k

%%% Shift all measurement elevations equally
avg_shift=zeros(num_verts,1);
for j=1:num_verts,
   avg_shift(j,1) = yz_data(vert_begin_pt(j),2) - ws_interp(j) + 5;
end
for i=1:length(yz_data),
   meas_pts(i,2) = yz_data(i,2) - mean(avg_shift(:,1));
end
clear i j

%%% Shift elevations so that they are relative to the depth and calculate
%%% the value of y/h for each measurement
j=2;
yh_ratio = zeros(length(meas_pts),1);
for i=1:length(meas_pts),
   if j == num_verts+1,
      meas_pts(i,2) = meas_pts(i,2) - bed_interp(num_verts,1);
      yh_ratio(i,1) = meas_pts(i,2)/depths(num_verts,1);
   elseif i < vert_begin_pt(j) && j ~= num_verts+1,
      meas_pts(i,2) = meas_pts(i,2) - bed_interp(j-1,1);
      yh_ratio(i,1) = meas_pts(i,2)/depths(j-1,1);
   else
      j=j+1;
      meas_pts(i,2) = meas_pts(i,2) - bed_interp(j-1,1);
      yh_ratio(i,1) = meas_pts(i,2)/depths(j-1,1);
   end
end
clear i j
```

```
output1 = [meas_pts(:,2),yh_ratio];
output2 = meas_pts(:,2);
output3 = mean(avg_shift(:,1));
```

Code calculates averages and standard deviations for filtered, un-rotated data to the cross section summary file. (Reads_process_WriteFiltered.m).

```
%%%%%%%%%% MUST MANUALLY INSERT 8 COLUMNS INBETWEEN COLUMNS Q &
%%%%%%%%%% R IN SUMMARY FILE BEFORE RUNNING CODE AND SAVE
%%%%%%%%%% SUMMARY FILE AS A .xls FILE

%%%% Enter cross section number - Modified from Craig Hill
prompts = {'Enter cross section # (1 to 10)'};
name = 'NCHRP cross section ADV processing';
numlines = 1;
xs_num = inputdlg(prompts, name, numlines);
xs_number = str2double(xs_num);

%%%% Select directory to work from - Modified from Craig Hill
working_directory = uigetdir('E:\','Choose working directory to work from');

%%%% Determine the file to write to - Modified from Craig Hill
[write_file, write_path] = uigetfile(strcat(working_directory,'\*.xls'),'Select the summary file to write
to');

%%%% Determine the number of measurements in the cross section (if more than 70 points, changes
%%%% will be needed)
meas_pts = xlsread(strcat(write_path,write_file), 'A2:A71');
num_pts = length(meas_pts);

%%%% Initiate arrays containing filtered averages and std deviations for each point
uvwV_filtered_avg = zeros(num_pts,4);
uvwV_filtered_stdev = zeros(num_pts,4);

%%%% Initiate waitbar
wbar_str = ['Writing filtered velocities for ',num2str(num_pts),' points'];
wbar = waitbar(0,wbar_str);

for j=1:num_pts,
   %%%% Update waitbar
   waitbar(j/num_pts)

   %%%% Read in ENTIRE timeseries_only.csv file for filtered, unrotated velocity components
   %%%%%%  ADV_TS_only COL10: filtered, un-rotated x-velocity component
   %%%%%%  ADV_TS_only COL11: filtered, un-rotated y-velocity component
   %%%%%%  ADV_TS_only COL12: filtered, un-rotated z-velocity component
   %%%%%%  ADV_TS_only COL13: filtered, un-rotated velocity magnitude
   read_file = ['XS',int2str(xs_number),'_Point',int2str(j),'_timeseries_data_only.csv'];
   ADV_TS_only = dlmread(strcat(write_path,read_file), ',' , 1, 0);

   %%%% Calculate the averages of filtered components and magnitude
   %%%%%%  uvwV_filtered_avg COL1: average filtered, un-rotated x-velocity component
   %%%%%%  uvwV_filtered_avg COL2: average filtered, un-rotated y-velocity component
   %%%%%%  uvwV_filtered_avg COL3: average filtered, un-rotated z-velocity component
   %%%%%%  uvwV_filtered_avg COL4: average filtered, un-rotated velocity magnitude
   uvwV_filtered_avg(j,1) = mean(ADV_TS_only(:,10));
   uvwV_filtered_avg(j,2) = mean(ADV_TS_only(:,11));
   uvwV_filtered_avg(j,3) = mean(ADV_TS_only(:,12));
```

```
    uvwV_filtered_avg(j,4) = mean(ADV_TS_only(:,13));

    %%%% Calculate the standard deviation of filtered components and magnitude
    %%%%%%  uvwV_filtered_stdev COL1: std deviation of filtered, un-rotated x-velocity
    %%%%%% component
    %%%%%%  uvwV_filtered_stdev COL2: std deviation of filtered, un-rotated y-velocity
    %%%%%% component
    %%%%%%  uvwV_filtered_stdev COL3: std deviation of filtered, un-rotated z-velocity
    %%%%%% component
    %%%%%%  uvwV_filtered_stdev COL4: std deviation of filtered, un-rotated velocity magnitude
    uvwV_filtered_stdev(j,1) = std(ADV_TS_only(:,10));
    uvwV_filtered_stdev(j,2) = std(ADV_TS_only(:,11));
    uvwV_filtered_stdev(j,3) = std(ADV_TS_only(:,12));
    uvwV_filtered_stdev(j,4) = std(ADV_TS_only(:,13));

    clear ADV_TS_only
end
clear j

%%%% Add headers to the eight new columns in the summary file
ufiltavgh = 'u_mean_filtered (m/s)';
vfiltavgh = 'v_mean_filtered (m/s)';
wfiltavgh = 'w_mean_filtered (m/s)';
Vfiltavgh = 'Vmag_mean_filtered (m/s)';
ufiltstdh = 'u_std_filtered';
vfiltstdh = 'v_std_filtered';
wfiltstdh = 'w_std_filtered';
Vfiltstdh = 'Vmag_std_filtered';
xlswrite(strcat(write_path,write_file),
[{ufiltavgh},{vfiltavgh},{wfiltavgh},{ufiltstdh},{vfiltstdh},{wfiltstdh},{Vfiltavgh},{Vfiltstdh}], 'R1:Y1');

%%%% Write u mean filtered to the summary file
ufilt_writestring = ['R2:R',int2str(num_pts+1)];
xlswrite(strcat(write_path,write_file), uvwV_filtered_avg(:,1), ufilt_writestring);

%%%% Write v mean filtered to the summary file
vfilt_writestring = ['S2:S',int2str(num_pts+1)];
xlswrite(strcat(write_path,write_file), uvwV_filtered_avg(:,2), vfilt_writestring);

%%%% Write w mean filtered to the summary file
wfilt_writestring = ['T2:T',int2str(num_pts+1)];
xlswrite(strcat(write_path,write_file), uvwV_filtered_avg(:,3), wfilt_writestring);

%%%% Write u standard deviation filtered to the summary file
ufiltstd_writestring = ['U2:U',int2str(num_pts+1)];
xlswrite(strcat(write_path,write_file), uvwV_filtered_stdev(:,1), ufiltstd_writestring);

%%%% Write v standard deviation filtered to the summary file
vfiltstd_writestring = ['V2:V',int2str(num_pts+1)];
xlswrite(strcat(write_path,write_file), uvwV_filtered_stdev(:,2), vfiltstd_writestring);

%%%% Write w standard deviation filtered to the summary file
wfiltstd_writestring = ['W2:W',int2str(num_pts+1)];
xlswrite(strcat(write_path,write_file), uvwV_filtered_stdev(:,3), wfiltstd_writestring);

%%%% Write Vmag mean filtered to the summary file
```

```
Vfilt_writestring = ['X2:X',int2str(num_pts+1)];
xlswrite(strcat(write_path,write_file), uvwV_filtered_avg(:,4), Vfilt_writestring);

%%%% Write Vmag standard deviation filtered to the summary file
Vfiltstd_writestring = ['Y2:Y',int2str(num_pts+1)];
xlswrite(strcat(write_path,write_file), uvwV_filtered_stdev(:,4), Vfiltstd_writestring);

clear ufiltavgh vfiltavgh wfiltavgh Vfiltavgh ufiltstdh vfiltstdh wfiltstdh Vfiltstdh
close (wbar);
```

Code shifts vertically all velocity measurements equally so that those closest to the surface are, on average, 5 cm from the water surface. It then estimates the depth-averaged values for each vertical profile using the trapezoidal approximation of integration. (depth_averaging_jrp.m).

```
function [depth_avgs] = depth_averaging_jrp(yzu_data,wsbed_prof)

%%%%%%%% VELOCITIES AT THE BED ARE ASSUMED ZERO AND VELOCITIES AT THE
%%%%%%%% SURFACE ARE LINEARLY EXTRAPOLATED USING THE TWO MEASURED
%%%%%%%% VALUES NEAREST THE SURFACE.

%%%% input matrix 'yzu_data' should contain:
%%%%% COL1: x-coordinate of known measurements in mm (transverse coordinate)
%%%%% COL2: y-coorindate of known measurements in cm (elevation)
%%%%% COL3: parameter to be averaged at the coordinate pair (x,y)

%%%% input matrix 'wsbed_prof' should contain:
%%%%% COL1: x-coordinate of original pt gauge measurements in mm (transverse coordinate)
%%%%% COL2: y-coordinate of original pt gauge bed measurements in cm (elevation)
%%%%% COL3: y-coordinate of original pt gauge water surface measurements in cm (elevation)

%%%% output matrix 'depth_avgs' contains:
%%%%% COL1: depth average of parameter at each vertical profile

%%%%%%%%%%%%%%%%%%%% CODE %%%%%%%%%%%%%%%%%%%%

%%% matrix 'wsbed_mod' contains bed and water surface profile data shifted
%%% to account for the offset of the point gauge from the ADV
wsbed_mod = zeros(length(wsbed_prof),2);
wsbed_mod(:,1) = (wsbed_prof(:,1) + 110)/10;  % COL1: shifted x-coordinate (cm)
wsbed_mod(:,2) = wsbed_prof(:,3) - wsbed_prof(:,2);  % COL2: depth (cm)

%%% matrix 'trans_coord' contains x-coordinate of known measurements in cm (transverse
%%% coordinate)
trans_coord = zeros(length(yzu_data),1);
trans_coord(:,1) = yzu_data(:,1)/10;  % COL1: x-coordinate of velocity measurement in cm

%%% Determine the number of vertical profiles and save what point they start at (if more than 22
%%% profiles, changes will be needed)
num_verts = 1;
temp_begin_pt = zeros(22,1);
temp_begin_pt(1) = 1;
m=2;
for j=2:length(trans_coord),
   if abs(trans_coord(j-1,1) - trans_coord(j,1)) > 0,
      num_verts = num_verts + 1;
      if temp_begin_pt(m) <= j && m <= length(temp_begin_pt),
         temp_begin_pt(m) = j;
         m=m+1;
      else
         m=m+1;
      end
   end
end
vert_begin_pt = zeros(num_verts,1);
```

```
for n=1:num_verts,
   vert_begin_pt(n)=temp_begin_pt(n);
end
clear j m n temp_begin_pt

%%% Matrix 'num_pts' contains the number of points in each vertical profile
num_pts = zeros(num_verts,1);
for i=1:num_verts,
   if i==num_verts && length(yzu_data)-vert_begin_pt(i) == 0,
      num_pts(i,1) = 1;
   elseif i==num_verts && length(yzu_data)-vert_begin_pt(i) ~= 0,
      num_pts(i,1) = length(yzu_data) - vert_begin_pt(i) + 1;
   else
      num_pts(i,1) = vert_begin_pt(i+1) - vert_begin_pt(i);
   end
end
clear i

%%% Determine the index of the ws and bed profiles to the right of the
%%% velocity measurements.  Used to interpolate and shift velocity
%%% measurements.
wsbed_indices = zeros(length(trans_coord),1);
for j=1:length(trans_coord),
   for k=1:length(wsbed_mod),
      if wsbed_mod(k,1) > trans_coord(j,1),
         wsbed_indices(j,1) = k;
         break
      end
   end
end
clear j k

%%% Interpolate water surface elevations at each vertical
ws_interp = zeros(num_verts,1);
for i=1:num_verts,
   ws_interp(i,1) = wsbed_prof(wsbed_indices(vert_begin_pt(i)),3) –
   (wsbed_mod(wsbed_indices(vert_begin_pt(i)),1)-
   (trans_coord(vert_begin_pt(i),1)))/(wsbed_mod(wsbed_indices(vert_begin_pt(i)),1)-
   wsbed_mod(wsbed_indices(vert_begin_pt(i))-
   1,1))*(wsbed_prof(wsbed_indices(vert_begin_pt(i)),3)-
   wsbed_prof(wsbed_indices(vert_begin_pt(i))-1,3));
end
clear i

%%% Interpolate bed elevations at each vertical
bed_interp = zeros(num_verts,1);
for j=1:num_verts,
   bed_interp(j,1) = wsbed_prof(wsbed_indices(vert_begin_pt(j)),2) –
   (wsbed_mod(wsbed_indices(vert_begin_pt(j)),1)-
   (trans_coord(vert_begin_pt(j),1)))/(wsbed_mod(wsbed_indices(vert_begin_pt(j)),1)-
   wsbed_mod(wsbed_indices(vert_begin_pt(j))-
   1,1))*(wsbed_prof(wsbed_indices(vert_begin_pt(j)),2)-
   wsbed_prof(wsbed_indices(vert_begin_pt(j))-1,2));
end
clear j
```

```
%%% Calculate the depth at each vertical
depths(:,1) = ws_interp(:,1) - bed_interp(:,1);

%%% Calculate measurement elevations relative to WS profile
avg_shift=zeros(num_verts,1);
yzu_mod(:,1)=yzu_data(:,1);
yzu_mod(:,3)=yzu_data(:,3);
for j=1:num_verts,
   avg_shift(j,1) = yzu_data(vert_begin_pt(j),2) - ws_interp(j) + 5;
end
for i=1:length(yzu_data),
   yzu_mod(i,2) = yzu_data(i,2) - mean(avg_shift(:,1));
end
clear i j

%%% Matrix 'top_widths' contains the difference between the WS elevation
%%% and the top-most measurement elevation.
top_widths = zeros(num_verts,1);
for i=1:num_verts,
   top_widths(i,1) = ws_interp(i,1) - yzu_mod(vert_begin_pt(i,1),2);
end
clear i

%%% Matrix 'bottom_widths' contains the difference between the bed elevation
%%% and the bottom-most measurement elevation.
bottom_widths = zeros(num_verts,1);
for j=1:num_verts,
   bottom_widths(j,1) = yzu_mod(vert_begin_pt(j,1)+num_pts(j,1)-1,2) - bed_interp(j,1);
end
clear j

%%% Matrix 'central_areas' contains the trapezoidal areas used to
%%% approximate the integral between measured points.
central_areas = zeros(num_verts,1);
for i=1:num_verts,
   temp_sum=0;
   for j=1:num_pts(i,1)-1,
      temp_sum = temp_sum + 0.5*(yzu_mod(vert_begin_pt(i,1)+j-1,2) –
      yzu_mod(vert_begin_pt(i,1)+j,2))*(yzu_mod(vert_begin_pt(i,1)+j-1,3) +
      yzu_mod(vert_begin_pt(i,1)+j,3));
   end
   central_areas(i,1) = temp_sum;
end
clear i j temp_sum

%%% Matrix 'top_areas' contains the trapezoidal areas used to approximate
%%% the integral between the WS elevation and the top-most measurement
%%% elevation.
top_areas = zeros(num_verts,1);
for j=1:num_verts,
   slope = (yzu_mod(vert_begin_pt(j,1)+1,2) –
   yzu_mod(vert_begin_pt(j,1),2))/(yzu_mod(vert_begin_pt(j,1)+1,3) –
   yzu_mod(vert_begin_pt(j,1),3));
   y_intercept = yzu_mod(vert_begin_pt(j,1),2) - slope*yzu_mod(vert_begin_pt(j,1),3);
   surface_value = (ws_interp(j,1) - y_intercept)/slope;
   top_areas(j,1) = 0.5*top_widths(j,1)*(yzu_mod(vert_begin_pt(j),3) + surface_value);
```

```
end
clear j

%%% Matrix 'bottom_areas' contains the triangle areas used to approximate
%%% the integral between the bed elevation and the bottom-most measurement
%%% elevation.  The bottom shapes are always triangles since the
%%% bed-velocity is assumed to be zero.
bottom_areas = zeros(num_verts,1);
for k=1:num_verts,
   bottom_areas(k,1) = 0.5*bottom_widths(k,1)*(yzu_mod(vert_begin_pt(k)+num_pts(k)-1,3));
end
clear k

%%% Matrix 'sum_areas' contains the approximation of integrated velocity
%%% profile for each vertical.
sum_areas(:,1) = bottom_areas(:,1) + top_areas(:,1) + central_areas(:,1);

%%% Create output matrix containing the depth averaged values at each
%%% vertical profile.
depth_avgs = zeros(num_verts,1);
for i=1:num_verts,
   depth_avgs(i,1) = sum_areas(i,1)/depths(i,1);
end
clear i
```